

HUMAN-INDUCED VERTICAL VIBRATION ON PEDESTRIAN
STRUCTURES: NUMERICAL AND EXPERIMENTAL ASSESSMENT

A Dissertation

Submitted to the Faculty

of

Purdue University

by

Daniel Gómez

In Partial Fulfillment of the

Requirements for the Degree

of

Doctor of Philosophy

August 2019

Purdue University

West Lafayette, Indiana

**THE PURDUE UNIVERSITY GRADUATE SCHOOL
STATEMENT OF DISSERTATION APPROVAL**

Dr. Shirley J. Dyke, Chair

School of Mechanical Engineering and Lyles School of Civil Engineering.

Dr. Shirley Rietdyk

Department of Health and Kinesiology.

Dr. Julio Ramirez

Lyles School of Civil Engineering.

Dr. Juan Caicedo

Civil and Environmental Engineering, University of South Carolina.

Approved by:

Dr. Dulcy M. Abraham

Head of the Burke Graduate Program.

To my wife and my parents.

ACKNOWLEDGMENTS

My deepest gratitude goes to my advisor, Professor Shirley J. Dyke. Her motivation, advice, confidence, modesty and patience have inspired me throughout these years at Purdue. I have no words to express my sincere thanks to her.

I also would like to thank Professor Shirley Rietdyk for her extensive guidance and support regarding human motor behavior. Professor Julio Ramirez for his experience and advice in the field of structural analysis and design. I would like to specially thank Professor Wei Song and his group at the University of Alabama for providing the equipment to conduct the full-scale test of an instrumented footbridge. Their help and support with the experiments are dearly appreciated. I thank Professor Juan Caicedo from University of South Carolina for reading this dissertation and offering constructive comments, and Professor Robert Connor from Purdue University for providing the steel beam used in this study.

I am extremely thankful to my friends and fellow graduate students in the Intelligent Infrastructure Systems Laboratory (IISL) for their sincere co-operation and providing a friendly atmosphere in the lab.

Finally, I would like to thank my family for their support and encouragement throughout these years. I must express my gratitude to Sandra, my wife, for her continued support and encouragement. I was continually amazed by her willingness to proof read countless pages of my writings.

This work was financially supported by the Colombia-Purdue Institute for Advanced Scientific Research (CPI), Colciencias, Colfuturo, the Universidad del Valle and Purdue University.

TABLE OF CONTENTS

	Page
LIST OF TABLES	viii
LIST OF FIGURES	ix
ABSTRACT	xiii
1 INTRODUCTION	1
1.1 Motivation	1
1.2 Literature review	3
1.2.1 Walking-induced load	3
1.2.2 Pedestrian-structure models	5
1.2.3 Guidelines and standards	6
1.3 Objectives and contribution	9
1.4 Overview of the dissertation	10
2 A SUBSTRUCTURE-BASED MODEL TO DESCRIBE PEDESTRIAN- STRUCTURE INTERACTION	13
2.1 Mathematical formulation	14
2.1.1 Bridge substructure	15
2.1.2 Pedestrian substructure	17
2.1.3 Pedestrian-bridge interaction model	20
2.2 Experimental verification	21
2.2.1 Experimental setup and parameter identification	21
2.2.2 Pedestrian parameters	25
2.2.3 Experimental verification of the PSI model	26
2.3 Summary	36
3 SPATIAL-TEMPORAL ASSESSMENT OF GAIT DYNAMICS IN WALKING- INDUCED VIBRATION	37
3.1 Introduction	38

	Page
3.2 Description of the experimental program	38
3.2.1 Participants	38
3.2.2 Equipment	39
3.2.3 Instrumented structure	40
3.3 Comparison of the gait kinematics on stationary and moving surfaces for a walking subject using a metronome	44
3.3.1 Step length and step width	44
3.3.2 Pace frequency and gait speed	44
3.4 Comparison of the gait kinematics on stationary and moving surfaces for a walking subject at self-selected pace	44
3.4.1 Step length and step width	46
3.4.2 Pace frequency and gait speed	47
3.5 Influence of the vibration level in the gait dynamics	48
3.6 Summary	52
4 STRUCTURED UNCERTAINTY FOR A PEDESTRIAN-STRUCTURE INTERACTION MODEL	55
4.1 Representing system uncertainties	56
4.1.1 Pedestrian subsystem definition	57
4.1.2 Structured parametric model uncertainty	58
4.1.3 Structural subsystem definition	63
4.1.4 PSI model with structured uncertainties	64
4.2 Experimental setup and procedure	67
4.2.1 Subjects and anthropometric data	67
4.3 Results and discussion	70
4.3.1 Response comparison for a walking subject using a metronome	71
4.3.2 Response comparison for a single subject walking at a self- selected pace	75
4.3.3 Response comparison between subjects using the metronome	77
4.3.4 Response comparison between subjects walking freely	79

	Page
4.4 Summary	80
5 EXPERIMENTAL AND NUMERICAL VIBRATION SERVICEABILITY ASSESSMENT OF A FOOTBRIDGE	82
5.1 Introduction	82
5.2 Footbridge description and experimental setup	83
5.2.1 Full scale measurements	84
5.2.2 Numerical modeling of the footbridge	84
5.3 Serviceability assessment for vertical vibration	89
5.3.1 Experimental assessment of pedestrian-induced vibration	90
5.3.2 Comparison with current standards	91
5.3.3 Numerical prediction of the structural response	93
5.4 Summary	95
6 CONCLUSIONS AND RECOMMENDATIONS	98
6.1 Future research perspectives	100
REFERENCES	102
A GAIT VARIABILITY	116
B STRUCTURAL RESPONSE FOR DIFFERENT PEDESTRIAN LOAD CON- DITIONS	126

LIST OF TABLES

Table	Page
1.1 Weight of a crowd of people as live load used for structural design purposes.	6
1.2 Recommended frequency and acceleration limits for vertical vibration serviceability assessment.	9
2.1 Bio-dynamic parameters obtained on a rigid floor.	26
3.1 Test subject parameters.	39
3.2 Obtained ranges for each gait parameter.	49
4.1 Biodynamic parameters used/obtained in PSI studies.	69
4.2 Perturbed biodynamic parameters obtained for a walking subject following an audible beat.	72
4.3 Perturbed biodynamic parameters obtained for a walking subject at self-selected pace frequency.	75
4.4 Perturbed biodynamic parameters obtained for walking subjects following an audible beat.	77
4.5 Perturbed biodynamic parameters obtained for walking subjects at self-selected pace frequency.	80
5.1 Experimental and FEM modal parameters of the footbridge.	89

LIST OF FIGURES

Figure	Page
1.1 Closed-loop system to represent the pedestrian-structure interaction. . . .	1
1.2 Noteworthy pedestrian bridges with reported excessive vibration problems.	4
1.3 Weight of a crowd based on work done by Johnson (1905).	7
1.4 Weight of a crowd based on work done by Nowak & Collins (2012).	8
2.1 Model of pedestrian-structure interaction system.	15
2.2 Structural subsystem dynamic model.	15
2.3 Pedestrian subsystem dynamic model.	19
2.4 Pedestrian-structure interaction model.	20
2.5 Flowchart of the solution procedure.	22
2.6 Experimental setup of full-scale steel beam.	23
2.7 Location of 18 accelerometers, with 12 in the vertical and 6 in the horizontal direction.	23
2.8 Structural subsystem acceleration measured response: (a) time history; (b) power spectral density (PSD).	24
2.9 COM acceleration in a rigid floor (subject SA).	27
2.10 Measured and predicted vertical acceleration responses and IRE comparison at midspan of the bridge for a single pedestrian.	29
2.11 Time-frequency representation of the measured responses of the bridge to single pedestrian. Zoom-in plot of a frequency range from the spectrogram including measured and predicted vertical acceleration variation responses.	31
2.12 Mean and standard deviation values of the NRMSE for test subjects. . . .	33
2.13 Peak acceleration for test subjects.	35
3.1 SmartGait TM system and test structure.	41
3.2 Experimental and identified transfer functions.	42

Figure	Page
3.3 Typical data results obtained using the SmartGait TM system shown the spatial-temporal gait representation measured in a trial. (a) Step length; (b) Step width; (c) Pace frequency; (d) Gait speed; (Note: the two vertical dashed lines indicate when the pedestrian enters and leaves the established walkway either on the beam or on the ground).	43
3.4 Comparison for pedestrian kinematic parameters using a metronome's beat. Each row depicts a kinematic parameter while each column represents a test subject both on the stationary and on the moving surface.	45
3.5 Percent change (PC) for pedestrian kinematic parameters vs. metronome's frequency. Each row depicts a kinematic parameters while each column represents a prescribed frequency. (Note: horizontal line at 0% indicates when the percentage increases and decreases).	46
3.6 Comparison for pedestrian kinematic parameters at self-selected pace. Each row depicts a kinematic parameters while each column represents a test subject both on the stationary and on the moving surface.	47
3.7 Percent change (PC) for pedestrian kinematic parameters at self-selected pace. Each row depicts a kinematic parameters while each column represents a test subject. (Note: horizontal line at 0% indicates when the percentage increases and decreases).	48
3.8 Peak acceleration as a function of pedestrian mass and coupled system's frequency.	50
3.9 Peak acceleration as function of pedestrian mass.	51
3.10 Influence of vibration amplitude in the pedestrian gait dynamics.	53
3.11 Influence of vibration amplitude in the pedestrian gait dynamics.	54
4.1 Model of the nominal pedestrian-structure interaction system.	57
4.2 Nominal pedestrian subsystem block diagram.	58
4.3 LFT of a linear uncertain system.	59
4.4 Pedestrian subsystem model with parametric uncertainties.	61
4.5 Input/output of the uncertain pedestrian subsystem.	63
4.6 Structural subsystem block diagram.	64
4.7 Pedestrian-structure interaction model with uncertainties	65
4.8 Test structure used in the experimental program.	67

Figure	Page
4.9 Single experimental record for a subject walking on the structure (solid line) and uPSI model prediction (gray region) at $F_m = 1.7$ Hz. The two vertical dashed lines indicate when the pedestrian is walking on the beam. (a) and (c) Midspan acceleration amplitude; (b) and (d) Spectrum of instantaneous frequencies versus time. The horizontal dotted line in (b) and (d) represents the first vertical natural frequency of the bare structure.	73
4.10 Single experimental record for a subject walking on the structure (solid line) and uPSI model prediction (gray region) at $F_m = 2.0$ Hz. The two vertical dashed lines indicate when the pedestrian is walking on the beam. (a) and (c) Midspan acceleration amplitude; (b) and (d) Spectrum of instantaneous frequencies versus time. The horizontal dotted line in (b) and (d) represents the first vertical natural frequency of the bare structure.	74
4.11 Single experimental record for a subject walking on the structure (solid line) and uPSI model prediction (gray region) at self-selected speed. The two vertical dashed lines indicate when the pedestrian is walking on the beam. (a) and (c) Midspan acceleration amplitude; (b) and (d) Spectrum of instantaneous frequencies versus time. The horizontal dotted line in (b) and (d) represents the first vertical natural frequency of the bare structure.	76
4.12 Single experimental record for a different subject walking on the structure (solid line) and uPSI model prediction (gray region) following a metronome. (a), (c) and (e) Midspan acceleration amplitude; (b), (d) and (f) Spectrum of instantaneous frequencies versus time.	78
4.13 Single experimental record for a different subject walking on the structure (solid line) and uPSI model prediction (gray region) at self-selected speed. The two vertical dashed lines indicate when the pedestrian is walking on the beam. (a) Midspan acceleration amplitude; (b) Spectrum of instantaneous frequencies versus time. The horizontal dotted line in (b) represents the first vertical natural frequency of the bare structure.	79
5.1 Hackberry Lane pedestrian bridge in Tuscaloosa Alabama.	83
5.2 Details of the instrumented pedestrian bridge.	85
5.3 Measured ambient response of the bridge (Channel No. 4).	86
5.4 Identified mode shapes of the footbridge. Mode 1: 1 st vertical. Mode 2: 1 st torsional. Mode 3: 1 st lateral . Mode 4: 2 nd vertical. Mode 5: 2 nd torsional. Mode 6: 3 rd vertical.	87
5.5 Analytical mode shapes of the footbridge. Mode 1: 1 st vertical. Mode 2: 1 st torsional. Mode 3: 1 st lateral . Mode 4: 2 nd vertical. Mode 5: 2 nd torsional. Mode 6: 3 rd vertical.	88

Figure	Page
5.6 Vertical accelerations due to a pedestrian walking at different frequencies (Channel No. 04).	91
5.7 Vibration serviceability assessment of a footbridge under pedestrian-induced loads.	94
5.8 Midspan acceleration amplitude of three experimental trials for a pedestrian walking on the footbridge (solid line) and uncertain PSI model prediction (gray region). The two vertical dashed lines indicate when the pedestrian enters and leaves the bridge.	96
A.1 Prescribed cadence: Subject S-1.	117
A.2 Prescribed cadence: Subject S-2.	118
A.3 Prescribed cadence: Subject S-3.	119
A.4 Prescribed cadence: Subject S-4.	120
A.5 Prescribed cadence: Subject S-5.	121
A.6 Prescribed cadence: Subject S-6.	122
A.7 Self-selected pace: Subject S-1.	123
A.8 Self-selected pace: Subject S-2.	123
A.9 Self-selected pace: Subject S-3.	124
A.10 Self-selected pace: Subject S-4.	124
A.11 Self-selected pace: Subject S-5.	125
A.12 Self-selected pace: Subject S-6.	125
B.1 Vertical accelerations due to two pedestrians walking at different frequencies (Channel No. 4).	126
B.2 Vertical accelerations due to three pedestrians walking at different frequencies (Channel No. 4).	127

ABSTRACT

Gómez, Daniel Ph.D., Purdue University, August 2019. Human-Induced Vertical Vibration on Pedestrian Structures: Numerical and Experimental Assessment. Major Professor: Shirley J. Dyke.

In recent years civil engineering structures such as floors, footbridges, and staircases, have reported unacceptable vibration when they are dynamically excited by pedestrians. When such structures have a particular combination of high structural flexibility and low inherent damping, there is potential for excessive vibration. Pedestrian-structure interaction (PSI) is especially noticeable when the lowest structural natural frequencies are close to the dominant pedestrian pace frequency or its harmonics. Although most of these structures are designed according to existing standards and guidelines, there are still many uncertainties in the human actions that may lead to unexpected structural behavior, increasing the vibration responses and exceeding serviceability limit states. How a pedestrian excites a structure and how that structure affects a pedestrian's gait is not fully understood. Therefore, a realistic analysis of PSI must be performed to properly incorporate these effects toward more rational structural designs. This study aims to identify, within this class of the walking-induced load problem, the vibration mechanisms, the mathematical models, and methods, to address excessive vibration in pedestrian structures. After conducting an in-depth evaluation of current guidelines and provisions for analysis and design of pedestrian structures, models to enable more realistic design under such uncertainties have been developed. The results establish a body of knowledge regarding human loads and structural responses, yielding the potential for more rational approaches to improve the analysis and design of pedestrian structures.

1. INTRODUCTION

1.1 Motivation

An increasing number of slender structures such as floors, footbridges, and staircases, have reported problems with excessive vibrations induced by pedestrians, even when most of them were designed to strictly follow current standards and guidelines (Cunha & Moutinho, 1999; Sachse et al., 2003; Gomez, Silva, et al., 2015). When such structures have particular combinations of high structural flexibility and low inherent damping, there is potential for excessive vibration, fatigue, and even failure. Pedestrian-structure interaction (PSI) (see Fig. 1.1) is especially noticeable when the lowest structural natural frequencies are close to the dominant pedestrian pace frequency or its harmonics (Ellingwood & Tallin, 1984; Bachmann et al., 1995; Cunha & Moutinho, 1999; Sachse et al., 2003). This condition exposes the pedestrian to excessive structural vibration modifying his/her gait characteristics that may lead unexpected structural behavior increasing the vibration responses and exceeding serviceability limit states (Danion et al., 2003; Dang & Živanović, 2015; García-diéguez & Zapico-Valle, 2018). Therefore, a more realistic analysis of PSI should be performed and incorporated it into structural analysis and design procedures.

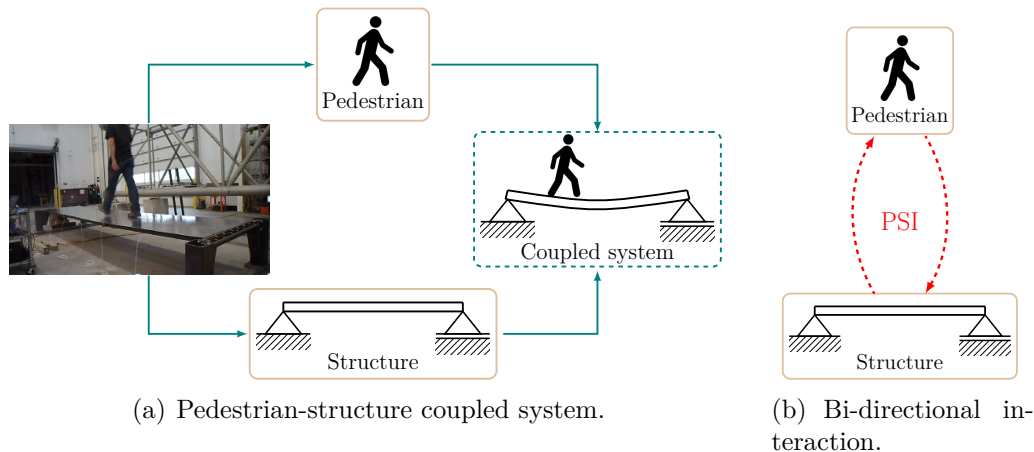


Fig. 1.1.: Closed-loop system to represent the pedestrian-structure interaction.

Rising concern regarding the potential for footbridge damages and even failures demonstrate that PSI effects remain a worldwide problem. However, because such structural issues have occurred sporadically in different countries over a few decades, the problem has not clearly been articulated ([Wolmuth & Surtees, 2003](#)). It is perhaps for this reason that the final design often deviates significantly from the predicted model response, such as the Millenium bridge in London, Solferino bridge in Paris, and Squibb Park bridge in New York, among others. As a result, the serviceability load conditions due to pedestrian activities are controlling the design for these structures ([Ellingwood & Tallin, 1984](#); [Bachmann et al., 1995](#)).

An examination of existing standards and guidelines yields a broad range of results demonstrating a clear lack of knowledge of the actual demands to consider, when common structures are exposed to dynamic and coupled pedestrian loads. Although there has been growing interest in this topic, and updates to some guidelines attempt to provide practical descriptions of the PSI effects, these are insufficient and the persistent concerns reported indicate that the level of this interaction is still difficult to estimate. Most international codes, including US design guidelines such as [AASHTO \(2009\)](#) and [ASCE-7/10 \(2010\)](#) consider the pure static effects of humans and crowds as live loads. As a consequence, the prediction of system's response is inaccurate and greatly depends on various uncertain parameters which the structural designer cannot anticipate readily. Thus, as the field proceeds to pursue innovative and sustainable solutions for designs, codes and procedures need to realistically consider the human influence on the structure with its considerable randomness and uncertainty in the structural response.

In summary, the increase of reported vibration problems in modern slender structures indicates that future structures should be designed with due consideration to the coupled dynamic loads induced by humans, to minimize the restrictions to architectural features of very slender or lightweight structures. Clearly research is critically needed because these serviceability load conditions due to human activities do control the design, especially in prominent structures where human occupants congregate such as stadiums, long-span floors, gymnasiums, footbridges and theaters. Thus, as society strives to build taller and longer, high-fidelity models and improved standards must enable the designer to perform an appropriate analysis to design reliable and robust structures that achieve desirable performance even with realistic response variations.

1.2 Literature review

1.2.1 Walking-induced load

The first notable consideration regarding excessive vibration in suspension bridges was published in a descriptive paper by [Stevenson \(1821\)](#). He noticed considerable movement when a passing regiment marched in regular time on the Montrose and Dryburgh bridges in Scotland. Based on his observations, he stated that this type of load should not be considered simply as dead load. Later, both the Broughton suspension bridge in England in 1831 and the Angers bridge in France in 1850 collapsed while groups of soldiers were marching across them. After the Broughton suspension bridge collapse, the British Army issued an order that soldiers crossing a bridge should break step.

A remarkable study conducted by [Tilden \(1913\)](#) developed an innovative experimental program to measure the dynamic effects of a single subject performing different activities such as standing up from crouching and sitting postures. Moreover, he led two other novel tests based on his observations when a crowd of people ran from one side to the other side of a bridge during a boat competition. In the first test, a man walked on a rigid floor while being recorded by an arrangement of several cameras. Using the sequential photos, professor Tilden was able to establish the movement of the center of mass (COM) of the pedestrian. By obtaining the acceleration from the displacements, an intent to estimate the horizontal forces exerted for a walker was made. In the second test, a man was running from one side to another side on three test bridges. Using a stop-watch, he calculated the speed of the runner based on the time and the covered distance. Using the kinetic energy produced by the runner, professor Tilden estimated the instantaneous horizontal force applied by the man on each side of the bridge.

Later sporadic reports for large vibration amplitudes were divulged in different countries. Several pedestrian bridges suffered annoying vibration in lateral and vertical direction during exceptional crowd events, such as marching soldiers, procession, crowd walking from one side to the another, crowd walking form one end to another, etc. ([Wolmuth & Surtees, 2003](#)). In 1958, the Parkovy pedestrian bridge in Ukraine was closed shortly after opening due to excessive lateral vibration. Frequency measurements revealed that the first natural frequency in lateral direction was 1 Hz, which is near the dominant frequency in the lateral direction of a walker ([Blekherman, 2005](#)). Another well documented example of excessive vibration occurred in

1989 when the Toda park bridge, a cable-stayed footbridge in Japan, was heavily used. This pedestrian bridge exhibited lateral vibration induced by crowd traffic due to its natural frequency in the lateral direction at 0.95 Hz (Fujino et al., 1992, 1993; Nakamura & Fujino, 2002). In vertical direction, the Jatujak Bridge in Thailand with a 2 Hz first vertical mode suffered large vibration response causing alarm to users (Poovarodom et al., 2003; Brand et al., 2017).

The most renowned examples of human-induced load took place when unexpected lateral vibration occurred in two iconic bridges: namely, the Solférino bridge in Paris (see Fig. 1.2(a)) and the Millennium bridge in London (see Fig. 1.2(b)). Such bridges, which were closed to the public due to excessive vibrations in 1999 and 2000, respectively, received wide attention from researchers, which demonstrated that structural engineers were not able to predict large responses due to human loads in their analysis. Moreover, this problem showed that the effects produced by human traffic and other activities such as dancing, running, jumping, and so on over structures are still not very well understood. Although, the lateral vibration problems of the Solférino and Millennium Bridge were unusual, this phenomenon is not unique and similar problems in the vertical direction have been observed in other structures. Therefore, guidelines and building codes show serious limitations to predict when large structural response amplitudes due to human loads will appear.



(a) Solférino bridge. (Adapted from [Skyscrapercity \(2015\)](#)).



(b) Millenium bridge. (Adapted from [London-Town \(2015\)](#)).

Fig. 1.2.: Noteworthy pedestrian bridges with reported excessive vibration problems.

1.2.2 Pedestrian-structure models

Several analytical models have been developed in the last three decades to predict footbridge responses due to human walking in the lateral and vertical direction. Many attempts to model human-induced effects in the lateral direction took place soon after the Millennium bridge exhibited unexpected large amplitude vibrations on its opening day in 2000 (Dallard et al., n.d.; Roberts, 2003; Ricciardelli & Pizzimenti, 2007; Eckhardt et al., 2007; Venuti et al., 2007; Macdonald, 2009). Also, of the several analytical models of human-induced vertical vibration that have been proposed, most of them consider a single pedestrian as a deterministic moving harmonic force (Živanović et al., 2005), neglecting the interaction as a bi-directional effect between the pedestrian and the oscillating bridge. Generally speaking, this approach is called the moving force problem. In this strategy, the vertical ground reaction force (GRF) generated by a pedestrian on a “rigid” floor is applied as a moving load. In fact, this straightforward approach is often adopted by the most common international standards and building codes (Archbold et al., 2011; Živanović et al., 2010).

Improving upon this approach, different mathematical models have been proposed to describe pedestrian-structure interaction. Using a spring-mass-damper system to represent a person crossing the bridge is one approach derived from the moving oscillator problem (Fanning et al., 2005; Toso et al., 2013; Pfeil et al., 2014; Gomez, Silva, et al., 2015), and a periodic force, which describes the GRF, is applied to the footbridge at the pedestrian location (Archbold et al., 2011; Jimenez-Alonso et al., 2016). Early developments in biomechanics and robotics representing the human locomotion as an inverted pendulum were explained by Mochon & McMahon (1980), Onyshko & Winter (1980), Alexander (1995), and Whittington & Thelen (2009). However, these bipedal models were initially created to describe a human while walking on a stationary surface. Recently, more detailed models have been motivated by these bipedal representations and were adapted for a moving surface (Bocian et al., 2013; Qin et al., 2013a,b). Despite the fact that the equations for the bipedal alone are quite simple, when the structure is included, the system equations become more complex, and accounting for the change of location of the pedestrian yields a time-varying system.

Historically, PSI models have been deterministic with the parameters of the pedestrian and structural models represented by specific quantities. However, for a walking pedestrian, the value of the biodynamic parameters vary not only from person to person, but also from trial to trial, even for the same subject performing a given activity

(Živanović et al., 2007; Racic et al., 2009). Thus, deterministic simulations conducted with a particular set of parameters may yield results that do not fully convey the types of responses that are possible. Recently, uncertainty has been taken into account in stochastic modeling under the premise that the pedestrian dynamic parameters can be defined by known probability density functions (Piccardo & Tubino, 2009; Pederesen & Frier, 2010; Ingólfsson & Georgakis, 2011; C. C. Caprani et al., 2012; Krenk, 2012; Zhang et al., 2016; Bruno & Corbetta, 2017). However, there is still a lack of sufficient data available to appropriately estimate the distributions of these random variables. Therefore, the available experimental data regarding human parameters, such as damping and stiffness, does not yet permit a probabilistic analysis (Wang et al., 2017; Tubino, 2017). Moreover, such measurements are often collected using pedestrians walking on rigid surfaces where the interaction effects between the pedestrian and the structure are not present (Brownjohn et al., 2004; Piccardo & Tubino, 2009; Ferrarotti & Tubino, 2016; Bruno & Corbetta, 2017; Gomez et al., 2018).

1.2.3 Guidelines and standards

Between 1860 to 1905, structural engineers and researchers were trying to establish the weight of a crowd for design purposes (see Table 1.1). However, the live load values used in the engineering practice at that time differ widely and in some case was understate. The load values traditionally used for a crowd ranged from 40 to 157 psf, revealing a vast criterion to design pedestrian structures.

Table 1.1.: Weight of a crowd of people as live load used for structural design purposes.

Authority	People in the test	Area [ft^2]	Weight avg. [$lbs/person$]	Total weight [lbs]	Weight of crowd [lbs/ft^2]	Year
Tredgold and Mr Nash (architects of Buckingham Palace)		314			120	1860
French practice					41	1881
Mr. Page, engineer to Chelsea bridge (London)					84	1881
Mr. E. W. Stoney	58	57	145	8404	147.4	1891
American highway bridges specifications					100	1892
Mr. W.N. Kernot (Working Men's College, Melbourne)	13	14		1761	126	1893
Mr. W.C. Kernot (Melbourne University)	17	18.23	153.3	2606.1	143.1	1893
Professor Spofford (MIT)					142.5	1904
Herr Hunscheidt in Bonn					144	1904
C.C. Schneider, USA (structural designer)					40-45	1904
Lewis J. Johnson (Harvard University)	40	36	163.2		134.2 - 156.9	1905

One of the earliest experimental tests to measure the static load produced by a group of people was conducted by Johnson (1905). He placed his students in a 36 ft^2 wood box to measure the weight of a different number of people as shown in Fig. 1.3.

He found that the maximum allowable load of 180 psf might occur in exceptional cases, but 160 psf seemed to be the reasonable value that might occur more often. It should be mentioned that the Canadian code ([Chaussé, 1906](#)) stated that 140 to 150 psf could be considered as the weight of a stationary group of people. However, for pedestrian structures in which the crowd is moving, the value of the live load might be considered greater in the analysis to take into account the effect of the human movement in the structural response.



(a) 10 men on 36 ft² (41 psf) (Adapted from [Johnson \(1905\)](#)).



(b) 37 men on 36 ft² (154 psf) (Adapted from [Johnson \(1905\)](#)).

Fig. 1.3.: Weight of a crowd based on work done by [Johnson \(1905\)](#).

At this time serviceability guidelines are limited in considering the fact that changes occur in the dynamic properties of pedestrian structures due to these dynamic interactions with moving pedestrians. Some standards still consider the maximum credible pedestrian loading as shown in the work done by professor Nowak in 2000 ([Nowak & Collins, 2012](#)) which is still used in the [AASHTO \(2009\)](#) as the maximum allowable pedestrian load neglecting the dynamic effect of the human movement. Serviceability guidelines do not accurately predict the structural dynamic response, and thus existing standards suffer from inconsistent and sometimes illogical design solutions, demonstrating significant gaps in knowledge remain ([Roos, 2009](#); [Zuo et al., 2012](#); [Van Nimmen et al., 2014](#)). Even with recent advances in load models and response predictions, measured responses from pedestrian bridges in operation often deviate greatly from those predicted ([Živanović et al., 2009](#)). The main reason for this gap is that experimental studies of PSI, as well as the analytical models available to

describe the loads produced by human walking, are unable to adequately reproduce the dynamic interaction between the two systems (Shahabpoor et al., 2013).



(a) Live load of 100 psf. (Adapted from AASHTO (2009)).



(b) Live load of 150 psf. (Adapted from AASHTO (2009)).

Fig. 1.4.: Weight of a crowd based on work done by Nowak & Collins (2012).

Current design codes and standards commonly address the vibration serviceability of structures at the design stage in a combination of one, two or even three approaches: (1) setting a lower bound for the static live load value, which must be increased by a factor to compensate for the lack of accuracy to estimate the structural dynamic response; (2) setting a lower bound value for the fundamental frequency of the structure with the intention to avoid the possibility of resonant response due to the human activities; or (3) setting an upper bound of the acceptability acceleration criterion limit as an assessment of vibration serviceability of pedestrian structures under walking-induced vibrations (Brownjohn et al., 2015). This procedure, which is described in different design codes (see Table 1.2) have several shortcomings, *e.g.*, incomplete and unrealistic characterization of the actual loads, neglected dynamic interactions between the humans and structures, and final designs that do not reflect the architectural and aesthetic appearance to maintain a harmony with the surrounding infrastructure. As a consequence, our ability to design for these loads is still limited. Because the vibration requirements due to human loads are a dominant factor in the actual structural response of pedestrian bridges, better modeling approaches are critically needed.

Table 1.2.: Recommended frequency and acceleration limits for vertical vibration serviceability assessment.

Guideline	Frequency, f (Hz)	Acceleration, a ($\text{m} \cdot \text{s}^{-2}$)
British Standards (BS5400, 1978)	> 5	$a < 0.5\sqrt{f}$
Ontario Guide (ONT95, 1995)	> 3	$a < 0.25f^{0.78}$
Eurocode 1 (EN 1991-2, 2002)	$f > 5$	$a < 0.7$
DIN 2003 (DIN-Fachbericht, 2003)	$\begin{cases} 1.6 > f > 2.4 \\ 3.5 > f > 4.5^h \end{cases}$	$a < 0.5\sqrt{f}$
Eurocode 5 (EN 1995-2, 2004) ^a	$\begin{cases} f \leq 2.5 \\ 2.5 < f \leq 5^h \end{cases}$	$\begin{cases} a < 200/(M\zeta)^c \\ a < 100/(M\zeta)^c \end{cases}$
Eurocode 5 (EN 1995-2, 2004) ^b	$\begin{cases} f \leq 2.5 \\ 2.5 < f \leq 5^h \end{cases}$	$\begin{cases} a < 46 \cdot n \cdot k_{vert}/(M\zeta)^d \\ a < 23 \cdot n \cdot k_{vert}/(M\zeta)^d \end{cases}$
Bro-2004 (Bro2004, 2004)	$f > 3.5$	$a_{\text{rms}} < 0.5$
Sétra (Sétra, 2006)	$\begin{cases} f \leq 1 \text{ or } f > 5 \text{ (neg.)}^g \\ 1 < f \leq 1.7 \text{ (med.)}^g \\ 1.7 < f \leq 2.1 \text{ (max.)}^g \\ 2.1 < f \leq 2.6 \text{ (med.)}^g \\ 2.6 < f \leq 5 \text{ (min.)}^g \end{cases}$	$\begin{cases} a \leq 0.5 \text{ (max.)}^e \\ 0.5 < a \leq 1 \text{ (med.)}^e \\ 1 < a \leq 2.5 \text{ (min.)}^e \\ a > 2.5 \text{ (Unacc.)}^e \end{cases}$
ISO 10137 (ISO-10137, 2007)	N/A	$a < 60\sqrt{2} \cdot a_{\text{rms}}^m$
HIVOSS (Heinemeyer et al., 2007)	$1.25 > f > 4.6$	$\begin{cases} a \leq 0.5 \text{ (max.)}^e \\ 0.5 < a \leq 1 \text{ (med.)}^e \\ 1 < a \leq 2.5 \text{ (min.)}^e \\ a > 2.5 \text{ (Unacc.)}^e \end{cases}$
LRFD Footbridge Guide (AASHTO, 2009)	> 3	N/A

^a For one pedestrian crossing the bridge.

^b For several pedestrians crossing the bridge.

^c M is the total mass of the bridge in kg. ζ is the damping ratio.

^d $n = 13$ for a distinct group of pedestrians, $n = 0.6 \cdot A$ for a continuous stream of pedestrians where A is the area of the bridge deck in m^2 . k_{vert} is defined in Fig. B-1 in EN 1995-2 (2004).

^e Level of comfort: max = maximum, med = medium, min = minimum, unacc = unacceptable.

^g Risk of resonance: max = maximum, med = medium, min = minimum, neg = negligible.

^h Might be excited by the 2nd harmonic of pedestrian loads.

^m a_{rms} is defined in Fig. C-1 (ISO-10137, 2007).

1.3 Objectives and contribution

The overarching research objective is to develop the necessary knowledge for understanding and modeling the effects of pedestrian-induced dynamic actions on a structure. To achieve the research objective, this comprehensive analysis and experimental program can be split into two main concepts: (1) spatial and temporal analysis of the variation in gait characteristics when a pedestrian is influenced by vertical vibrating conditions, and (2) the sensitivity of the structural response to pedestrian-induced loads including biodynamic parameter variations. A common

point of interest between human motor behavior, feedback systems, and serviceability design of structures is pursued in this dissertation. By melding these three disciplines, the research developed in this dissertation leverages tools and theories from: (1) kinesiology to analyze and describe pedestrian gait characteristics and uncertainties in biodynamic parameters. (2) control theory, to capture the salient features in of pedestrian-structure system as coupled subsystems that interact dynamically. (3) structural engineering, to interpret these models and establish rational serviceability limits toward improve structural designs to meet realistic limit state specifications. By blurring these research boundaries, the understanding of pedestrian-structure interaction is pushed further, enabling structural designers to perform an appropriate analysis and design that achieve desirable performance with realistic response variations.

The main contribution of this research is to significantly advance awareness and understanding regarding PSI. This knowledge will be valuable for the accurate structural response prediction based on the development of a novel substructuring model that is able to simulate the interaction between a pedestrian and structure adequately (Gomez et al., 2018) (Chapter 2). Furthermore, by studying the effects of a lively structure and their influence on the pedestrian gait characteristics, the kinematic variation in terms of step length, step width, pace frequency, and gait speed are obtained, and the synchrony in PSI where a walking person matches his/her pace frequency with the structure's natural frequency is revealed (Gomez et al., 2019a) (Chapter 3). Then, a systematic approach to combine the developed feedback model with gait variability and intra- and inter-subject biodynamic uncertainties is implemented to provide a robust model suited to highlight the sensitivity of the structural response to pedestrian parameter randomness (Gomez et al., 2019b) (Chapter 4). Therefore, the results here establish a clear understanding of walking-induced load effects in structures, yielding rational knowledge for improving the analysis procedures and design guidelines for pedestrian structures where vibration leads to a reduction in serviceability.

1.4 Overview of the dissertation

This dissertation is organized in six chapters.

Chapter 2 presents a novel mathematical substructuring approach used to represent a pedestrian-structure coupled system dynamics. The equations for each subsystem are described, and a discussion of how the inputs and outputs of each

substructure interact with each other are provided. Then, an experimental study is described and the associated bridge and pedestrian models are constructed. Test subjects with different physical characteristics are considered, and a method is developed to characterize each pedestrian using data obtained while walking on a rigid floor. Finally, the predicted results of the PSI model are validated against the experimental bridge responses due to a single pedestrian, and are also compared with the results obtained using traditional models in both time and frequency domains. The methodology and results presented in this chapter has been published as:

Gomez, D., Dyke, S. J., & Rietdyk, S. (2018). Experimental verification of a substructure-based model to describe pedestrian-bridge interaction. *Journal of Bridge Engineering*, 23(4), 1–14. [doi.org/10.1061/\(ASCE\)BE.1943-5592.0001204](https://doi.org/10.1061/(ASCE)BE.1943-5592.0001204).

Chapter 3 studies the stride kinematics and quantifies the variability among passing subjects on a beam such as a moving surface under real structural conditions. Overground data for a particular subject is first used as a baseline measurement. Then it is used to compare the same length of walkway data obtained for the same subject on an oscillatory beam. The main findings regarding changes in spatio-temporal gait measures might be implemented to develop high-fidelity models providing a better serviceability prediction of the structural response. The methodology and results presented in this chapter will be submitted with minor changes as:

Gomez, D., Dyke, S. J., & Rietdyk, S. (2019). Spatial-temporal assessment of gait dynamics in walking-induced vibration. (To be submitted to *Engineering Structures*).

Chapter 4 describes the uncertain system modeling concept and develops a structured parametric description of the pedestrian subsystem. The coupled equation governing the dynamics of the system with these uncertainties are provided, and their closed-loop representation is established. The experimental program is described, including the characteristics of the pedestrian test subjects and the structure. Then, simulated structural response envelopes using the uncertain model and measured acceleration data are compared. Finally, the main findings are discussed and potential applications for this model are considered. The methodology and results presented in this chapter has been submitted as:

Gomez, D., Dyke, S. J., & Rietdyk, S. (2019). Structured uncertainty for a pedestrian-structure interaction model. (Submitted for review to *Journal of Sound and Vibration*).

Chapter 5 examines the vibration serviceability limit states of an in-service footbridge. An experimental program is conducted to obtain the dynamic properties of the structure under service conditions, and a model of the footbridge is built for evaluation purposes. Current guidelines are evaluated to assess the pedestrian comfort criteria. Finally, numerical simulations using the uncertain model developed in Chapter 4 are conducted and compared with recorded experimental data. Findings are discussed regarding the serviceability limit state of the footbridge and the comfort criteria established by design codes.

Chapter 6 presents the main findings, conclusions and future lines that have emerged from this research.

It should be mentioned that the organization of this dissertation were initially written as journal papers. Each chapter was adjusted from a written manuscript. The chapters are organized in a sequenced assemblage of those papers. Thus, some level of redundancy in the information during the dissertation is inevitable.

2. A SUBSTRUCTURE-BASED MODEL TO DESCRIBE PEDESTRIAN-STRUCTURE INTERACTION

In this chapter a new PSI model is developed to predict the vertical dynamic response of a footbridge traversed by a single pedestrian. A modular approach is used to represent the pedestrian-structure system as coupled subsystems that interact dynamically with each other. Thus, feedback links that represent the dynamic interaction between the two subsystems as the pedestrian traverses the bridge are directly integrated into the model. This modular approach is based on state space equations, and offers two distinct advantages. First, the bridge can be modeled using standard linear, time-invariant techniques (*e.g.*, a finite element model), and second, this approach permits the inclusion of significantly different levels of damping in each subsystem. With this model, changes in the modal characteristics are included by shifting the location of the pedestrian, and applying the interactive inputs directly into the bridge substructure based on the position of the pedestrian. No external disturbance is applied, although a non-zero velocity is used to model the energy inserted into the system by the pedestrian. Thus, the coupled model framework described herein will support a variety of future investigations of human-induced vibrations in footbridges, and it also facilitates structural analysis conducted for design purposes. To evaluate this framework, the PSI model is created and its performance, in terms of both a pedestrian's vertical acceleration of the body center of mass and the structural response of the bridge, are compared with experimental data. The results demonstrate that the framework can be an efficient tool for the determination of the pedestrian biodynamic parameters, as well as the prediction of bridge response under a single pedestrian.

This chapter is organized as follows. In Section 2.1, the mathematical substructuring approach used to represent the system dynamics is developed. The equations for each subsystem are described, and a discussion of how the inputs and outputs of each substructure interact with each other are provided. In Section 2.2, an experimental study is described and the associated bridge and pedestrian models are constructed. Test subjects with different physical characteristics are considered, and a method is developed to characterize each pedestrian using data obtained while walking on a

rigid floor. Finally in Section 2.2.3, the predicted results of the PSI model are validated against the experimental bridge responses due to a single pedestrian, and are also compared with the results obtained using traditional models in both, time and frequency domain.

2.1 Mathematical formulation

To represent the coupled subsystems, a model is developed that directly incorporates the bi-directional interactions between the bridge and pedestrian at the contact point (*i.e.*, the pedestrian location). This system is partitioned into two dynamic substructures. One substructure is the footbridge, which is modeled here as a finite element (FE) model. The second substructure is the pedestrian, which is modeled as a mass-spring-damper (an oscillator). These two dynamic substructures are coupled, and each will have an influence on the other. Coupling of the two substructures is achieved by computing the response of each system at the interface, (*i.e.*, the contact location at each point in time), and using it as the appropriate input for the other subsystem. This approach results in a time-varying system that considers the responses of each system as inputs to the other system (Gomez, Dyke, & Maghareh, 2015). Furthermore, this framework offers flexibility through the ready use of a well-defined FE footbridge model together with a simple pedestrian biodynamic model.

In this coupled model the interaction effects, and thus the modal characteristics of the combined system, change with the position of the contact location (see Fig. 2.1). By decomposing the PSI system into two substructures, and feeding the inputs from the complementary dynamic system into each substructure, the dynamic interaction is directly included. The contact force generated by the pedestrian is the input to the bridge, and the structure's vertical acceleration is the input to the pedestrian model. The individual substructure equations do not vary, and to model the fully coupled system the contact location must only be modified at each time step. In the following subsections, the PSI model and the formulation of each of the substructures is discussed. Then, the interactions between the bridge and pedestrian are described such that the PSI can be represented as a feedback system.

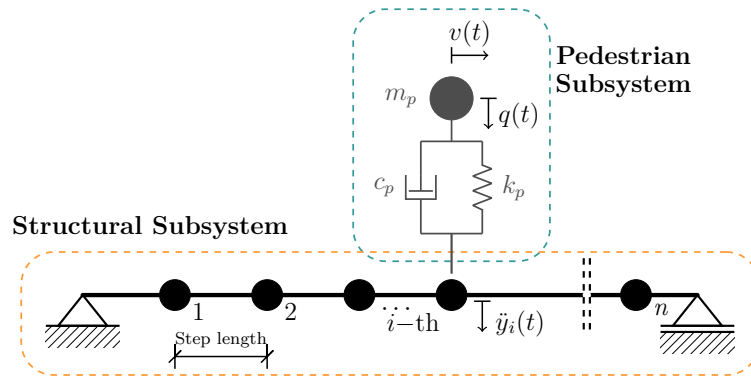


Fig. 2.1.: Model of pedestrian-structure interaction system.

2.1.1 Bridge substructure

A typical FE model of a bridge is shown in Fig. 2.2. The bridge is represented as a linear, time-invariant 2-D or 3-D FE model discretized as a series of beam elements for this particular case. To demonstrate the method, only the n vertical degrees of freedom (DOFs) are considered in the analysis, while the remaining DOFs have been condensed. The number and location of each node are determined by the approximate step length of a pedestrian, and this value should be considered to be an input of the method.

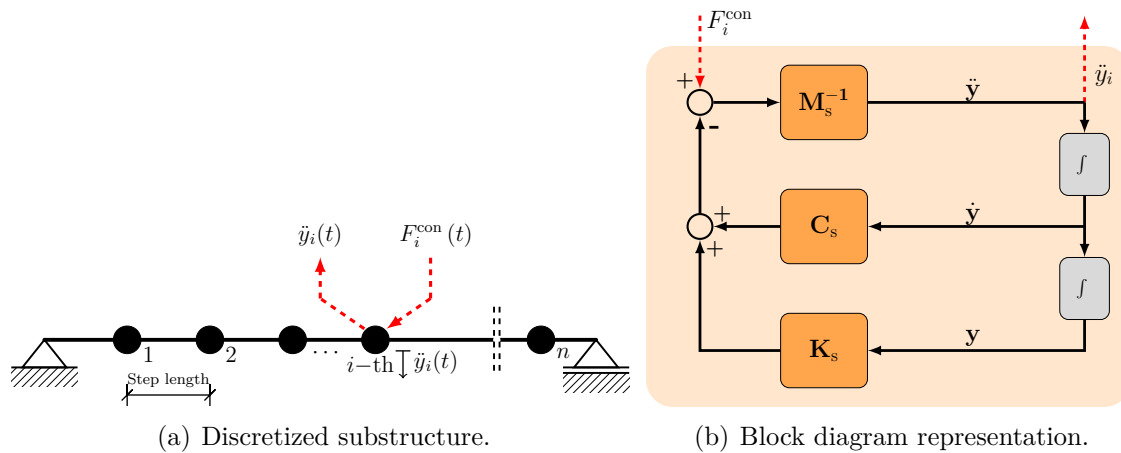


Fig. 2.2.: Structural subsystem dynamic model.

The equation of motion of the general bridge substructure (BS) is represented by

$$\mathbf{M}_s \ddot{\mathbf{y}}(t) + \mathbf{C}_s \dot{\mathbf{y}}(t) + \mathbf{K}_s \mathbf{y}(t) = \mathbf{\Gamma} F_i^{\text{con}}(t) \quad (2.1)$$

$$F_i^{\text{con}}(t) = c_p \dot{q}(t) + k_p q(t) \quad (2.2)$$

$$\mathbf{\Gamma} = \left[0 \quad 0 \quad \dots \quad \underbrace{1}_{i\text{-th}} \quad \dots \quad \underbrace{0}_n \right]^T \quad (2.3)$$

where \mathbf{M}_s , \mathbf{C}_s , and $\mathbf{K}_s \in \mathbb{R}^{n \times n}$ are the mass, damping, and stiffness matrices of the bare structure after condensation. $\mathbf{\Gamma} \in \mathbb{R}^n$ is a column vector which varies with time and is defined by the spatial location of the pedestrian on the bridge. This vector is populated with zero entries except at the DOF corresponding to nodal displacement of the deck where the pedestrian is acting. $F_i^{\text{con}}(t)$ represents the force imparted by the pedestrian on the bridge at the i -th point of contact. Here, $\ddot{\mathbf{y}}(t)$, $\dot{\mathbf{y}}(t)$, and $\mathbf{y}(t) \in \mathbb{R}^n$ are vectors containing the nodal acceleration, velocity and displacement responses, respectively. Note, $\ddot{y}_i(t)$ is the nodal acceleration at the i -th point, which is the point of contact. This output of the bridge subsystem will be used as the input to the pedestrian substructure. As a result, at the i -th iteration step, the only input applied to the bridge substructure is the distribution vector $\mathbf{\Gamma}$ times the contact force $F_i^{\text{con}}(t)$. These feedback links are shown in Fig. 2.2(a). For a graphical relationship between the signals in the bridge substructure, the matrix expression in Eq. ((2.1)) is presented in block diagram form in Fig. 2.2(b).

The equation for the bridge substructure in Eq. ((2.1)) can be written in state space form. The input to this subsystem is represented by the scalar $F_i^{\text{con}}(t)$ described previously. The state variables are assembled in the vector $\mathbf{x}_s = [\mathbf{y}(t) \quad \dot{\mathbf{y}}(t)]^T \in \mathbb{R}^{2n \times 1}$ known as the state vector. The subsystem outputs are selected to include the displacement y , velocity \dot{y} , and acceleration \ddot{y} responses at the nodes of the bridge, represented by the vector $\mathbf{z}_s = [\mathbf{y} \quad \dot{\mathbf{y}} \quad \ddot{\mathbf{y}} \quad \ddot{y}_i]^T \in \mathbb{R}^{(3n+1) \times 1}$. The nodal acceleration \ddot{y}_i is included in the output vector to readily be used as an input to the pedestrian substructure at each iteration. The resulting state space equation is:

$$\begin{bmatrix} \dot{\mathbf{x}}_s \\ \mathbf{z}_s \end{bmatrix} = \begin{bmatrix} \mathbf{A}_{\text{str}} & | & \mathbf{B}_{\text{str}} \\ \mathbf{C}_{\text{str}} & | & \mathbf{D}_{\text{str}} \end{bmatrix} \begin{bmatrix} \mathbf{x}_s \\ F_i^{\text{con}} \end{bmatrix} \quad (2.4)$$

where

$$\begin{aligned}
 \mathbf{A}_{\text{str}} &= \begin{bmatrix} \mathbf{0}_{n \times n} & \mathbf{I}_{n \times n} \\ -\mathbf{M}_s^{-1} \mathbf{K}_s & -\mathbf{M}_s^{-1} \mathbf{C}_s \end{bmatrix}_{2n \times 2n} & \mathbf{B}_{\text{str}} &= \begin{bmatrix} \mathbf{0}_{n \times 1} \\ \mathbf{M}_s^{-1} \mathbf{\Gamma} \end{bmatrix}_{2n \times 1} \\
 \mathbf{C}_{\text{str}} &= \begin{bmatrix} \mathbf{I}_{n \times n} & \mathbf{0}_{n \times n} \\ \mathbf{0}_{n \times n} & \mathbf{I}_{n \times n} \\ -\mathbf{M}_s^{-1} \mathbf{K}_s & -\mathbf{M}_s^{-1} \mathbf{C}_s \\ -\mathbf{\Gamma}^T \mathbf{M}_s^{-1} \mathbf{K}_s & -\mathbf{\Gamma}^T \mathbf{M}_s^{-1} \mathbf{C}_s \end{bmatrix}_{(3n+1) \times 2n} & \mathbf{D}_{\text{str}} &= \begin{bmatrix} \mathbf{0}_{2n \times 1} \\ \mathbf{M}_s^{-1} \mathbf{\Gamma} \\ \mathbf{\Gamma}^T \mathbf{M}_s^{-1} \mathbf{\Gamma} \end{bmatrix}_{(3n+1) \times 1}
 \end{aligned} \tag{2.5}$$

and n , in Eq. ((2.5)), is the number of degrees of freedom of the condensed FE structure model.

2.1.2 Pedestrian substructure

Typically the pedestrian is modeled as a moving force traversing the bridge. At each step, a force profile is imparted on the bridge based on the force a pedestrian imparts on a rigid floor while walking. This method is based on measurements of ground reaction forces (GRF) using fixed force plates, which thus yield the force profile used for each step. However, this procedure does not fully account for the interactions between the pedestrian and the structure. To address this limitation, a dynamic pedestrian substructure model is used here, consisting of a single-DOF (SDOF) oscillator with a non-zero vertical initial velocity condition as a source of excitation rather than using a ground reaction force.

In general, the energy in a human-structure coupled system is not conserved. Energy can be added by the pedestrian, or it can be dissipated by both the pedestrian and the structure itself. Therefore, an external energy source must be provided to simulate how a human adds energy through his/her body. A non-zero vertical initial velocity condition of the pedestrian mass is included here to incorporate the energy exchange that occurs during human gait described by (Winter, 2009) and (Whittle, 2014). With the human gait, two different acceleration-based sources of energy take place during the stride period. The main excitation source to this system is produced when the heel strikes the ground. The second excitation source is related to swinging of the limbs during walking (Yli et al., 2015). By directly incorporating the first source of excitation, the vertical movement of the COM can be reproduced more accurately. In a subsequent section, a comparison is made between the measured

vertical acceleration with the PSI predicted output in a rigid floor, showing that the model is able to add energy to the system.

The pedestrian substructure (PS) is modeled here using the biodynamic characteristics as well as input parameters which have been reported in several studies (Toso et al., 2013; Pfeil et al., 2014; Ortiz & Caicedo, 2019). The biodynamic parameters consist of a lumped mass m_p attached to a linear spring and a viscous linear dashpot with coefficients k_p and c_p , respectively. The additional input parameter is the value of the non-zero initial velocity condition $\dot{q}(t_o)$. An excitation in the PS is initiated, at each iteration, by imparting a vertical initial velocity $\dot{q}(t_o)$ to the pedestrian mass at the time defined as the instant when the heel strikes the ground. This approach is capable of representing the vertical movement of the COM as it generates the transient effects in the bridge response due to the heel strike.

$$m_p\ddot{q}(t) + c_p\dot{q}(t) + k_pq(t) = -m_p\ddot{y}_i(t) \quad (2.6)$$

Eq. (2.6) represents the pedestrian dynamics, where $\ddot{q}(t)$, $\dot{q}(t)$, and $q(t)$ are the vertical acceleration, velocity and displacement of the pedestrian's COM relative to the bridge, respectively. The input to the pedestrian substructure is the vertical acceleration of the bridge $\ddot{y}_i(t)$ at the contact point. The output, which was defined as the input of the complementary system in Eq. (2.2), is the contact force $F_i^{\text{con}}(t)$, applied to the bridge by the pedestrian, as shown in Fig. 2.3(a). The equation of motion is also schematically depicted as a block diagram in Fig. 2.3(b).

The pedestrian subsystem is also written in compact state space form. In this case, the state variables, including the relative displacement and relative velocity, are assembled in the state vector as $\mathbf{x}_p = [q(t) \quad \dot{q}(t)]^T \in \mathbb{R}^2$. The input is represented by $\ddot{y}_i(t)$. The outputs are represented by the vector $\mathbf{z}_p = [q \quad \dot{q} \quad \ddot{q} \quad F_i^{\text{con}}]^T \in \mathbb{R}^4$. The state space form is

$$\begin{bmatrix} \dot{\mathbf{x}}_p \\ \mathbf{z}_p \end{bmatrix} = \begin{bmatrix} \mathbf{A}_{\text{ped}} & | & \mathbf{B}_{\text{ped}} \\ \hline \mathbf{C}_{\text{ped}} & | & \mathbf{D}_{\text{ped}} \end{bmatrix} \begin{bmatrix} \mathbf{x}_p \\ \ddot{y}_i \end{bmatrix} \quad (2.7)$$

where

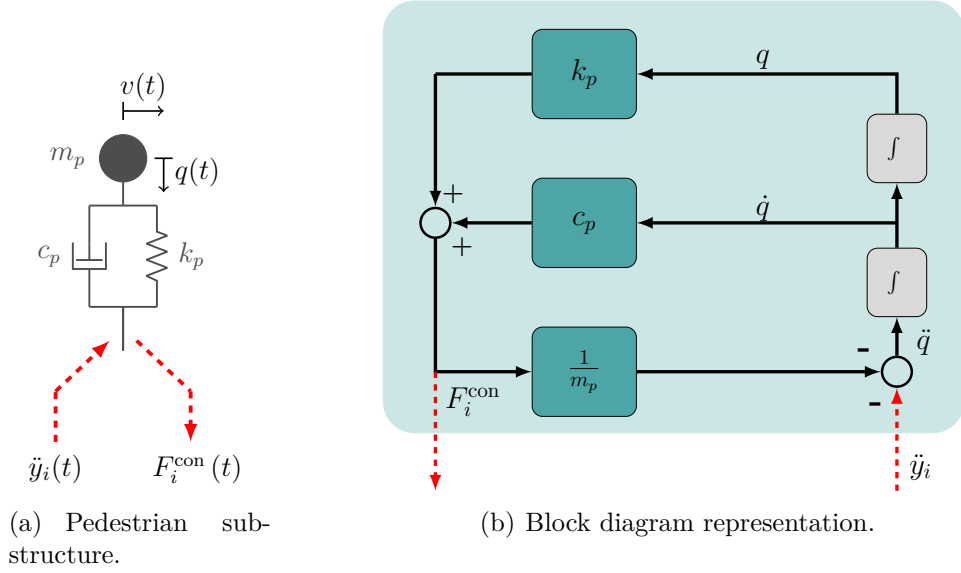


Fig. 2.3.: Pedestrian subsystem dynamic model.

$$\mathbf{A}_{\text{ped}} = \begin{bmatrix} 0 & 1 \\ -\frac{k_p}{m_p} & -\frac{c_p}{m_p} \end{bmatrix}_{2 \times 2} \quad \mathbf{B}_{\text{ped}} = \begin{bmatrix} 0 \\ -1 \end{bmatrix}_{2 \times 1} \quad \mathbf{C}_{\text{ped}} = \begin{bmatrix} 1 & 0 \\ 0 & 1 \\ -\frac{k_p}{m_p} & -\frac{c_p}{m_p} \\ k_p & c_p \end{bmatrix}_{4 \times 2} \quad \mathbf{D}_{\text{ped}} = \begin{bmatrix} 0 \\ 0 \\ -1 \\ 0 \end{bmatrix}_{4 \times 1} \quad (2.8)$$

In this study, it is assumed that the pedestrian walks at a constant velocity, which is included in the biodynamic model using the step length and pacing frequency. Furthermore, the model assumes continuous contact between the pedestrian and structure, and does not distinguish between the single and double phase portions of the stance. Therefore, the possibility of separation of the pedestrian from the bridge is not considered, and the position of the pedestrian defines the contact point at each instant in time. This model could readily be extended in the future to consider a running or jumping human, or to consider variable walking speeds, as needed.

2.1.3 Pedestrian-bridge interaction model

Next, consider the interactions between the pedestrian and bridge substructures that must be included to establish the PSI feedback system. The dynamic response of the beam is affected not only by the position of the moving mass, but also by the vertical motion of the pedestrian. Thus, during the passage of a pedestrian walking across the bridge, the pedestrian excites the bridge through the contact force at the contact point, while the bridge only excites the pedestrian by its own movement at this same contact point. With this closed-loop approach, the dynamic interaction is directly integrated into the model.

The solution to these equations is obtained with a procedure that has the advantage of being simple, accurate, and explicit, yielding a global response of the coupled system. When these subsystems are solved together, this coupled and time-varying model is able to capture the interactions between the human and the structure as the position of the pedestrian on the bridge changes. In other words, the linear time-invariant pedestrian and bridge subsystems are coupled and use a time-dependent contact point, as shown in Fig. 2.4. Thus, this closed-loop system can be classified as a linear, time-varying dynamic system. This interactive response can be obtained for any discretized bridge and any pedestrian activity, making this pedestrian-structure model a flexible tool.

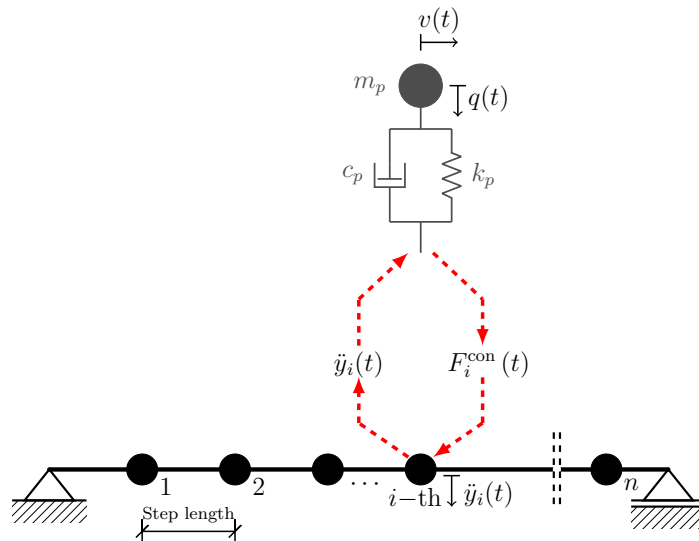


Fig. 2.4.: Pedestrian-structure interaction model.

To solve for the response of this system, the equations of motion are solved numerically for the time period $S_t = 1/F_p$ within each pedestrian step (the average step time taken by the pedestrian). Then, to simulate the response during the next step length, the final conditions of the system at the end of that step length are used as the initial conditions for the next step length. To begin, set the time to $t_k = 0$, the pedestrian first step as $i = 1$, and the initial conditions (ICs). Select a time increment Δt for the numerical integration. Typically the integration time step is chosen to correspond to a frequency that is at least 10 times the frequency of the highest mode of the bridge model. The steps in the iterative procedure are summarized in the flowchart shown in Fig. 2.5.

2.2 Experimental verification

To verify the PBI model, a series of experiments were conducted to measure typical structural responses induced by a single walking pedestrian. The experimental specimen that serves as the bridge was selected based on its suitability for walking safely, its large size, and its dynamic properties. Three test subjects having different body characteristics were considered as pedestrians, and measurements were taken under various walking conditions. The objective here is to provide a realistic testbed that would exhibit significant, but representative, dynamic interactions that will be useful for assessment and verification of the model. Thus, vertical motion of the footbridge was perceptible in all tests. Comparisons are made between the measured vertical responses of this experimental specimen and the PBI model predictions. Additionally, the study considers the moving force model and moving oscillator model to assess of the capabilities and limitations of all three classes of models.

2.2.1 Experimental setup and parameter identification

A simply-supported beam, representative of a typical girder from a full-scale bridge deck, is used as the bridge. Based on the dynamic properties of this beam, it is relatively sensitive to pedestrian-induced excitation with a pedestrian walking at a typical pace. The structure is a $W_{30 \times 132}$ steel beam A992 ($F_y = 345$ MPa and $E = 200$ GPa) and each end rests on a concrete block. The entire beam has a length of 15.24 m and a weight of 29.4 kN. For these experiments, the unsupported distance between the two end supports is 14.64 m (see Fig. 2.6).

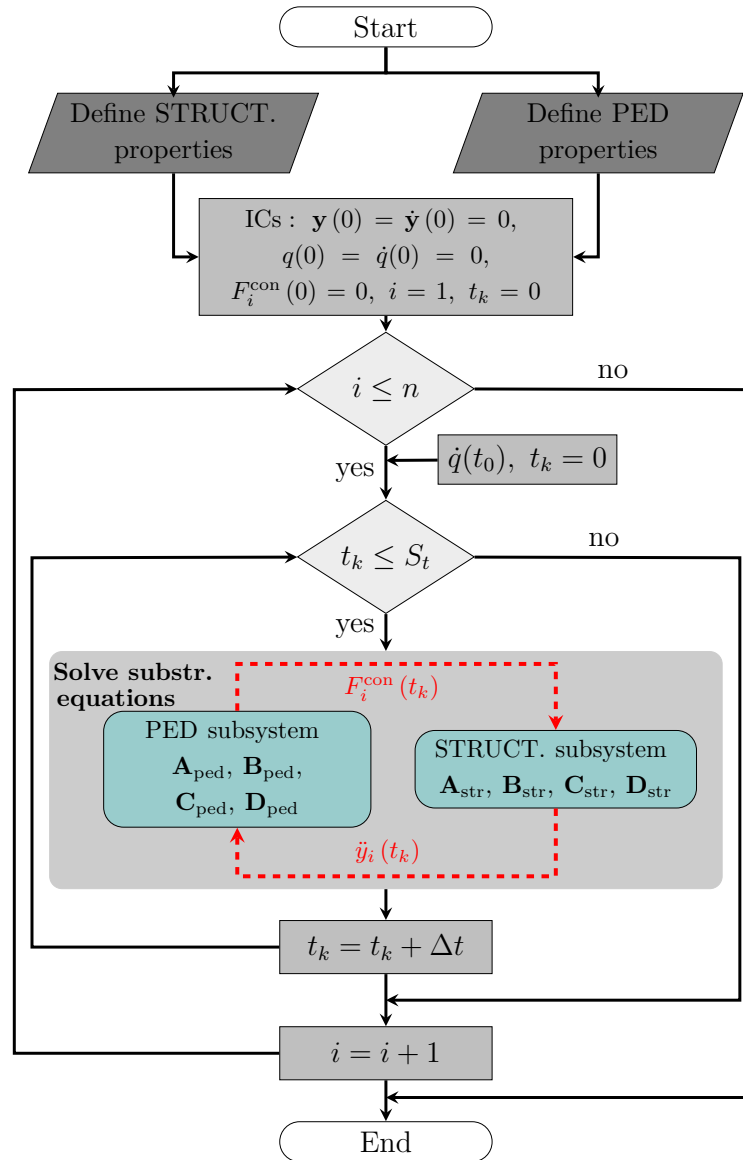


Fig. 2.5.: Flowchart of the solution procedure.

Eighteen uniaxial accelerometers are used in the experimental setup to capture the vibrations of the beam, with twelve in the vertical direction and six in the lateral (perpendicular to the long axis of the beam) direction as depicted in Fig. 2.7. The accelerometers are PCB Piezotronics piezoelectric sensors model 333B40 with a sensitivity of $(\pm 10\%) 500 \text{ mV} \cdot \text{g}^{-1}$ and a frequency range from 0.5 to 3 kHz.

To identify the dynamic properties of the bridge alone in this configuration, forced vibration testing is first conducted. The bridge is excited using an electrodynamic shaker placed at 1.2 m from the midspan, with the objective of capturing structural

Fig. 2.7) are shown in Fig. 2.8. Based on the experimental data, the modal characteristics of the bridge are identified. A common curve fitting method is applied to the experimental complex frequency response function to identify the system as a ratio of polynomials in the Laplace variable s (Dyke et al., 1996). The first three vertical modes are at 2.15 Hz, 8.31 Hz and 18.12 Hz. Thus, noticeable interactions would be expected due to human-induced vibration because the first vertical natural frequency of this bridge is within the normal range of the human gait (*i.e.*, 1.6-2.4 Hz) (Bachmann et al., 1995; Sétra, 2006). The first two torsional modes are at 5.77 Hz and 15.25 Hz. Also, a single lateral mode is present at 10.75 Hz. These were obtained using an analyzed frequency range from 0.5 to 20 Hz. Also, the damping ratios associated with the first three vertical modes are identified to be 0.28%, 0.48% and 0.31%, respectively.

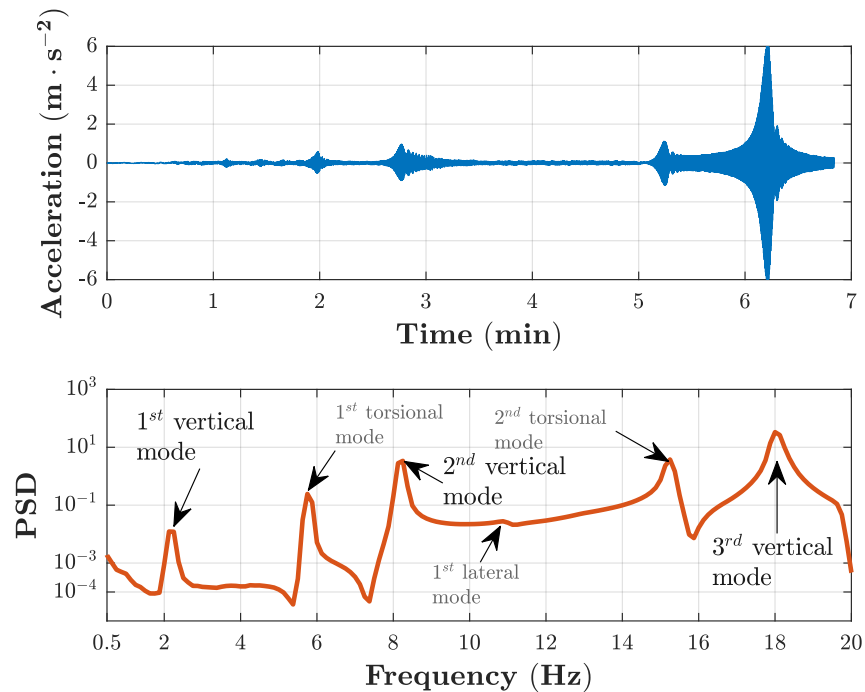


Fig. 2.8.: Structural subsystem acceleration measured response: (a) time history; (b) power spectral density (PSD).

A two-dimensional FE model is developed based on the physical properties of the bridge. Torsional and lateral modes are neglected here as their effects are assumed to be insignificant for this analysis. The 2-D model is then updated using the measured modal characteristics. To build the FE model, a simply-supported,

homogeneous Euler-Bernoulli beam is discretized into $n + 1$ beam elements. The n lumped masses are located at regular distances according to the average step length of a pedestrian, and only the vertical and rotational degrees-of-freedom (DOF) are considered. Proportional damping is assumed to generate a damping matrix for the bridge substructure. The rotational DOF are condensed, yielding a bridge model with n DOF. In the condensed model the \mathbf{M}_B , \mathbf{C}_B , and \mathbf{K}_B matrices in Eq. (2.1) are thus defined, forming the bridge substructure described in Eq. (2.4).

2.2.2 Pedestrian parameters

Three healthy subjects, (SA, SB, and SC), with no history of postural problems, participated in a series of experiments. The applicable ethics committee approved this study, and all human subjects signed informed consent forms prior to participation. Two types of tests were conducted. In the first type of test, each subject was instructed to walk according to his/her self-selected pace. In the second type of test, a metronome was used to guide the walking pace frequency, denoted here as F_p . When the metronome was used, several pacing rates were used ranging from slow to fast (1.7, 1.8, 1.9, 2.0, 2.1, and 2.2 Hz). For each subject, the tests were first conducted on a rigid floor, and then on the flexible bridge. These tests were useful for model comparisons, as well as for parameter estimation.

The pedestrian motion was captured using a portable and non-invasive, triaxial accelerometer (STMicroelectronics k330 3-axis accelerometer). The accelerometer has a range of ± 2 g and a resolution of $61 \mu\text{g}$. The data were sampled at 100 Hz, and an elliptical low-pass filter with cut-frequency at 50 Hz was used. This device was placed close to the subject's COM with a belt around the waist. The device was affixed to the subject firmly above the sacrum along the spine to record trunk acceleration in the vertical direction.

To identify the parameters of the biodynamic model of the pedestrian, the experimental vertical accelerations, obtained with the pedestrian walking on a rigid floor, were used. The PSI model was used to simulate the COM vertical accelerations, with the bridge substructure stiffness set to a high value to minimize any dynamic interactions. Using this simulation model, the biodynamic parameters c_p and k_p as well as $\dot{q}(t_o)$ were identified through a standard constrained optimization in MATLAB[®] that minimizes the error between the experimental vertical COM acceleration and the simulated vertical acceleration of the pedestrian mass during around 20 sec. The param-

eter m_p is the known mass of the pedestrian. The pedestrian substructure parameters obtained for each test subject are given in Table 2.1. Mass ratios indicated in this table are calculated as a ratio of the mass of each subject divided by the modal mass of the first mode of the bridge alone, which is approximately 1500 kg. Note that all of these values are well within the normal range found in the literature (Archbold et al., 2011; Shahabpoor et al., 2013).

Table 2.1.: Bio-dynamic parameters obtained on a rigid floor.

	\mathbf{m}_p [kg]	\mathbf{c}_p [kg · s ⁻¹]	\mathbf{k}_p [N · m ⁻¹]	$\dot{\mathbf{q}}(\mathbf{t}_o)$ [m · s ⁻¹]	Mass ratio [%]
SA	56	212.5	14000	0.30	3.73
SB	97	501.4	20000	0.38	6.47
SC	72	273.2	18000	0.22	4.80

A typical time-history of the measured acceleration (solid line) and simulated acceleration (dashed line) of the human subject and the corresponding floor acceleration (dash-dotted line) are shown in Fig. 2.9. Here the subject SA was instructed to walk at $F_p = 1.9$ Hz using a metronome. And as an input to the model, an initial velocity, as stated previously, was used here to emulate the effect when the heel strikes the floor in each step, as shown with the dash-dotted line in Fig. 2.9. Clearly, the PSI model is able to capture the fundamental behavior of the vertical COM acceleration on a stationary surface without the use of an external force.

2.2.3 Experimental verification of the PSI model

The next step is the verification of the PSI model, in terms of its ability to capture the human-structure dynamic interactions. To do this two independently identified models with the established parameters that best model the pedestrian subsystem and the structural subsystem are used. A dynamic simulation is performed to obtain the response of the feedback system described in Eqs. (2.4) and (2.7) using a single pedestrian. The identified biodynamic parameters shown in Table 2.1 are used. Additionally, the moving force (MF) and moving oscillator (MO) models are considered to assess the relative capabilities and limitations of the modeling methods when interaction is present.

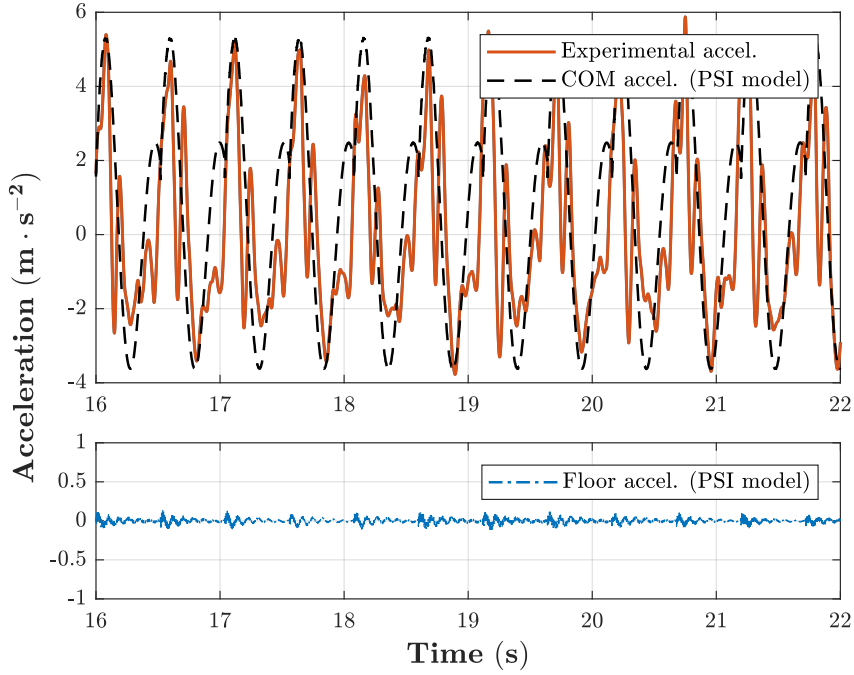


Fig. 2.9.: COM acceleration in a rigid floor (subject SA).

For all simulations, the identified model of the beam is used. The MO model described in (Fanning et al., 2005; Dang & Živanović, 2013) uses a secondary dynamic system based on a lumped mass connected by a spring and damper with the bridge, to represent a pedestrian. For purposes of comparison, this model also utilizes the biodynamic characteristics of the pedestrian given in Table 2.1. Alternatively, the MF model uses a moving force determined based on the weight of the pedestrian. Both of these models also include a periodic function that has been shown to represent the vertical force applied by a walker (Bachmann et al., 1995). This function is expressed as a Fourier series multiplied by the mode shape to obtain the effective modal force, as in

$$F_v(t) = \alpha W \cdot \sin(2\pi F_p t - \varphi) \cdot \phi(ct) \quad (2.9)$$

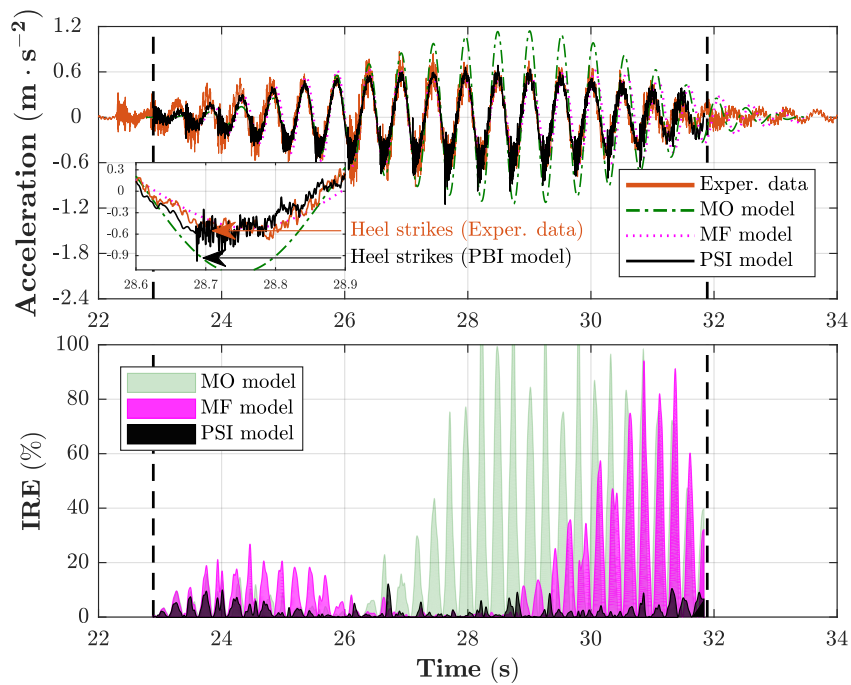
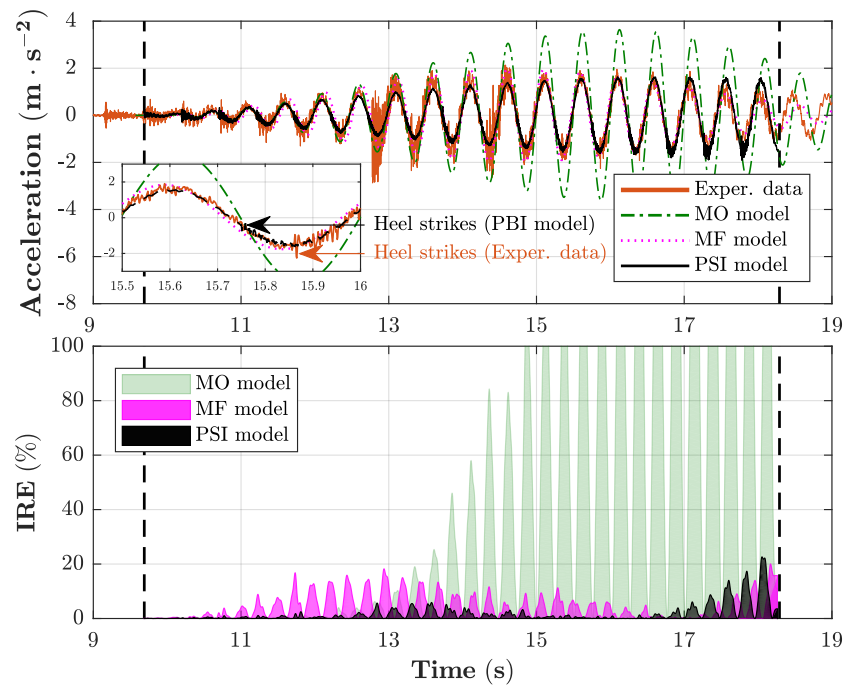
From Eq. ((2.9)), the single-step forcing function $F_v(t)$ is represented by an amplitude corresponding to the weight of the pedestrian W , and a dynamic function, which includes the harmonic components of the pedestrian load. However, this periodic function may be limited and resolved, for practical reasons, only for the first

harmonic vertical component (Sétra, 2006). Thus, α and φ are the Fourier coefficient and phase lag of the first harmonic, respectively. The pace frequency is defined by F_p , c is the constant anterior-posterior velocity of the pedestrian, $\phi(\cdot)$ is the normalized fundamental mode shape of the bridge, and t is the variable representing the time that has elapsed. The values of the first harmonic amplitude and phase lag have been chosen in this study as 0.4 and 0, respectively. Also, W , F_p , and c are defined for each individual test based on the experimental data.

To quantitatively evaluate the models, the vertical experimental acceleration at the midspan of the footbridge is compared with the corresponding predictions from each of the models. The response is compared using an instantaneous relative error (IRE) and a normalized root mean square error (NRMSE). The difference between the simulated response $\ddot{Y}_{sim}(t_m)$, and the measured response $\ddot{Y}_{exp}(t_m)$, is computed at each time sample t_m , and appropriately normalized and compared. The IRE is a measure of the instantaneous normalized error, and is computed at each individual time step across the N samples of the time history. The NRMSE is a measure of the overall response, and is computed using the complete response history. The IRE and NRMSE are calculated using Eqs. (2.10) and (2.11).

$$\text{IRE}(t_m) = \frac{|\ddot{Y}_{exp}(t_m) - \ddot{Y}_{sim}(t_m)|}{|\ddot{Y}_{exp}(t_m)|} \times 100\% \quad (2.10)$$

$$\text{NRMSE} = \frac{\sqrt{\frac{1}{N} \sum_{m=1}^N [\ddot{Y}_{exp}(t_m) - \ddot{Y}_{sim}(t_m)]^2}}{\max(|\ddot{Y}_{exp}(t_m)|)} \times 100\% \quad (2.11)$$

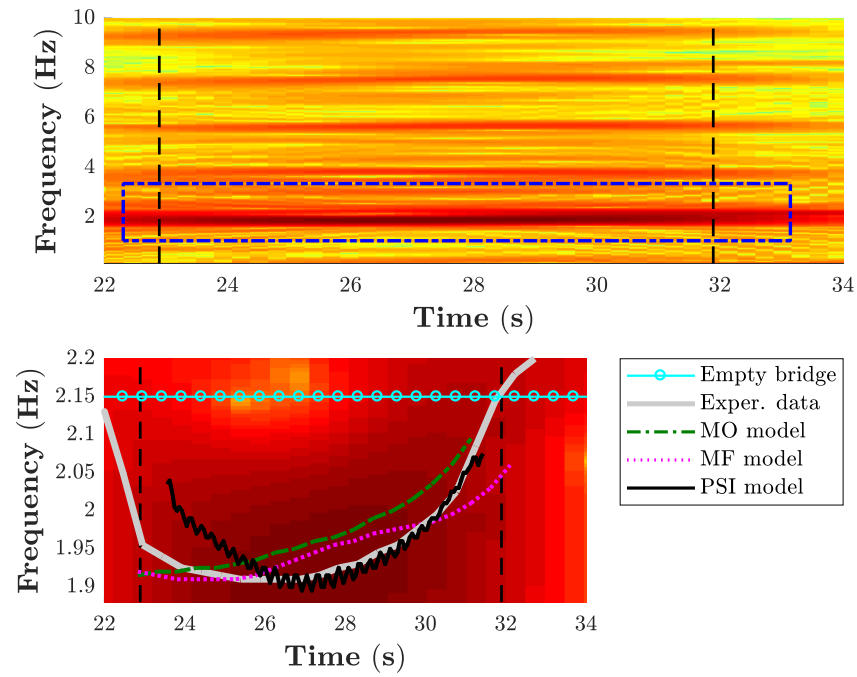
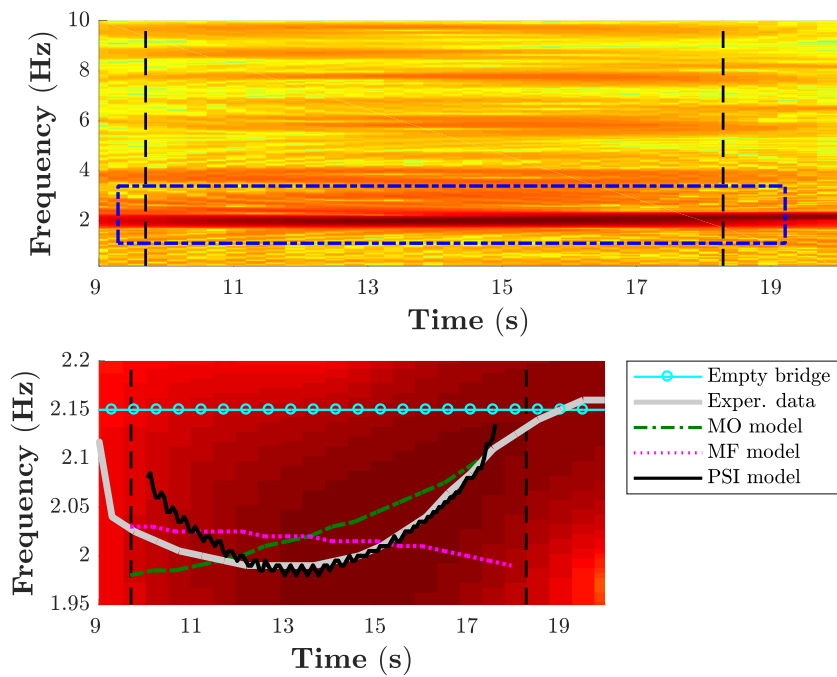
(a) Following the metronome at $F_p = 1.9$ Hz.

(b) Self-selected pace frequency.

Fig. 2.10.: Measured and predicted vertical acceleration responses and IRE comparison at midspan of the bridge for a single pedestrian.

A total of 81 tests were conducted with the three subjects. 57 of these were recorded while a metronome guided the pace of the pedestrian's steps, and in the remaining 24 tests the pedestrian walked at a self-selected pace. Two representative time-histories, for two different test subjects, are shown in Fig. 2.10. Here the measured and simulated responses are shown, along with the corresponding value of the IRE for each individual time sample. The response of the bridge (solid line) remains zero before the pedestrian enters, gradually builds up during the pedestrian's passage, and attenuates in free vibration after the pedestrian has left the bridge. In Fig. 2.10(a) subject SA was instructed to walk at $F_p = 1.9$ Hz following the beat of a metronome. However, in Fig. 2.10(b) subject SC was instructed to walk at a self-selected rate and his average pace frequency was 1.98 Hz. The dashed vertical lines in Figs. 2.10 and 2.11 indicate the times at which the pedestrian enters and leaves the bridge.

The results for these two cases demonstrate that the PSI model (dashed line) reproduces the transient effects observed due to the heel-strike for each footfall in the same manner that the data exhibits this behavior for a walking person. To assess the performance of the PSI model, IRE values *vs.* time are shown in Fig. 2.10. The instantaneous relative error measure is significantly smaller with the PSI model as compared to the values obtained with the MF (dash-dotted line) and MO (dotted line) models in those representative trials. Because this system is time-varying, a time-frequency representation of the responses is adopted to investigate the non-stationary characteristics using spectrograms. The experimental and simulated response data for each model are provided (see Fig. 2.11). Fig. 2.11 shows the time-frequency analysis of the measured data only, for clarity. Obvious horizontal stripes exist in each figure around 2, 4, 6, 8 and 10 Hz due to the dominant harmonics resulting from the pace frequency associated with the pedestrian walking on the bridge. Clearly the amplitude of the structural response increases significantly in the frequency range between 1.7 and 2.3 Hz because this dominant first harmonic is close to the first vertical natural frequency of the bridge ($F_1 = 2.15$ Hz).

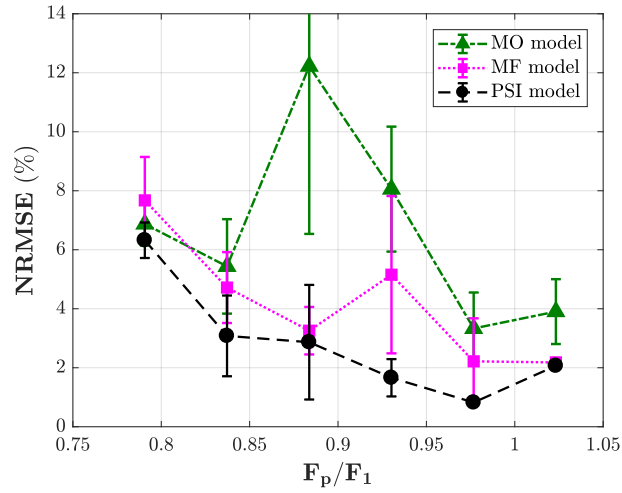
(a) Following the metronome at $F_p = 1.9$ Hz.

(b) Self-selected pace frequency.

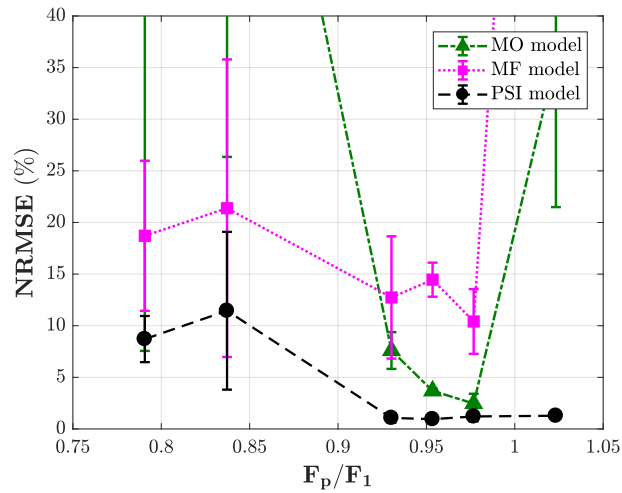
Fig. 2.11.: Time-frequency representation of the measured responses of the bridge to single pedestrian. Zoom-in plot of a frequency range from the spectrogram including measured and predicted vertical acceleration variation responses.

The frequency variations that occur with the various models (MF, MO, and PSI models), as compared to the frequency variations present in the measured responses are also examined. Fig. 2.11 shows a zoomed-in plot over a limited frequency range extracted from the spectrogram. Here one can observe the variations in the power spectral density when a pedestrian crosses the bridge. The horizontal dotted line represents the fundamental frequency of the empty bridge, where it is not affected by the presence of the pedestrian. The solid line indicates the frequency associated with the maximum value of the power spectral density at each point in time. In both cases, when the subject walks at a specified pace of 1.9 Hz (see Fig. 2.11(a)) or at a self-selected rate with an estimated average pace frequency of 1.98 Hz (see Fig. 2.11(b)), there is a significant variation in the frequency content of the experimental response with time. This variation can be attributed to a combination of: (1) the mass distribution due to the pedestrian's location; and (2) the forced response in the pedestrian-bridge system due to the quasi-periodic loading at pace frequency F_p and its harmonics. Additionally, the corresponding lines that are provided for the MF and MO models indicate that in this case these models do not account for the significant dynamic interaction effects. The variations in the accuracy of the predicted responses of the coupled-system are more pronounced when the pace frequency is closer to the vertical natural frequency of the structure. Better agreement is observed with the PSI model in those representative trials.

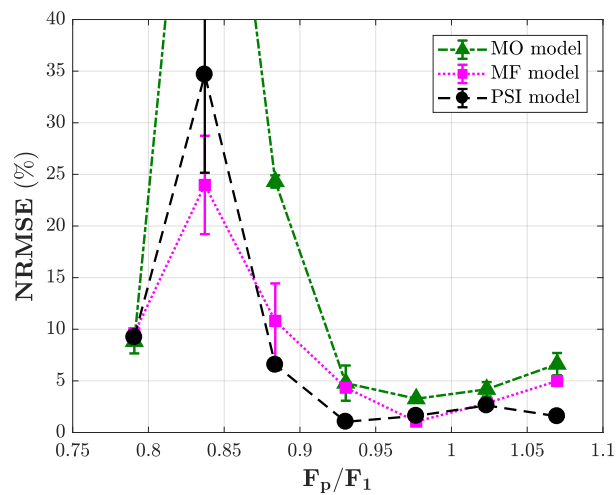
The NRMSE obtained with each model was used to obtain a single value for each of the 57 metronome-based experimental trials, and these results are summarized in Figs. 2.12(a-c). Because several repetitions were performed for each of the tests, the mean value and standard deviation of the NRMSE values are computed for each test configuration. These values are shown for each of the corresponding pace frequencies considered, where the pace frequencies are normalized against the first vertical natural frequency of the structure F_1 . The NRMSE values associated with the responses of the MF and MO models are typically larger than those of the PSI model. Moreover, the MF and MO models produce particularly large NRMSE values when the frequency ratio F_p/F_1 are in the range between 0.7 to 0.9. Here, the dynamic interaction is low and the behavior is dominated by the forced response of the structure. Furthermore, both the MF and MO models overestimate the system response when the F_p/F_1 is close to unity (*i.e.*, 0.9 to 1.05).



(a) Subject SA.



(b) Subject SB.



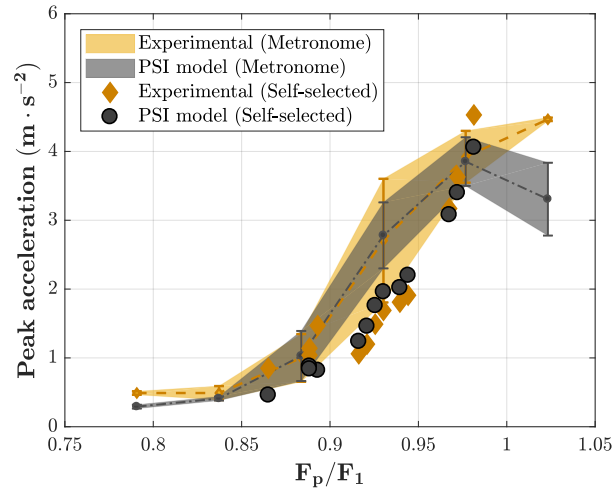
(c) Subject SC.

Fig. 2.12.: Mean and standard deviation values of the NRMSE for test subjects.

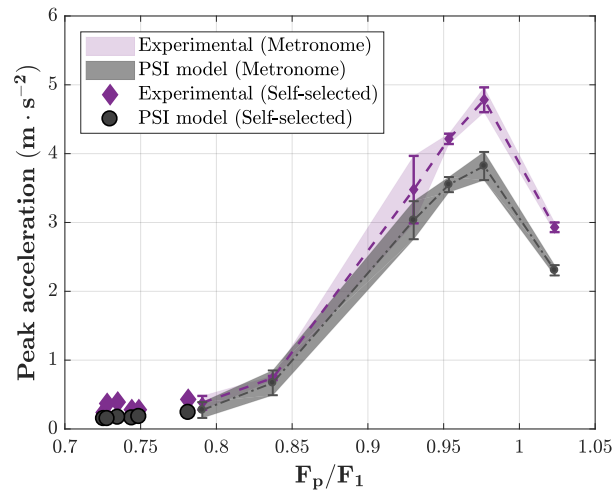
This result means that MF and MO have limited capacity to take into account the interaction between the two subsystems. However, the PSI model exhibits significantly smaller normalized errors because the model accounts for the influence of the bridge on pedestrian on the dynamics.

The responses are examined from an alternate perspective in Figs. 2.13(a-c). These figures show the range of variation of the peak estimated acceleration of the responses versus the normalized pace frequency. The upper and lower bounds provided are defined by the mean and standard deviation of the maximum absolute values of the response. Both the experimental and PSI prediction results are given for each frequency ratio of interest in the tests using the metronome. Here the mean of the peak values of the simulated responses have nearly the same amplitude as the peaks of the measured responses. And as expected, more dynamic interaction occurs between the two subsystems when the frequency ratio is close to one. Additionally, 24 experiments were conducted at a self-selected pace frequency. These responses were analyzed and the corresponding peak responses are represented with diamonds in Figs. 2.13(a-c).

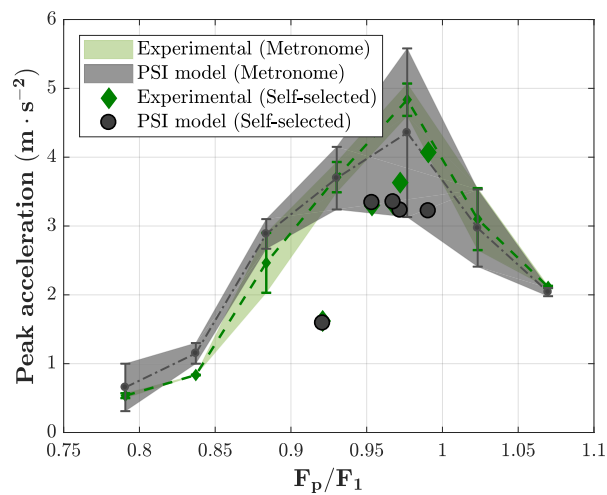
It can be concluded that the PSI model yields an accurate prediction of the peak acceleration of the pedestrian-bridge system as indicated by the discrete circles, even when the pedestrian walks naturally. Indeed for SB, a pedestrian that walked at a slower speed than in the metronome, the responses are typically in agreement with the experimental data. Clearly the PSI model is able to capture the dominant coupled dynamics of the pedestrian-structure system.



(a) Subject SA.



(b) Subject SB.



(c) Subject SC.

Fig. 2.13.: Peak acceleration for test subjects.

2.3 Summary

In this chapter a pedestrian-structure interaction model has been presented herein for predicting the dynamic response of a structure traversed by a single pedestrian. The predicted acceleration responses with the PSI, the MF, and the MO models were compared with real acceleration data. Different gait speeds were considered while a single human subject traversed a previously identified steel beam that served as a bridge. Three different human subjects participated. The PSI model was found to be better at predicting the variations in the natural frequency of the coupled system, as well as the peak responses of the coupled system. The PSI model is thus effective for predicting the structural response when dynamic interactions are present.

3. SPATIAL-TEMPORAL ASSESSMENT OF GAIT DYNAMICS IN WALKING-INDUCED VIBRATION

Pedestrian structures regularly exhibit excessive vibrations when they are dynamically excited by human activities. Although several pedestrian models have been proposed to capture the influence that humans have on such structures, current representations simplify the human effect, potentially compromising the structure's serviceability. Thus, better walking-induced load models have to be developed to allow structural designers to deal appropriately with realistic pedestrian-structure coupled effects. Current modeling approaches neglect, due to the lack of suitable data, the temporal and spatial kinematic changes when pedestrians are walking on a moving surface such as a slab, footbridge, or stair.

Even though several studies have successfully looked at characterizing the variability of the human gait, most of these were conducted overground for medical and biomechanical purposes. This study provides a more complete spatial and temporal analysis of the human gait parameters when the pedestrian is influenced under vertical vibrating conditions. The results show a pedestrian's tendency to adapt one's gait to the oscillating conditions of the structure, providing a better understanding of the pedestrian intra-subject gait changes on a lively surface. These findings will enable structural engineers to incorporate gait changes in realistic pedestrian models in the analysis and design of structures.

The goal of this chapter is to quantify the spatio-temporal gait measures when subjects walking on a beam such as a moving surface (MS) under real conditions. Overground (OG) data is used as a baseline measurement to compare the same length of walkway data obtained for the same subject on an oscillatory beam. Two gait modes, at self-selected pace and following a metronome, are examined and their effects in the structural response are also explored. The main findings regarding changes in spatio-temporal gait measures and how gait is adapted might be implemented to develop high-fidelity pedestrian-induced load models providing a better serviceability prediction of the structural response.

3.1 Introduction

Numerous studies have been conducted to examine gait variability and functional mobility during locomotion (Grieve & Gear, 1966; Yamasaki et al., 1991; Maki, 1997; Hausdorff et al., 2001; McAndrew Young & Dingwell, 2012; Collins & Kuo, 2013; Svoboda et al., 2017; Cahill-Rowley & Rose, 2017; Begue et al., 2018). The approach used to control stride variation during travel on altered, overground, compliant, uphill, and downhill surfaces has received much attention over the last four decades across many fields. The variability in the subject's kinematic parameters are regarded as an essential measure of motor skills, and its analysis provides an assessment of the gait performance and even health (Sekiya et al., 1997; Zijlstra, 2004; Bailey et al., 2017).

Although these experimental programs were conducted with subjects walking under different conditions, all of them were conducted on rigid surface. These procedures do not fully account for the interaction between the pedestrian and an oscillating surface. Therefore, how the movement of a pedestrian structure, especially in the vertical direction, influences the human gait has not been fully studied. Despite this and to the best of author's knowledge, the only experimental study to address this limitation was conducted by Dang & Živanović (2016), which was intended to quantify the human locomotion under low-frequency vertical vibration and their effects in the stride characteristics on three test subjects. In the experimental program a stationary pedestrian walked on a treadmill that was placed at the midspan of a bridge. They found that vertical vibration levels lead to a marginal increase in the pacing rate of 8%, and a slight decrease in the step length of 8%. However, they suggested that the minimal differences are only circumstantial and should be further investigated. The fact that a fixed speed provided by the treadmill might influence the gait behavior (Dingwell et al., 2001; Jordan et al., 2007; García-Diéguez & Zapico-Valle, 2017; Choi et al., 2017), shows that there are still considerable uncertainties regarding human locomotion under vertical excitation that need to be researched in a more natural environment.

3.2 Description of the experimental program

3.2.1 Participants

Six subjects (four males) are enrolled in the study (see Table 3.1). No participants have any disease or disorder that impacted their gait, as verified by self-report. All

participants signed an informed consent approved by the Institutional Review Board of Purdue University. The subjects walked both OG and on the MS. Two gait modes are examined: (1) prescribed cadence, where the participant walked at a frequency (F_m) set by a metronome, and (2) self-selected speed. Each pass on the beam or on the floor is considered a trial. Ten trials at a self-selected speed and seven trials at a prescribed cadence were completed, where the prescribed metronome’s frequency was selected between 1.7 and 2.3 Hz (in increments of 0.1 Hz) in each trial. The metronome was set at a specific frequency and seven trials were conducted at this frequency. Later the frequency was adjusted randomly at a different value to conduct seven test at a new frequency. This procedure was applied to avoid psychological bias and anticipation in the subject’s gait movement. A total of 708 trials were collected and analyzed in this experimental program. All test subjects participated in both experiments walking OG and on the MS the same length, for a fair comparison.

Table 3.1.: Test subject parameters.

Subject	Age (years)	Mass (kg)	Height (m)	Gender
S-1	31	55	1.67	Female
S-2	29	87	1.65	Male
S-3	39	89	1.81	Male
S-4	38	77	1.69	Male
S-5	34	109	1.76	Male
S-6	29	49	1.53	Female

3.2.2 Equipment

A wearable device, which uses the video and inertial sensors of a smartphone records subject gait data of each step (SmartGaitTM, (A. Kim et al., 2015)). Step length (SL), step width (SW), step time (ST), and gait speed (GS) are recorded on both, overground and on the moving surface. To capture foot movements, reflective markers are attached to the top of each shoe centered over the proximal phalanges. The smartphone is attached to the trunk with a belt. SmartGaitTM has modest to excellent agreement with a pressure-sensing walkway, with an average absolute error of 6% or less of standard (A. Kim et al., 2015). SL is the distance between two steps

in the anterior-posterior direction at double support phase. SW is the medial-lateral distance between the foot markers at the same time. ST is the temporal difference between two consecutive steps. Pace frequency (PF) is the inverse of ST with units of Hz. Finally, GS is estimated by the SmartGaitTM on-board software as

$$GS = SL \cdot PF \quad (3.1)$$

with units of ($\text{m} \cdot \text{s}^{-1}$).

3.2.3 Instrumented structure

The test structure that serves as a vibrating surface is selected for its dynamic characteristics, and it exhibits significant vertical vibration where, in extreme cases, the acceleration reaches 1 g. The simple-support beam and a subject wearing the SmartGaitTM are shown in Fig. 3.1. The structure is a $W_{30 \times 132}$ steel beam A992 ($F_y = 345$ MPa and $E = 200$ GPa) that is simply supported on top of two concrete blocks, one at each end (see Fig. 3.1(c)). Cross section of the steel beam is depicted in Fig. 3.1(c). The length of the beam is 15.24 m with an unsupported distance between the two concrete blocks of 14.6 m. Two 3 m elevated wood platforms are installed as starting and ending surfaces to allow subjects to reach steady-state walking conditions before entering the beam. The entire structure weighs 29.4 kN. Twenty-two vertical accelerometers are used to measure the structural responses, with locations schematically depicted in Fig. 3.1(c). An additional accelerometer (No. 19 not included in Fig. 3.1(c)) is used as a trigger to indicate the time stamps at which the subject enters and leaves the beam. The installed accelerometers are piezoelectric sensors model 333B40 with a sensitivity of ($\pm 10\%$) $500 \text{ mV} \cdot \text{g}^{-1}$ and a frequency range from 0.5 to 3 kHz (PCBPiezotronics, Depew, New York).

A series of forced vibration tests are conducted to measure the response of the bare structure. For characterization testing performed in advance of pedestrian tests, the structure is excited using an electrodynamic shaker located 1.82 m from the midspan with a 1.8 kg moving mass in vertical direction. The shaker is fixed in the vertical direction on the structure (referenced with a square in Fig. 3.1(c)) with an accelerometer on the base (accelerometer No. 7) and another accelerometer on the moving mass (accelerometer No. 22). In each test, the shaker is driven with an input that is either a linear or logarithmic swept-sine signal with a frequency range of 0.4 to 22 Hz spanning 480 s. The high-fidelity data acquisition system sampled all 22

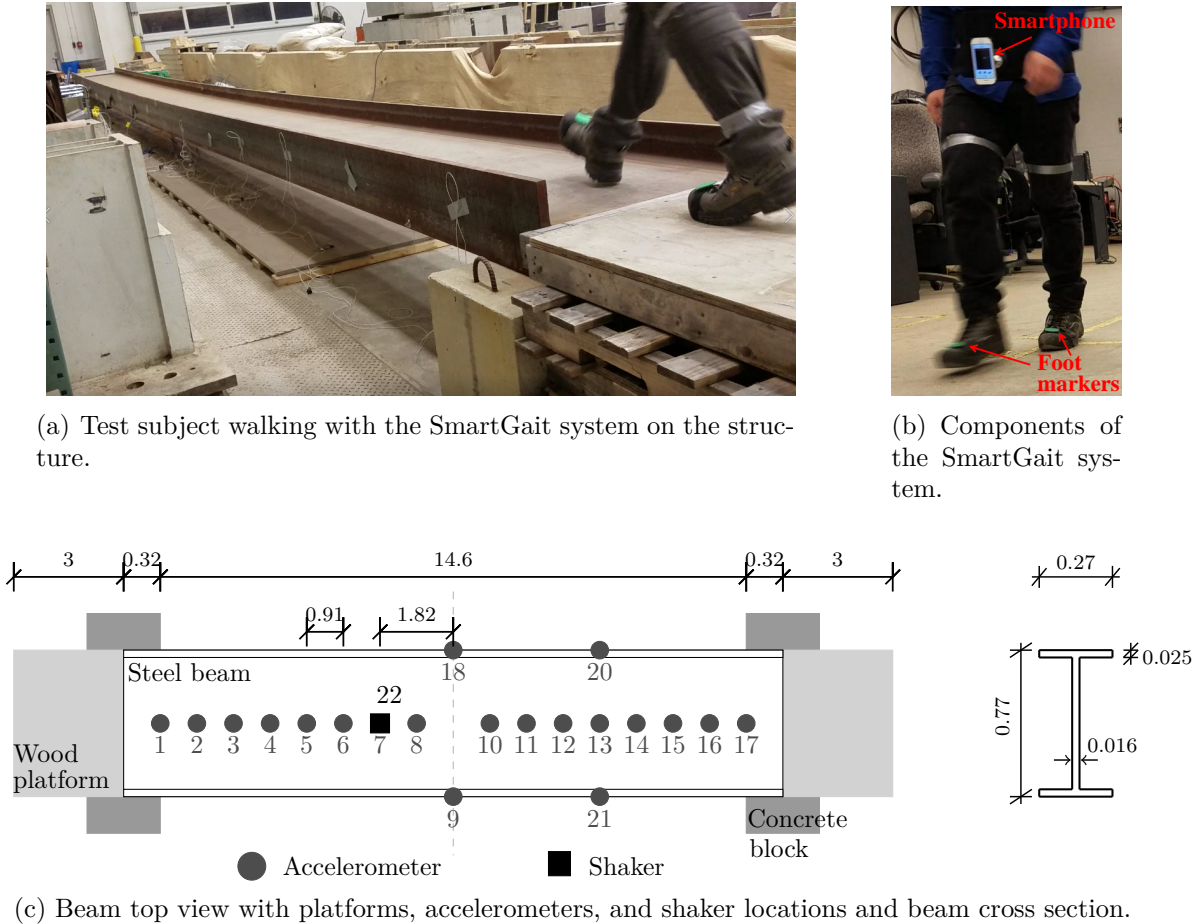


Fig. 3.1.: SmartGait™ system and test structure.

channels at 1024 Hz with excitation signal amplitudes ranging from 1 to 5 V. The 22 accelerometers recorded only vertical acceleration responses.

Modal analysis is performed to identify the dynamic properties of the test structure. Based on the experimental input/output signal relations, transfer functions of the dynamic system are calculated and plotted as magnitude and phase. Then, a ratio of two polynomials in the Laplace variable s is fit to the experimental frequency response functions (Dyke et al., 1996). Specifically, the transfer functions from the relative acceleration of the moving mass to each of the measured responses are estimated. A representative Bode plot for the experimentally determined transfer function from the relative acceleration of the moving mass to the response at accelerometer No. 20 is shown in Fig. 3.2. The first three vertical modes are identified at 2.08 Hz, 8.06 Hz, and 18.18 Hz with associated damping ratios of 0.07%, 0.13%,

and 0.07%, respectively. Two torsional modes are identified at 5.69 Hz and 15.06 Hz. Additionally, a single lateral mode is later obtained at 10.47 Hz with a horizontal arrangement of accelerometers that are not included in Fig. 3.1(c).

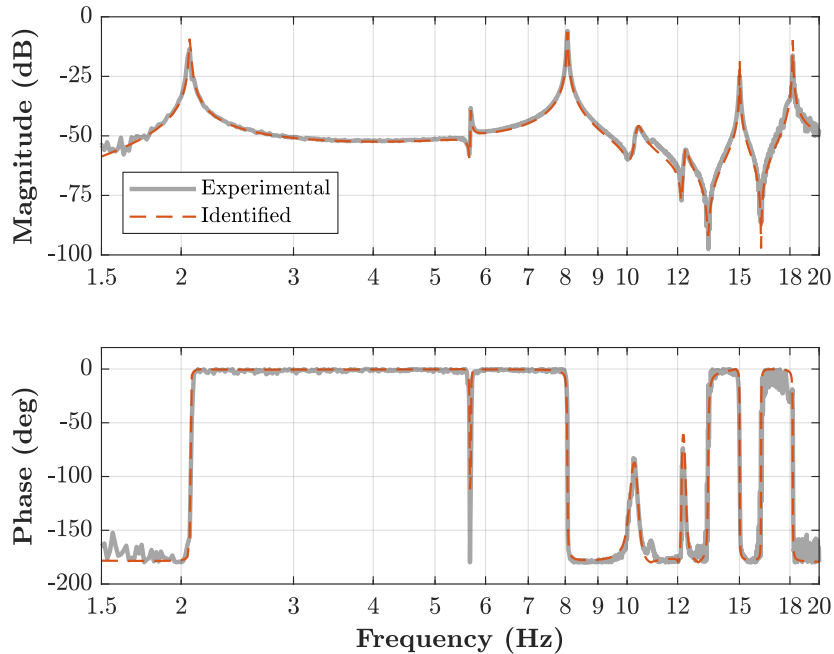


Fig. 3.2.: Experimental and identified transfer functions.

The SmartGait data are processed to obtain the SL, SW, PF, and GS (Fig. 3.3(a-d)). The corresponding data for the same pedestrian position on both surfaces are determined in each recorded data to compare the measurements across the trials. As a location reference, two vertical dashed lines are used in the figures to indicate when the pedestrian is on the beam and its counterpart on the floor. The same step positions are identified in each trial to directly compare these measurements within walking location for the same subject. For each test, the average value between the right and left foot for each step is obtained to represent each particular test as a line (see Appendix A for a detail representation of the gait variability for each pedestrian). Box-and-whisker plots of each pedestrian’s kinematic parameter are used here to represent the variability of the data. On each box, the central line indicates the median, and the box indicates the upper and lower quartiles (25th and 75th percentiles). The whiskers represent the distribution of the individual results

extended to the most extreme data points not considered outliers, and the outliers are plotted individually using the + symbol.

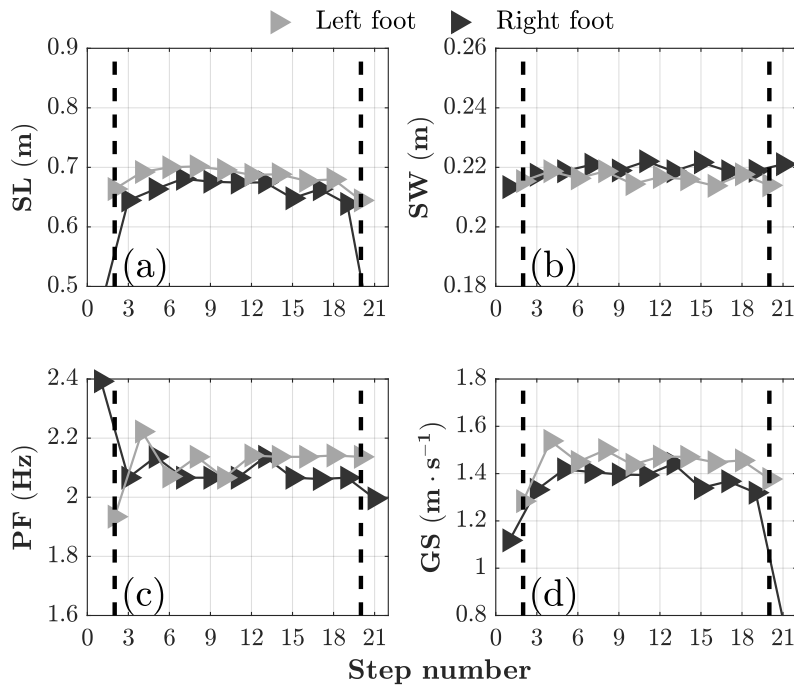


Fig. 3.3.: Typical data results obtained using the SmartGaitTM system shown the spatial-temporal gait representation measured in a trial. (a) Step length; (b) Step width; (c) Pace frequency; (d) Gait speed; (Note: the two vertical dashed lines indicate when the pedestrian enters and leaves the established walkway either on the beam or on the ground).

The percent change (PC) is calculated to report the differences between (OG_{median}) and (MS_{median}) quantities for the same subject. The PC is a measure of the instantaneous difference and is computed when pedestrian is in the middle of both on the beam and on the ground. If the result is positive it means that a kinematic quantity increases, and if the result is negative, that quantity decreases. PC is defined as

$$PC = \frac{MS_{\text{median}} - OG_{\text{median}}}{OG_{\text{median}}} \times 100\%. \quad (3.2)$$

3.3 Comparison of the gait kinematics on stationary and moving surfaces for a walking subject using a metronome

In this section, the variability in the gait dynamics is compared on both MS and OG surfaces when the test subject walked using a metronome. Pedestrian kinematic parameters are presented for four selected metronome's frequencies in the middle of the walkway (Fig. 3.4).

3.3.1 Step length and step width

Under MS conditions, at $F_m=1.7$ and 2.3 Hz the PC of the SL slightly increases from 6% to 9% for four of six subjects (Fig. 3.5). At $F_m=2.0$ and 2.1 Hz, SL increases until 17% for all the individuals (Fig. 3.5) probably to keep a comfortable SL on the vibrating surface with an increasing vertical deck acceleration, as shown later in Fig. 3.8. With regard to SW, it is difficult to draw a conclusion due to apparent differences in the subjects' results.

3.3.2 Pace frequency and gait speed

At $F_m=1.7$ and 2.3 Hz, the PF has PC values between $\pm 2\%$ (Fig. 3.5). However, at $F_m=2.0$ and 2.1 Hz the results show that is difficult for the pedestrian to follow the beat and keep the PF constant due to the deck's movement ranging the PC between $\pm 6\%$ for high vertical accelerations from 4 to 6 $\text{m}\cdot\text{s}^{-2}$ (Fig. 3.8). The GS increases up to PC=16% during the walking tests on the structure at $F_m=1.7$ and 2.3 Hz for four of six subjects. At $F_m=2.0$ and 2.1 Hz, GS also increases for four of six subjects until 17%.

3.4 Comparison of the gait kinematics on stationary and moving surfaces for a walking subject at self-selected pace

In this series of tests, each subject walked at his/her self-selected pace OG and on an MS. The gait parameter comparison at both surfaces are shown in Fig. 3.6.

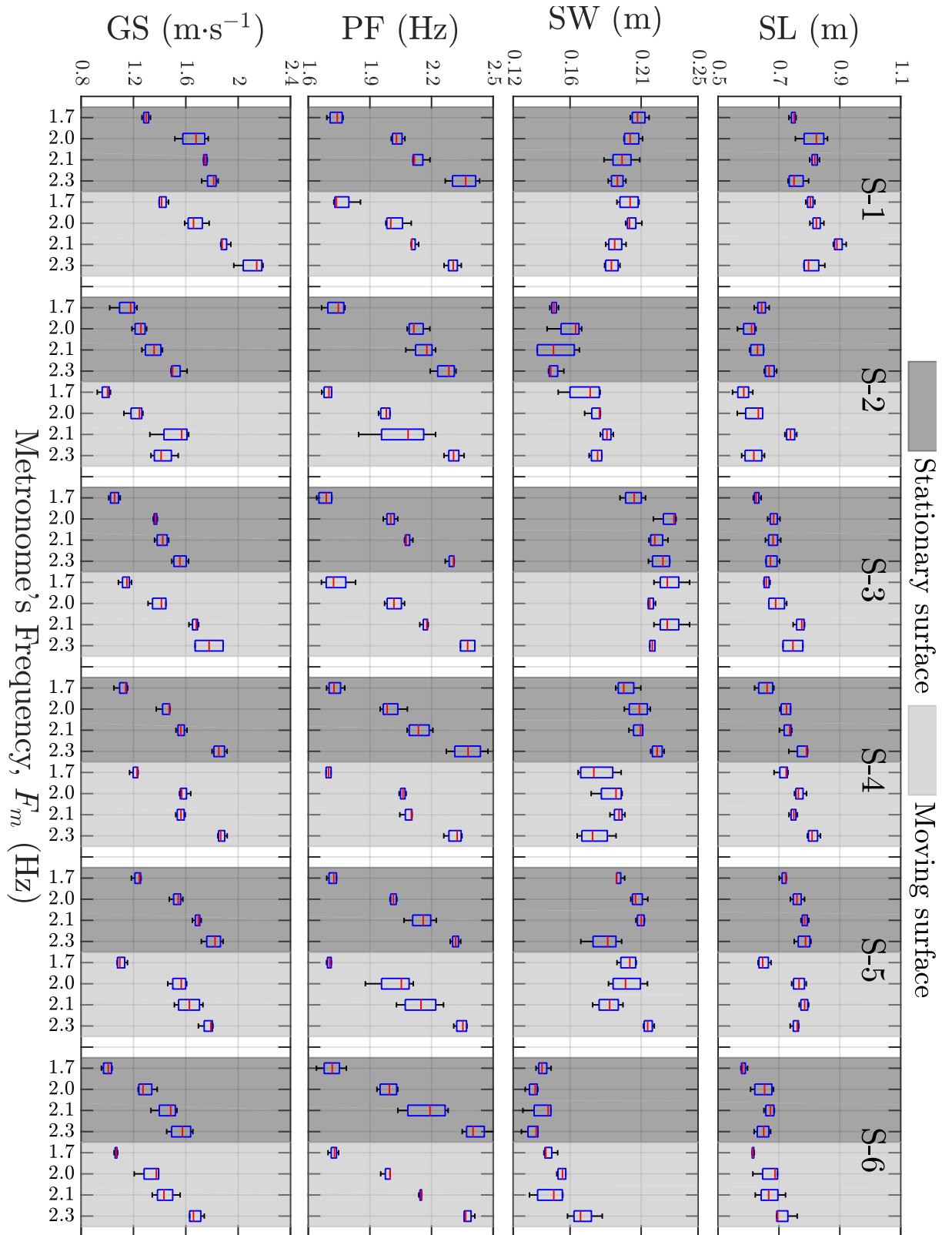


Fig. 3.4.: Comparison for pedestrian kinematic parameters using a metronome's beat. Each row depicts a kinematic parameter while each column represents a test subject both on the stationary and on the moving surface.

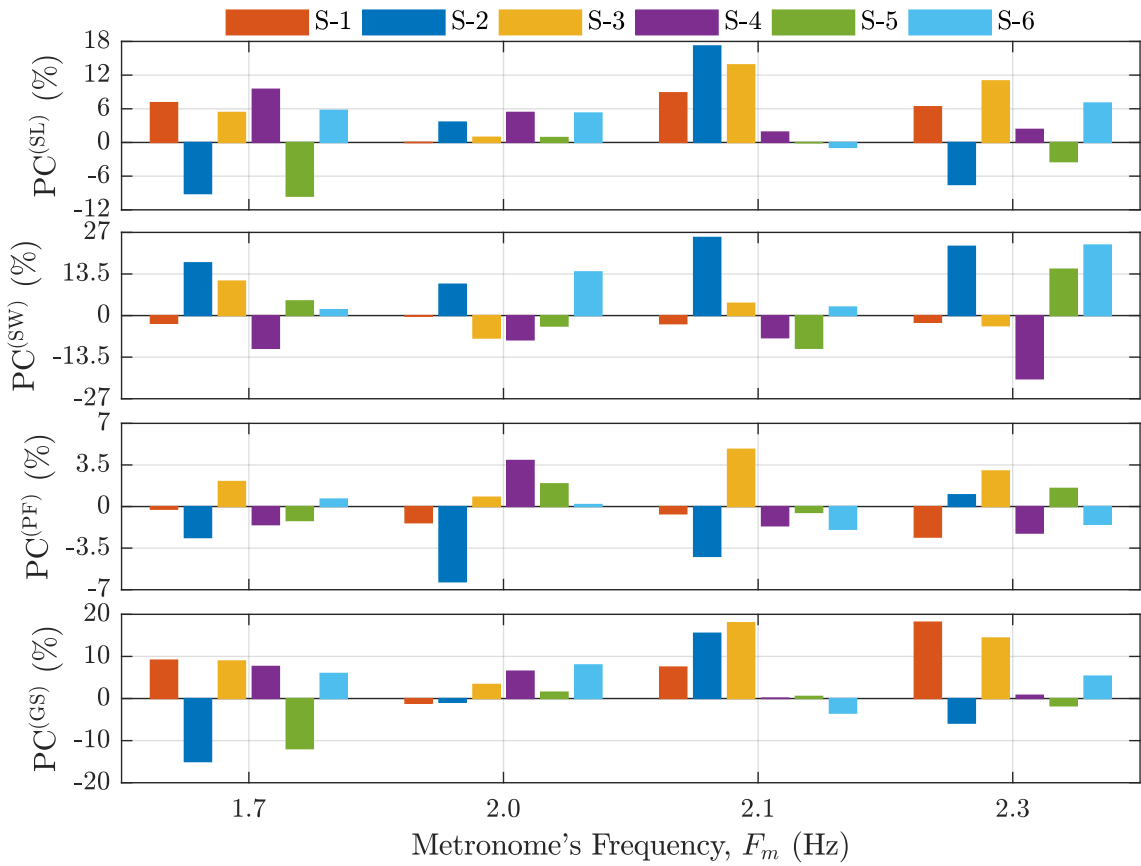


Fig. 3.5.: Percent change (PC) for pedestrian kinematic parameters vs. metronome's frequency. Each row depicts a kinematic parameters while each column represents a prescribed frequency. (Note: horizontal line at 0% indicates when the percentage increases and decreases).

3.4.1 Step length and step width

When subjects walked at a preferred PF on the beam, the SL are kept similar in both surfaces for five of six subjects (see Fig 3.7). The results show that walkers tried to preserve their SL even with significant vibration amplitudes as shown in Fig. 3.8. However, the SW increased for five subjects with a broad range from 8 to 38% (see Fig. 3.7). It seemed that in each trial when the structural vibration increased, their SW also tended to increase probably to improve the balance when vertical movement of the surface is noticeable.

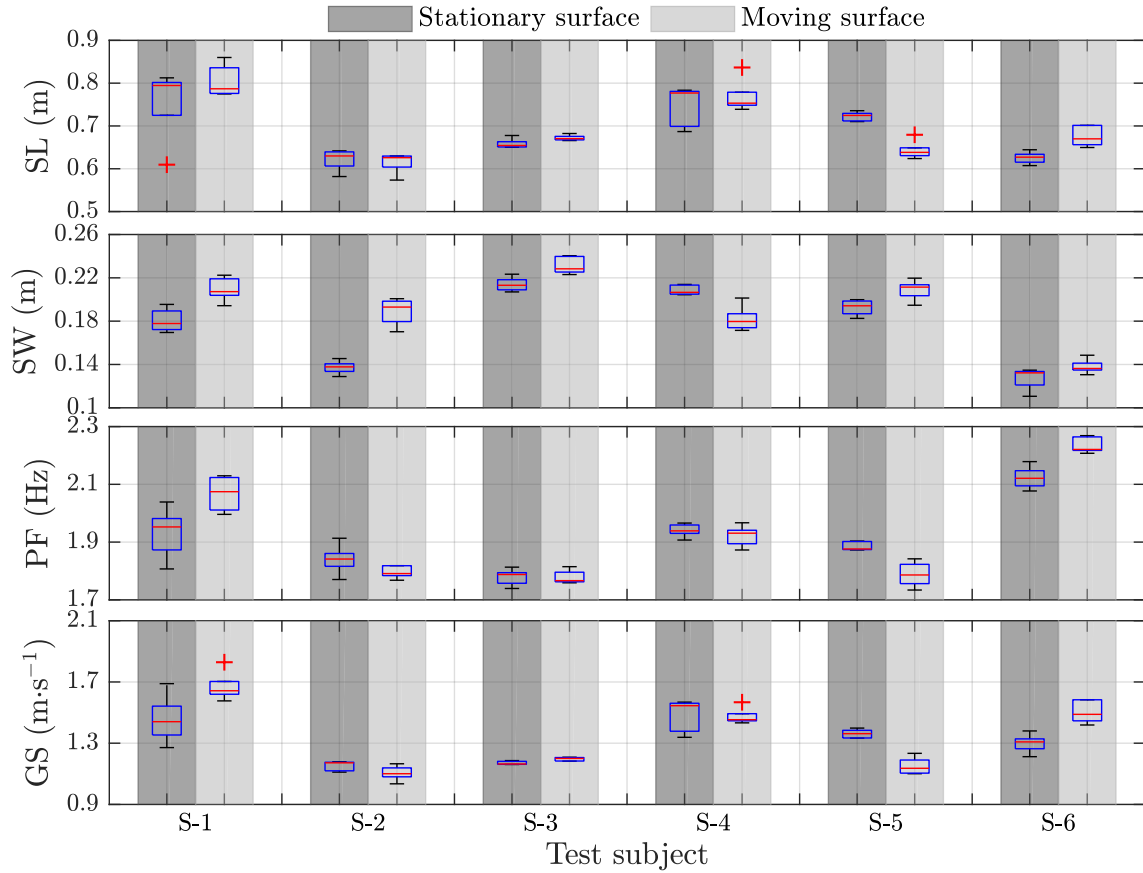


Fig. 3.6.: Comparison for pedestrian kinematic parameters at self-selected pace. Each row depicts a kinematic parameters while each column represents a test subject both on the stationary and on the moving surface.

3.4.2 Pace frequency and gait speed

Subjects S-2, S-3, S-4, and S-5 slightly decreased their PF parameter keeping them around PC=-6% as shown in Fig. 3.7. In contrast, subjects S-1 and S-6 increase their PF to 7.5% and 5%, respectively. However, there is one case that is of special interest. When subject S-1 walked on the beam near the dominant frequency of the combined pedestrian-structure system, he/she shifted his/her PF in phase with the structure's oscillation and kept it close to PF=2.08 Hz most of the trials. This synchronization could generate a deck's vertical impulse on the subject at the same time that he/she increased the dynamic load when the heel struck the structure in a positive feedback loop. This effect may explain the obtained peak acceleration values (until $6.5 \text{ m}\cdot\text{s}^{-2}$) with a body mass of 55 kg (see the black circles in Fig. 3.8). The PC of the GS

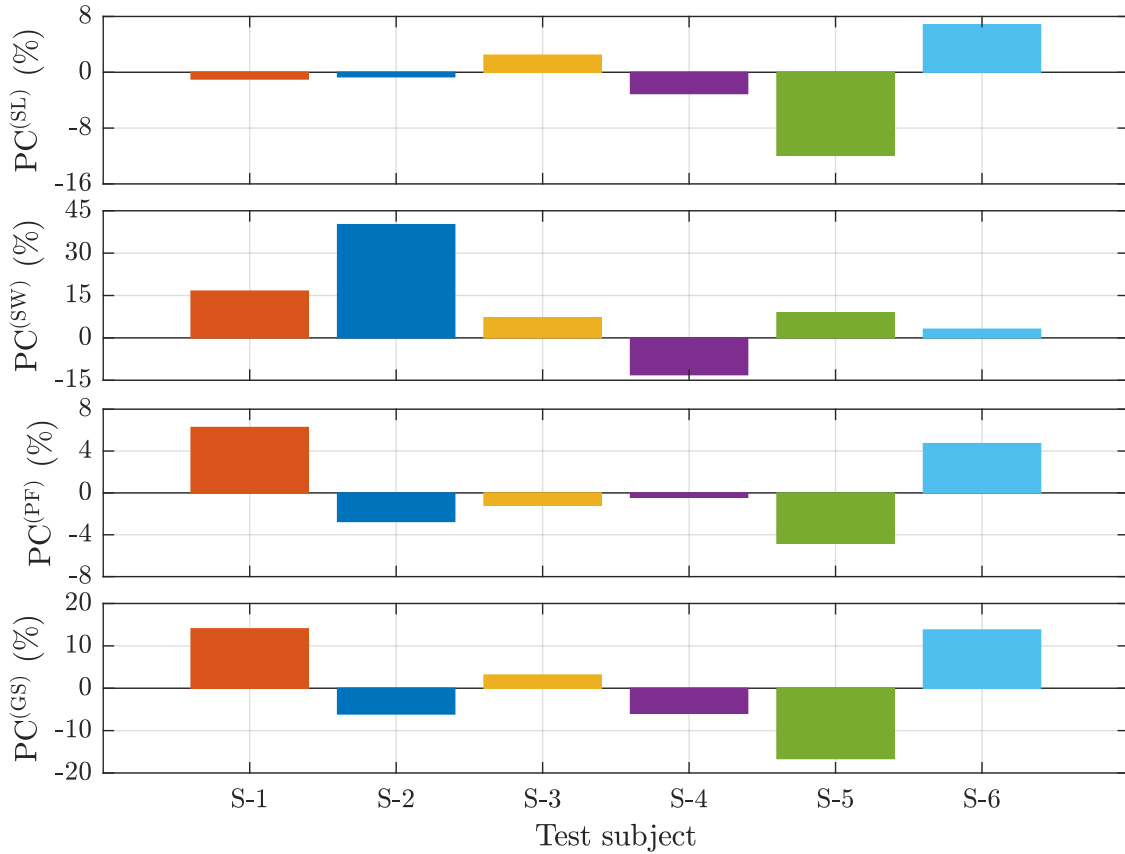


Fig. 3.7.: Percent change (PC) for pedestrian kinematic parameters at self-selected pace. Each row depicts a kinematic parameters while each column represents a test subject. (Note: horizontal line at 0% indicates when the percentage increases and decreases).

parameter for subject S-1, S-3, and S-6 increase until $PC=14\%$. Subjects S-2, S-4, and S-5 decrease their PC from -6% to -18% .

A summary of the variations on gait characteristics based on the experimental results are indicated in Table 3.2.

3.5 Influence of the vibration level in the gait dynamics

In this section, the influence of the vibration level in the gait dynamics is evaluated. Fig. 3.8 shows the peak vertical response of the beam in terms of accelerations produced by each single walker. The filled circles depict the peak acceleration in the middle of the structure with its corresponding frequency for each pedestrian during

Table 3.2.: Obtained ranges for each gait parameter.

Gait parameter	Metronome's beat		Self-selected
	F_m (Hz)	PC (%)	PC (%)
SL	1.7 & 2.3	[-9 to 11]	[-12 to 8]
	2.0 & 2.1	[-2 to 18]	
SW	1.7 & 2.3	[-17 to 17]	[-15 to 40]
	2.0 & 2.1	[-13 to 28]	
PF	1.7 & 2.3	[-2.5 to 2.5]	[-6 to 7]
	2.0 & 2.1	[-6 to 5]	
GS	1.7 & 2.3	[-15 to 18]	[-18 to 13]
	2.0 & 2.1	[-4 to 19]	

metronomic walking. The black circles represent the peak acceleration response when a pedestrian walked at self-selected pace. The results reveal that resonance occurs at a frequency lower than the natural frequency on the empty bridge. This variation can be attributed to the pedestrian mass, stiffness, and damping that behaves as an attached dynamic oscillator and modified the dynamic properties of the bare structure (Gomez et al., 2018). The gray volume in Fig. 3.8 is obtained by estimating the change in the frequency of the pedestrian-structure system by adding the maximum lumped mass for the tested subjects ($m = 109$ kg) in the middle of the beam. The peak responses for each pedestrian following the beat laid in the gray volume, however their magnitude varied for each trial until 30% revealing the intrinsic lack of consistency (intra-subject variability) in human locomotion and their effect when interact with a structure.

In Fig. 3.9 the mass of each test subject is plotted against the maximum value of the structural acceleration response in the midspan. Four different metronome's frequencies are selected in the analysis. $F_m=1.7$ and 2.3 Hz are plotted because they are the lowest and highest prescribed cadence frequency values, respectively. $F_m=2.0$ and 2.1 Hz are also selected due to their proximity to the beam's first vertical frequency of vibration ($f_1 = 2.08$ Hz), where dynamic amplification in the pedestrian-structure system's response is expected. Fig. 3.9 shows that when the metronome's frequency was set to 1.7 and 2.3 Hz, the peak acceleration values are not influenced by the pedestrian mass. However, when F_m was set to 2.0 and 2.1 Hz, the dynamic response increases when the mass increases for most of the pedestrians. Clearly, the structural response is also highly influenced by the biodynamic damping and stiffness,

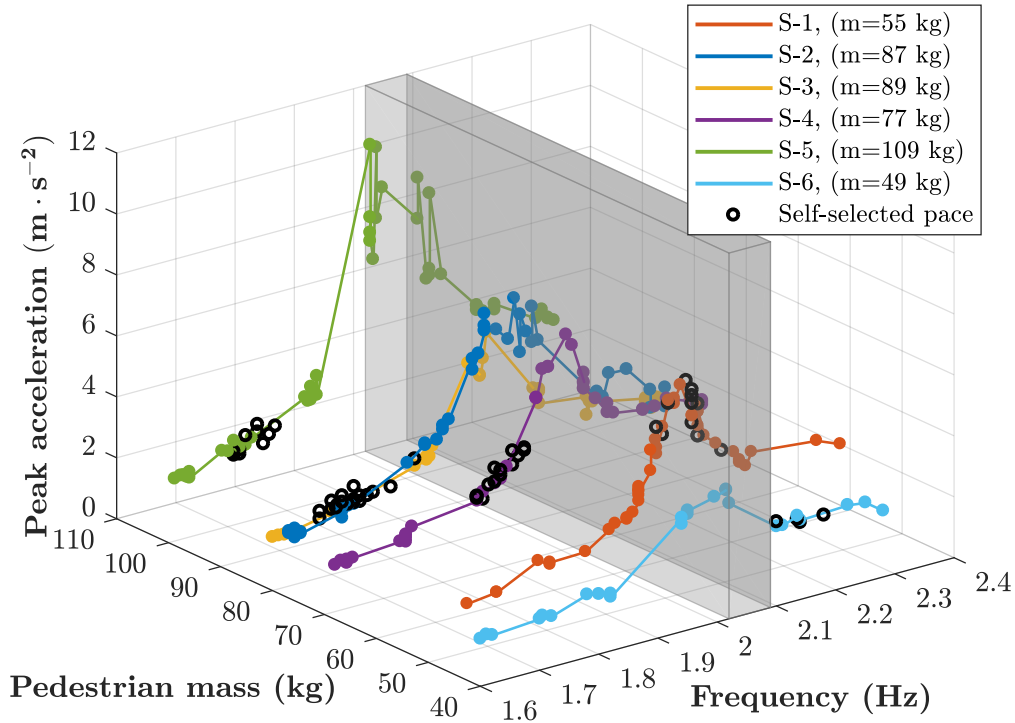


Fig. 3.8.: Peak acceleration as a function of pedestrian mass and coupled system's frequency.

but the mass seems like a meaningful parameter that can be easily measured for a preliminary structural response estimation.

Based on the percent changes obtained in Section 3.3, the midspan peak acceleration of the moving surface is related with each gait parameter. Figs. 3.10 and 3.11 depict the influence of the vibration levels in the the gait characteristics of the test subjects. When the metronome was set to 1.7 and 2.3 Hz, the pedestrian was subjected, in most of the cases, to vibration levels up to $2.5 \text{ m}\cdot\text{s}^{-2}$ approximately, which is near the maximum acceptable value ($2.5 \text{ m}\cdot\text{s}^{-2}$) in guidelines and standard (*e.g.*, Sétra (2006) and Heinemeyer et al. (2007)). The obtained PC ranges for SL, SW, PF, and GS (-9 to 11%, -17 to 17%, -2.5 to 2.5%, and -15 to 18%, in in Table 3.2) are in agreement with the reported results by Dang & Živanović (2016). However, when the metronome was set to 2.0 and 2.1 Hz, the PF was near to the structure's natural frequency producing higher vibration amplitudes and important variations in the walking locomotion. With vertical acceleration amplitudes higher than $2.5 \text{ m}\cdot\text{s}^{-2}$, the gait parameters showed notable PC changes between both surfaces for SL, SW, PF, and GS (-2 to 18%, -13 to 28%, -6 to 5%, -4 to 19%, in Table 3.2). These might

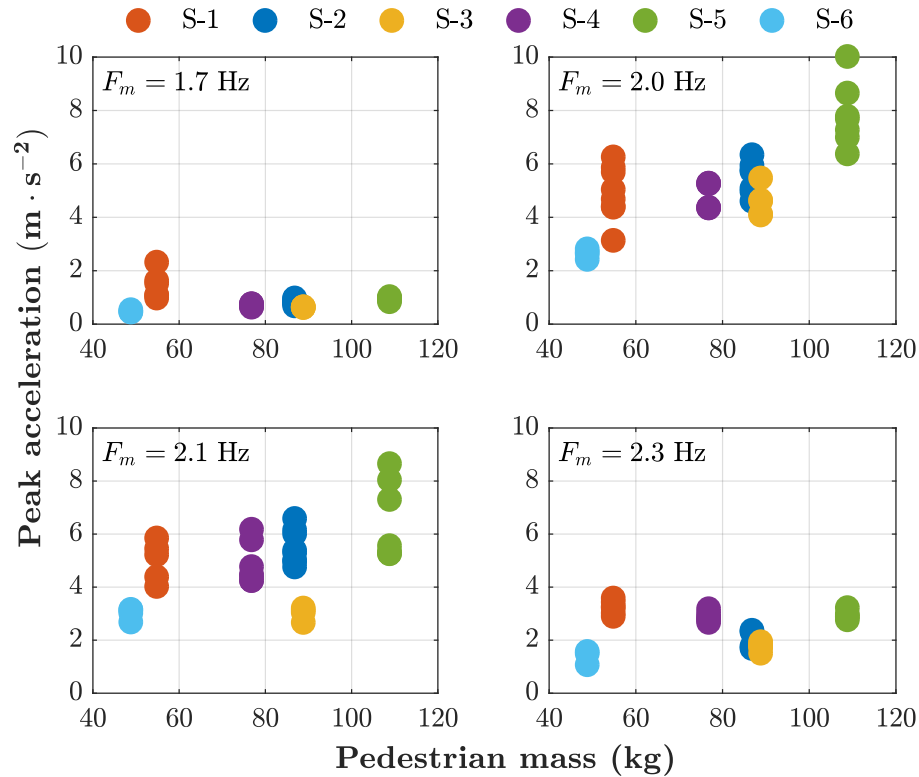


Fig. 3.9.: Peak acceleration as function of pedestrian mass.

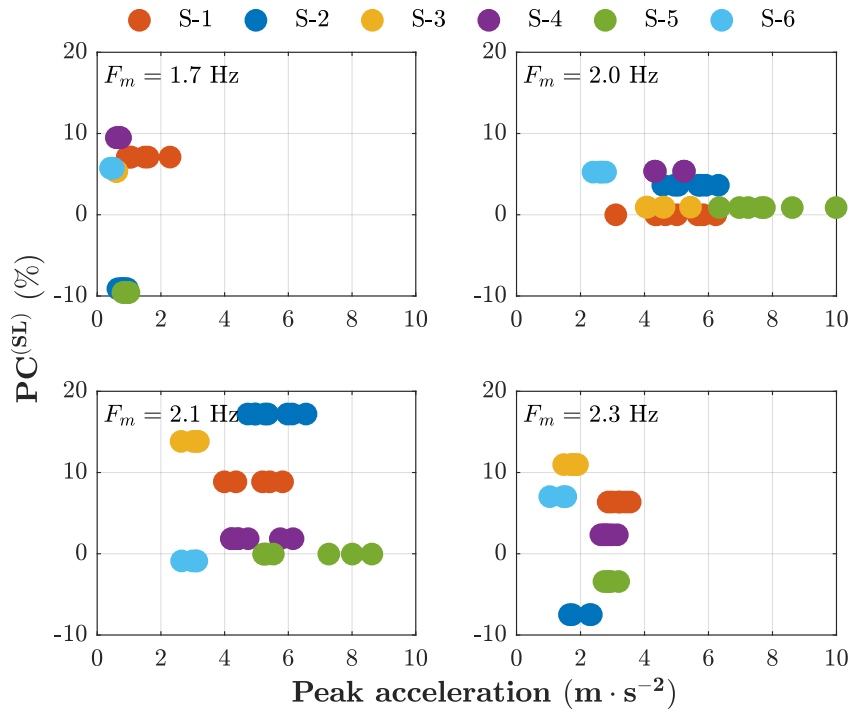
be associated with maximizing gait stability on an oscillatory surface without any concern to minimize expended metabolic energy. Thus, the subject seemed to provide extra energy when the pacing frequency was close to the vertical frequency of the structure to maintain the required cadence. This implies that the subject spent more energy in the walking process to adapt and modulate the gait at an unnatural pace frequency, consistent with published experimental observations (Holt et al., 1995).

When the PF was not prescribed by a metronome's beat, pedestrians were able to walk freely on both surfaces. While four of them decreased their PF on the MS, one subject walked on the beam with a pace frequency higher than 2.08 Hz (subject S-6), and the other one shifted his/her pace frequency in phase to the natural frequency of the pedestrian-beam system (subject S-1) (See the obtained PC ranges for SL, SW, PF, and GS in Table 3.2). The results showed that subjects that walked with a PF far from the structural frequency did not modify their gait parameters significantly because of the low level of vibration. However, when the level of vibration was noticeable at a frequency close to the natural pace frequency, the subject could either

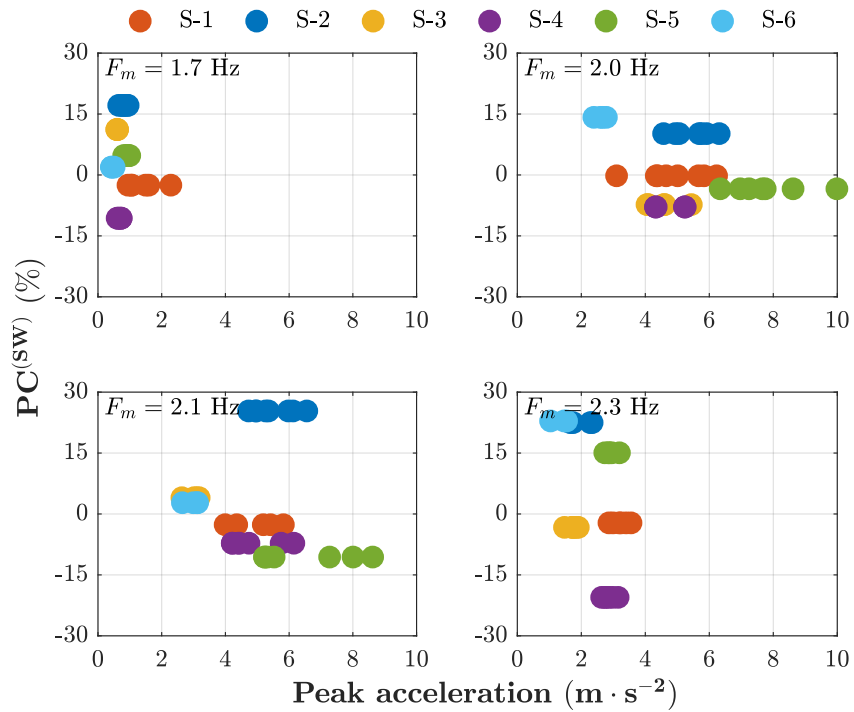
decrease his/her gait parameters to avoid an increase in the surface vibration or shift his/her PF with the surface movement to walk in synchrony with the structure. It seems that subjects might be susceptible to use the vertical impulse during the swing phase to reduce the metabolic cost of walking by taking advantage of the structural movement. This phenomenon might be evidence for vertical lock-in in pedestrian-structure interaction where the pedestrian tries unconsciously to modify their gait characteristics in order to minimize his/her metabolic energy, as was demonstrated in the lateral direction by (Strogatz et al., 2005; Joshi & Srinivasan, 2015, 2018).

3.6 Summary

In this chapter the spatial-temporal intra-subject gait parameter changes for a pedestrian walking both OG and MS conditions were quantified. A previous study showed the influence of low-frequency vertical vibration on human walking by using a treadmill on top of a bridge (Dang & Živanović, 2016). Besides, they used a shaker to produce stationary levels of vibration at the same time the pedestrian was walking on the treadmill. However, treadmill walking might not fully reflect natural gait dynamics when the stride speed is constrained. From this perspective, we extended their initial results adapting a beam that served as a lively structure to measure vertical vibrations under real conditions while a pedestrian wore a non-invasive gait analyzer device. As a result, the structural vibration amplitude caused in the experimental study was appreciable for all of the subjects while walking, exposing them to different self-induced vertical acceleration levels. The main findings are: (1) the obtained ranges for each gait parameter based on different levels of vertical accelerations when the pacing frequency was controlled by a metronome, (2) the gait parameter changes in terms of ranges when the subject walked freely at self-selected pace showing the gait adaptation to the moving conditions, and (3) the relation between the gait parameters and how these changes affect the structural response.

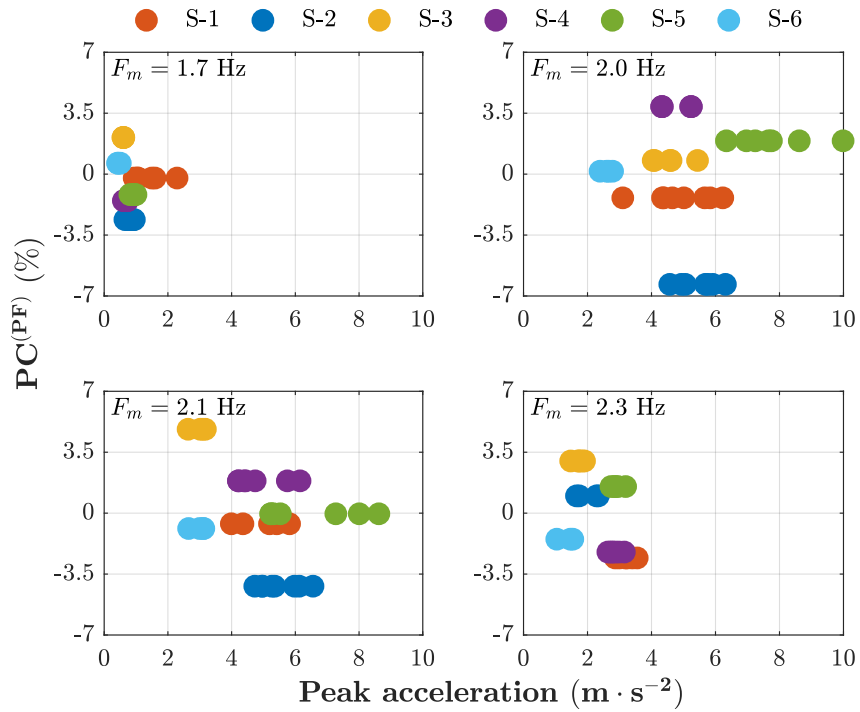


(a) Step length percentage change as function of the peak acceleration.

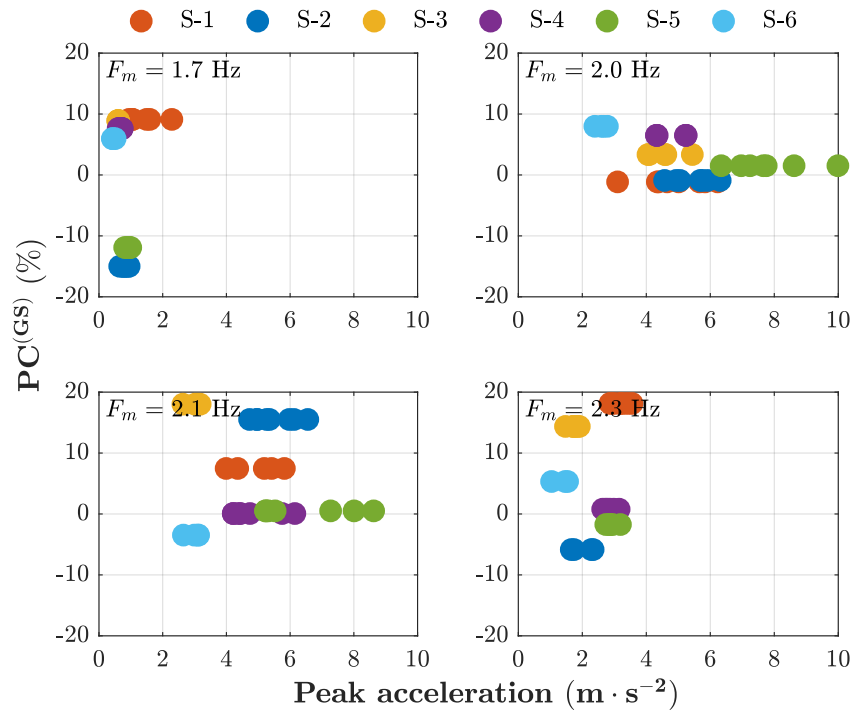


(b) Step width percentage change as function of the peak acceleration.

Fig. 3.10.: Influence of vibration amplitude in the pedestrian gait dynamics.



(a) Pace frequency percentage change as function of the peak acceleration.



(b) Gait speed percentage change as function of the peak acceleration.

Fig. 3.11.: Influence of vibration amplitude in the pedestrian gait dynamics.

4. STRUCTURED UNCERTAINTY FOR A PEDESTRIAN-STRUCTURE INTERACTION MODEL

Model variability in control engineering is often represented using perturbations. Specifically, in interval analysis (Moens & Vandepitte, 2007; Henriques, 2008; Moore et al., 2009) and robust control (Packard, 1998; Skogestad & Postlethwaite, 2007), uncertain variables can be defined in closed-bounded real intervals as *parametric uncertainties*. The uncertainty in each parameter can be modeled with a nominal value and a range of possible variations where the perturbations are organized in a structured manner (Paw & Balas, 2008). The parametric uncertainty technique has been applied to civil infrastructure to suppress the dynamic response (*e.g.*, Venini (1998), Marinova & Stavroulakis (2007), and Huo et al. (2016) among others). They developed robust control approaches that consider parametric uncertainties in designing a control algorithm for a structural frame with an active mass damper. In these studies, the linear fractional transformation (LFT) is used as an effective approach to include parametric uncertainties in the dynamic system. By separating what is known from what is unknown in the dynamic subsystem, a feedback-like connection can be transformed into an LFT structured uncertainty model (Moreno & Thomson, 2010). Therefore, the model with uncertainties obtained using the LFT method has the advantage of relating each of the uncertainties with a physically meaningful parameter in the system. As a result, parametric perturbation modeling, as a non-probabilistic method, facilitates the calculation of structural system response bounds.

In this chapter a new analytical approach to include such uncertainties in pedestrian-structure interaction analysis is developed and verified. A coupled model is used in which the pedestrian is modeled as a moving dynamic subsystem represented by a single degree-of-freedom (SDOF) oscillator. The structure is modeled as a multiple degree-of-freedom (MDOF) mechanical system. To represent the variability of the pedestrian's dynamic characteristics, uncertainty is included in the pedestrian subsystem. Parameters, including the mass, viscous damping, elastic stiffness, pace frequency, and the initial velocity in the vertical direction of the body center of mass, are considered to be uncertain model quantities using the LFT. To characterize the uncertainties in this pedestrian model, experimental data collected with test subjects

walking on a flexible surface are used. The capabilities of the model are evaluated in terms of their ability to predict the structural responses. The analysis considers the variability in the human-induced load among several single pedestrians (inter-subject variability) as well as the variability overall in the human-induced load for various pedestrians (intra-subject variability) are verified. Through the comparisons between the experimental data and the simulated envelope responses using the uncertain model, the capabilities of the approach to capture the combined system response is demonstrated in both the time and frequency domains.

The contribution of this chapter is to develop a systematic approach to describe the uncertainty of the pedestrian subsystem that provides a robust model suited for adoption in current design procedures. The model highlights the sensitivity of the structural response to pedestrian parameter variations. Thus, it enables the designer to perform an appropriate analysis and design reliable and robust structures that achieve desirable performance even with realistic response variations.

The organization of this chapter is as follows. In Section 4.1, the uncertain system modeling concept is explained, and the structured parametric description of the pedestrian subsystem is developed. The coupled equations governing the dynamics of the system are provided with these uncertainties, and their closed-loop representation is discussed. In Section 4.2, the experimental program is described, including the characteristics of the pedestrian test subjects and the structure. Section 4.3 provides the results, where parametric uncertainties are determined and simulated structural response envelopes using the uncertain model are compared to the measured acceleration data. Finally, the main findings are discussed and potential applications for this model are considered in the Summary.

4.1 Representing system uncertainties

The PSI model established in Chapter 2 is adopted here in order to develop an approach to consider parametric uncertainties. The pedestrian is assumed to walk at a constant velocity $v(t)$, which is represented in the biodynamic model with the step length and the pace frequency F_p . The PSI model assumes continuous contact of the pedestrian with the structure by means of a contact point, which defines the pedestrian's position at each instant in time. This coupled system is partitioned into two dynamic subsystems as shown in Fig. 4.1. One subsystem represents the

pedestrian, and is modeled as a traveling oscillator. The other subsystem represents the structure, and is represented as a finite element model (see Section 4.1.3).

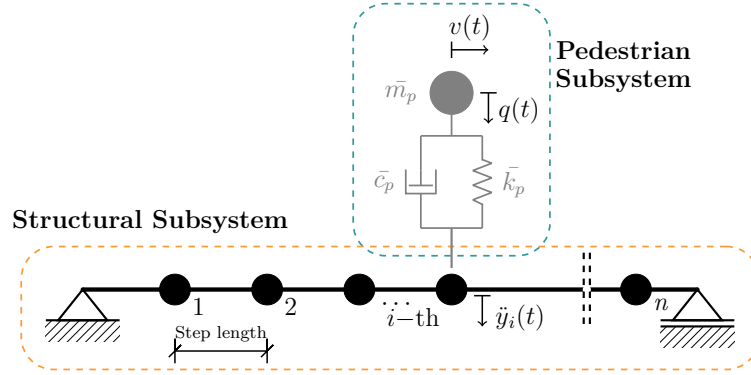


Fig. 4.1.: Model of the nominal pedestrian-structure interaction system.

4.1.1 Pedestrian subsystem definition

The pedestrian subsystem includes the biomechanical characteristics of the pedestrian represented as a linear oscillator (*i.e.*, a mass-spring-damper (MSD)). Nominal biodynamic parameters include a lumped mass \bar{m}_p that is attached to a linear spring and a viscous linear dashpot with coefficients \bar{k}_p and \bar{c}_p , respectively. The nominal pedestrian subsystem dynamics are governed by the differential equation

$$\bar{m}_p \ddot{q}(t) + \bar{c}_p \dot{q}(t) + \bar{k}_p q(t) = -\bar{m}_p \ddot{y}_i(t) \quad (4.1)$$

where $q(t)$, $\dot{q}(t)$, $\ddot{q}(t)$ are the vertical displacement, velocity, and acceleration of the body COM relative to the structure, respectively, and $\ddot{y}_i(t)$ is the i -th structural nodal acceleration at the pedestrian's point of contact (this is used as the input to the pedestrian subsystem at each time step). The output of this subsystem model is the force imparted by the pedestrian to the structure at the i -th point of contact, defined as $F_i^{\text{con}}(t)$ and given by

$$F_i^{\text{con}}(t) = \bar{c}_p \dot{q}(t) + \bar{k}_p q(t). \quad (4.2)$$

The block diagram of this nominal pedestrian subsystem model is illustrated in Fig 4.2.

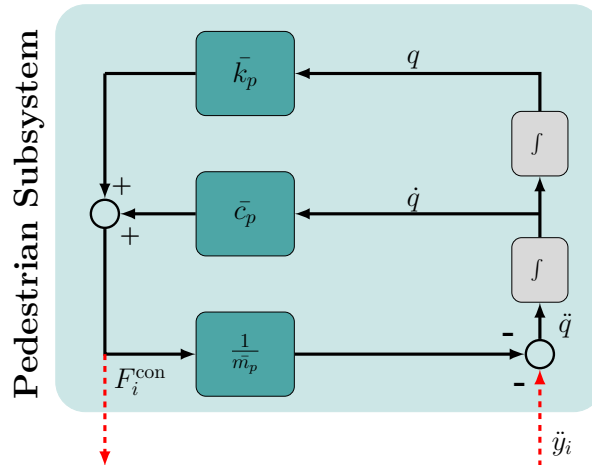


Fig. 4.2.: Nominal pedestrian subsystem block diagram.

As the pedestrian travels horizontally, this model considers one additional parameter, a non-zero vertical initial velocity condition $\dot{q}(t_o)$ that is imparted on the dynamic oscillator at each step. This initial velocity is equivalent to an impulse excitation at each step (at the instant when each foot hits the ground). To define the pedestrian's time-varying position, a vector is created

$$\mathbf{\Gamma} = [0 \ 0 \ \dots \ 1 \ \dots \ 0]^T \quad (4.3)$$

where $\mathbf{\Gamma}$ is used to represent the position of the pedestrian at each time, and thus defines the point where the contact force $F_i^{\text{con}}(t)$ is applied to the structure in the system of equations. The length of this vector corresponds to the number of possible discrete pedestrian positions on the bridge. All components of this vector are equal to zero except the one that specifies the pedestrian location at a particular time.

4.1.2 Structured parametric model uncertainty

In general, the precise mass, damping, and stiffness for a pedestrian will not be known, either because they are hard to measure or due to inter- or intra-subject variability (C. Caprani & Ahmadi, 2016; Racic & Brownjohn, 2011). Intrinsic uncertainties in the human body are included in the MSD biodynamic model as parametric uncertainties. Thus, the dynamic response of a pedestrian-structure system with uncertain-but-bounded pedestrian parameters can then be determined by representing the uncertain quantities as an LFT. By considering a suitable range of possible

values for the biodynamic parameters to represent our lack of knowledge about the pedestrian, realistic variability in pedestrian characteristics may be considered in the analysis, and subsequently incorporated into the design process.

Uncertainty in a given parameter is modeled using a nominal value and an associated range of possible variations, where the perturbations Δ are organized in a structured manner (Skogestad & Postlethwaite, 2007). In this study, the LFT is used to include such parametric uncertainties in the pedestrian subsystem. The LFT is defined as the closed-loop transfer matrices from $w \mapsto z$ and is represented by the operator $F_u(\mathbf{N}, \Delta)$, the upper LFT of \mathbf{N} and Δ (Marinova & Stavroulakis, 2007; Moreno & Thomson, 2010; K. Zhou & Doyle, 1998) as shown in Fig. 4.3. Thus, an uncertain model obtained using the LFT method has the advantage of directly relating each uncertainty with a physically meaningful parameter in the pedestrian subsystem.

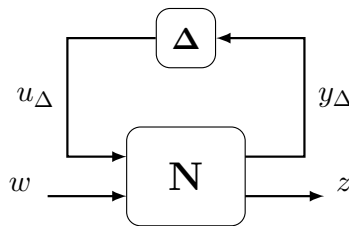


Fig. 4.3.: LFT of a linear uncertain system.

Here, the realization of the LFT model, $F_u(\mathbf{N}, \Delta)$, is achieved through the derivation of the \mathbf{N} and Δ matrices from the pedestrian subsystem. \mathbf{N} is the coefficient matrix. It is decomposed as shown in Eq. (4.4) into the known and unknown parts of the uncertain system. \mathbf{N}_{22} represents the nominal system, and the remaining matrices describe how the system varies with the perturbed parameters. The matrix \mathbf{N} is represented as

$$\mathbf{N} = \begin{bmatrix} \mathbf{N}_{11} & \mathbf{N}_{12} \\ \mathbf{N}_{21} & \mathbf{N}_{22} \end{bmatrix}. \quad (4.4)$$

Thus, with some manipulations of the input and output signals of the block \mathbf{N} in Fig. 4.3, we can show

$$\begin{aligned}
y_\Delta &= \mathbf{N}_{11}u_\Delta + \mathbf{N}_{12}w \\
z &= \mathbf{N}_{21}u_\Delta + \mathbf{N}_{22}w \\
u_\Delta &= \mathbf{\Delta}y_\Delta.
\end{aligned} \tag{4.5}$$

Assuming that $(\mathbf{I} - \mathbf{N}_{11}\mathbf{\Delta})^{-1}$ exists, the LFT can be reduced to a linear function $F_u(\mathbf{N}, \mathbf{\Delta})$ where

$$z = \underbrace{\left[\mathbf{N}_{22} + \mathbf{N}_{21}\mathbf{\Delta}(\mathbf{I} - \mathbf{N}_{11}\mathbf{\Delta})^{-1}\mathbf{N}_{12} \right]}_{F_u(\mathbf{N}, \mathbf{\Delta})} w. \tag{4.6}$$

The uncertainty block $\mathbf{\Delta}$ in Eq. (4.6) contains the unknown portions of the uncertain system, included in a structured manner with real scalar system model uncertainties along its diagonal. These model uncertainties are assumed to be bounded as

$$\mathbf{\Delta} = \{ \delta \in \mathbb{R} \mid -1 < \delta < 1 \}. \tag{4.7}$$

The inputs and outputs of $\mathbf{\Delta}$ are represented by y_Δ and u_Δ , respectively. As a result, the parametric uncertainties are defined as the set of all possible values and are parameterized using this uncertainty block.

The uncertain biodynamic parameters of the model, m_p , c_p , and k_p represent the possible perturbations of each parameter in the pedestrian subsystem. The nominal value of \bar{m}_p , \bar{c}_p , and \bar{k}_p are the average values of mass, damping and stiffness of a pedestrian, respectively. The uncertainty, or the variation from the nominal value, is expressed as a percentage of the nominal value of the mass, damping, and stiffness are defined by p_m , p_c , and p_k , respectively. The perturbations in the pedestrian mass, damping, and stiffness, defined as δ_m , δ_c , and δ_k , respectively, are unknown but lie in the interval $[-1, 1]$, and can be lumped as

$$\mathbf{\Delta} = \begin{bmatrix} \delta_m & & \\ & \delta_c & \\ & & \delta_k \end{bmatrix}. \tag{4.8}$$

As a result, the constant block diagram representation of the nominal model in Fig. 4.2 is modified to include each parameter with its specific known intervals, as is depicted in Fig. 4.4.

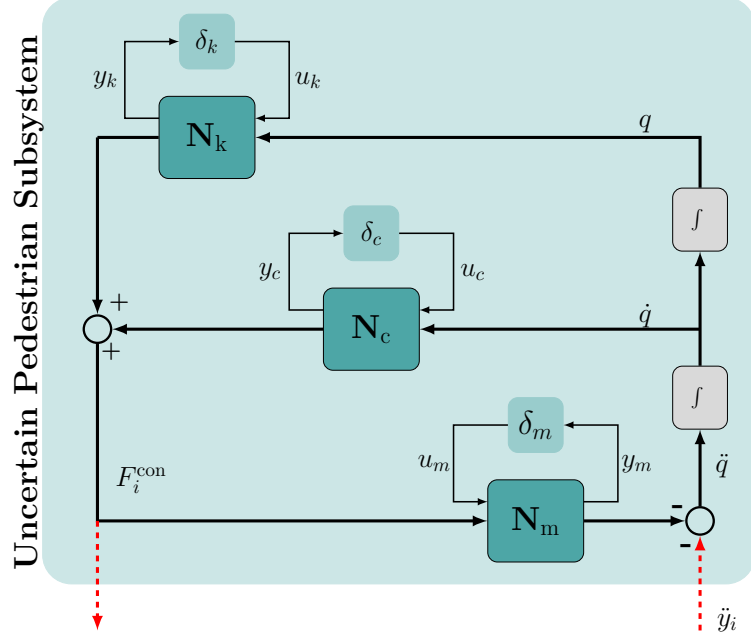


Fig. 4.4.: Pedestrian subsystem model with parametric uncertainties.

The structured dynamic representation to model the perturbed pedestrian parameters uses an LFT in δ represented as $F_u(\mathbf{N}, \delta)$. Using this approach, the mass m_p is expressed as an inverse multiplicative uncertainty, and its upper LFT representation in δ_m is

$$\begin{aligned} \frac{1}{m_p} &= \frac{1}{\bar{m}_p (1 + p_m \delta_m)} = \underbrace{\frac{1}{\bar{m}_p}}_{N_{22}} + \underbrace{(-p_m)}_{N_{21}} \delta_m \left(1 - \underbrace{(-p_m)}_{N_{11}} \delta_m \right)^{-1} \underbrace{\frac{1}{\bar{m}_p}}_{N_{12}} \\ &= F_u(\mathbf{N}_m, \delta_m) \quad \text{with} \quad \mathbf{N}_m = \begin{bmatrix} -p_m & \frac{1}{\bar{m}_p} \\ -p_m & \frac{1}{\bar{m}_p} \end{bmatrix}, \end{aligned} \quad (4.9)$$

while the damping c_p and stiffness k_p coefficients are expressed as multiplicative uncertainties that can be represented as an LFT using δ_c and δ_k , respectively, as

$$\begin{aligned}
c_p &= \bar{c}_p (1 + p_c \delta_c) = \underbrace{\bar{c}_p}_{N_{22}} + \underbrace{p_c}_{N_{21}} \delta_c \left(1 - \underbrace{0}_{N_{11}} \delta_c \right)^{-1} \underbrace{\bar{c}_p}_{N_{12}} \\
&= F_u(\mathbf{N}_c, \delta_c) \quad \text{with} \quad \mathbf{N}_c = \begin{bmatrix} 0 & \bar{c}_p \\ p_c & \bar{c}_p \end{bmatrix},
\end{aligned} \tag{4.10}$$

and

$$\begin{aligned}
k_p &= \bar{k}_p (1 + p_k \delta_k) = \underbrace{\bar{k}_p}_{N_{22}} + \underbrace{p_k}_{N_{21}} \delta_k \left(1 - \underbrace{0}_{N_{11}} \delta_k \right)^{-1} \underbrace{\bar{k}_p}_{N_{12}} \\
&= F_u(\mathbf{N}_k, \delta_k) \quad \text{with} \quad \mathbf{N}_k = \begin{bmatrix} 0 & \bar{k}_p \\ p_k & \bar{k}_p \end{bmatrix}.
\end{aligned} \tag{4.11}$$

Within the structured uncertainty configuration in Fig. 4.4, the equations relating all inputs to their corresponding outputs around those perturbed parameters are obtained (Gu et al., 2005). The perturbed system can be arranged into an uncertain state-space (uSS) model, as described in detail by Packard (1998). The augmented interconnected system in Fig. 4.4 is given by

$$\begin{bmatrix} \dot{x}_1 \\ \dot{x}_2 \\ \text{---} \\ y_m \\ y_c \\ y_k \\ \text{---} \\ F_i^{\text{con}} \end{bmatrix} = \underbrace{\begin{bmatrix} 0 & 1 & | & 0 & 0 & 0 & | & 0 \\ -\frac{\bar{k}_p}{\bar{m}_p} & -\frac{\bar{c}_p}{\bar{m}_p} & | & p_m & -\frac{p_c}{\bar{m}_p} & -\frac{p_k}{\bar{m}_p} & | & -1 \\ \text{---} & \text{---} \\ \frac{\bar{k}_p}{\bar{m}_p} & \frac{\bar{c}_p}{\bar{m}_p} & | & -p_m & \frac{p_c}{\bar{m}_p} & \frac{p_k}{\bar{m}_p} & | & 0 \\ 0 & \bar{c}_p & | & 0 & 0 & 0 & | & 0 \\ \bar{k}_p & 0 & | & 0 & 0 & 0 & | & 0 \\ \text{---} & \text{---} \\ \bar{k}_p & \bar{c}_p & | & 0 & p_c & p_k & | & 0 \end{bmatrix}}_{\mathbf{G}_{\text{ped}}} \begin{bmatrix} x_1 \\ x_2 \\ \text{---} \\ u_m \\ u_c \\ u_k \\ \text{---} \\ \ddot{y}_i \end{bmatrix} \tag{4.12}$$

where \mathbf{G}_{ped} is the uSS realization of the perturbed pedestrian subsystem. \mathbf{G}_{ped} has four inputs (u_m , u_c , u_k , and \ddot{y}_i), four outputs (y_m , y_c , y_k , and F_i^{con}) and two states

(x_1, x_2) , as shown in Eq. (4.12). The effects of uncertain pedestrian parameters on the system \mathbf{G}_{ped} are lumped in a matrix form as

$$\mathbf{u}_{\Delta} = \Delta \mathbf{y}_{\Delta} \quad (4.13)$$

with the outputs and inputs of the perturbation block Δ defined as $\mathbf{u}_{\Delta} = [u_m \ u_c \ u_k]^T$ and $\mathbf{y}_{\Delta} = [y_m \ y_c \ y_k]^T$, respectively. The \mathbf{G}_{ped} matrix in Eq. (4.12) includes the input/output dynamics of the pedestrian subsystem, including the uncertainties in the parameters shown in Eq. (4.13) (see Fig. 4.5). Note that a major advantage of this approach is that \mathbf{G}_{ped} is completely defined by the average biodynamic values \bar{m}_p , \bar{c}_p , and \bar{k}_p , and the percentages of uncertainties p_m , p_c , and p_k .

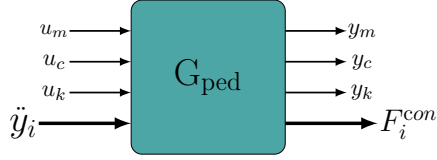


Fig. 4.5.: Input/output of the uncertain pedestrian subsystem.

4.1.3 Structural subsystem definition

The equation of motion for a conventional finite element model of a structure with a point force excitation can be expressed in matrix form as

$$\mathbf{M}_s \ddot{\mathbf{y}}(t) + \mathbf{C}_s \dot{\mathbf{y}}(t) + \mathbf{K}_s \mathbf{y}(t) = \mathbf{\Gamma} F_i^{\text{con}}(t) \quad (4.14)$$

where the matrices \mathbf{M}_s , \mathbf{C}_s , and \mathbf{K}_s are the global mass, damping, and stiffness condensed matrices, respectively. The output vector of the structural subsystem may be selected to include the displacement $\mathbf{y}(t)$, velocity $\dot{\mathbf{y}}(t)$, and acceleration $\ddot{\mathbf{y}}(t)$ responses at the nodes of the model. The i -th structural nodal acceleration output at the pedestrian's point of contact $\ddot{y}_i(t)$ is used as the input to the pedestrian subsystem. The vertical force imparted by the pedestrian $F_i^{\text{con}}(t)$ is applied at the i -th point of contact, simulating each individual step of the pedestrian. For the sake of simplicity, no uncertainties in this subsystem are considered. A block diagram representation of the structural subsystem is depicted in Fig. 2.2 but is reproduced below for convenience.

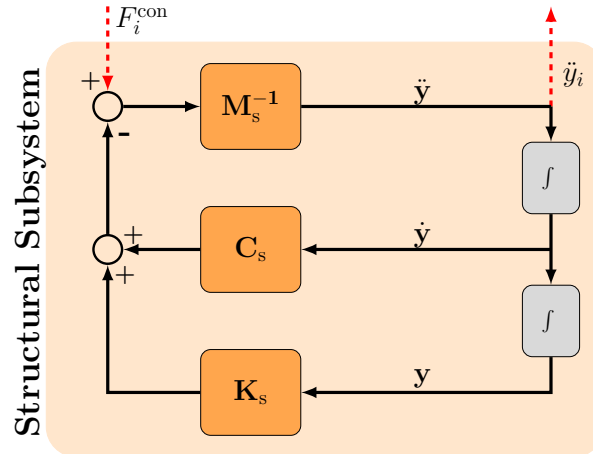


Fig. 4.6.: Structural subsystem block diagram.

4.1.4 PSI model with structured uncertainties

Using the perturbed pedestrian subsystem and the deterministic structural subsystem, a pedestrian-structure interaction model with structured uncertainties (uPSI) is assembled to consider the influence of a walker with unknown dynamic parameters on a structure, as depicted in Fig. 4.7. The bidirectional interaction between the structure and pedestrian is included by using dynamic substructuring, capturing the effect of each subsystem on the other. By simulating the coupled set of equations, this time-varying model has been shown to capture the interacting system dynamics. Then, as the coupled system is perturbed, a family of responses is obtained. Consequently, the range of responses of this closed-loop system (*i.e.*, the envelope of responses) can be easily obtained for any discretized structure (Gomez et al., 2018).

To obtain the envelope of structural responses for this perturbed, dynamically-coupled model, the two subsystems are solved together to include the interaction based on the location of the pedestrian as the pedestrian traverses the structure. The procedure for this uncertain analysis is broken into seven main steps as described below:

1. Establish the nominal values of the pedestrian's biodynamic parameters, including mass \bar{m}_p , damping \bar{c}_p , stiffness \bar{k}_p , pace frequency \bar{F}_p , and vertical initial velocity $\bar{q}(t_o)$. Then, define uncertainties as a percentage of each parameter's nominal value to define the uncertain intervals.

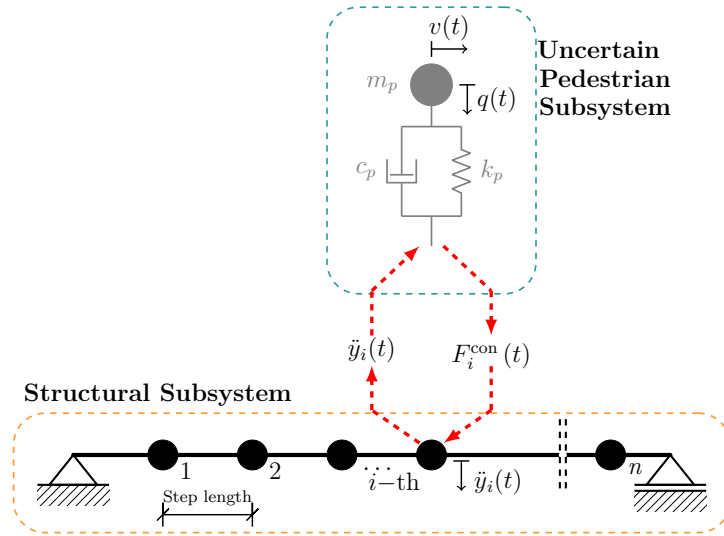


Fig. 4.7.: Pedestrian-structure interaction model with uncertainties

2. Obtain the LFT realization using Eqs. 4.9, 4.10, and 4.11 for each pedestrian characteristic. By deriving \mathbf{N} and $\mathbf{\Delta}$ from the uncertain subsystem, the augmented input/output model, shown in Fig. 4.4, is built.
3. Obtain the uSS model for the pedestrian subsystem using the augmented input/output expressions defined by Eqs. 4.12 and 4.13.
4. Assemble and condense the matrices of the structural subsystem \mathbf{M}_s , \mathbf{C}_s , and \mathbf{K}_s , using the step length as the distance between the lumped masses given by Eq. 4.14.
5. Initialize the states of the structural subsystem ($\mathbf{y}(0) = \dot{\mathbf{y}}(0) = \mathbf{0}$) and the pedestrian subsystem ($q(0) = \dot{q}(0) = F_i^{con}(0) = 0$).
6. Select an appropriate time increment Δt to perform the numerical integration. Typically the integration time step is chosen to correspond to a frequency that is at least ten times the natural frequency of the highest mode of the structural model.
 - (a) The iterative procedure starts defining the number of pedestrian strides as the vector $i = 1..n$, where n is the number of pedestrian spatial locations on the structure subsystem, as:

- i. The length of the i -th iteration is defined by $t_k = 0.. \Delta t .. S_t$, and represents the time duration between two strides of the pedestrian as $S_t = 1/F_p$. By using the output of the uSS model, the family of perturbed responses can be obtained as follows:
- Compute $F_i^{\text{con}}(t_k)$ as the family of forces applied to the structure subsystem at the i -th pedestrian location using Eq. 4.2, while the family of nodal responses of the structural subsystem, in terms of displacement $\mathbf{y}(t_k)$, velocity $\dot{\mathbf{y}}(t_k)$, and acceleration $\ddot{\mathbf{y}}(t_k)$, are calculated by solving the equation of motion given by Eq. 4.14 as an interactive system.
 - Extract the family of nodal vertical accelerations $\ddot{y}_i(t_k)$ at the i -th contact point which is the interface point between the pedestrian and the structure, and apply them as inputs in Eq. 4.1.
 - Compute the family of relative responses in displacement $q(t_k)$ and velocity $\dot{q}(t_k)$ of the uncertain pedestrian model using the uSS model defined in step 3, and obtain the new $F_i^{\text{con}}(t_{k+1})$ to be applied in the next iteration.
- ii. Repeat Step 6(a)i until S_t is reached. This means that the pedestrian has completed stride i and a new stride, $i + 1$, will begin.
- (b) Set the initial state values of the structural subsystem for loop $i + 1$ equal to the final state values from the previous iteration i , as

$$\begin{aligned} \mathbf{y}_{i+1}(0) &= \mathbf{y}_i(S_t) \\ \dot{\mathbf{y}}_{i+1}(0) &= \dot{\mathbf{y}}_i(S_t). \end{aligned} \tag{4.15}$$

The initial states in the pedestrian subsystem must also be set equal to the final state values from the previous iteration. Moreover, an initial COM vertical velocity $\dot{q}(t_o)$, to add energy at each stride, is applied as follows

$$\begin{aligned} q_{i+1}(0) &= q_i(S_t) \\ \dot{q}_{i+1}(0) &= \dot{q}_i(S_t) + \dot{q}(t_o) \end{aligned} \tag{4.16}$$

- (c) The new position of the pedestrian at location $i + 1$ will start from Step 6a.

7. Repeat Steps 6a to 6c until the pedestrian exits the footbridge when $i = n$.

4.2 Experimental setup and procedure

The experimental study described herein is conducted to measure typical structural responses induced by a single walking pedestrian. The test beam that serves as the experimental structure was described in detail in Section 3.2.3. The vibration amplitude of the simple-support beam shown in Fig. 4.8 is appreciable for all of the subjects while walking during the test program, exhibiting significant pedestrian-structure interaction. However, only the first three vertical modes are included in the structural subsystem model.



Fig. 4.8.: Test structure used in the experimental program.

4.2.1 Subjects and anthropometric data

Fifteen participants (five females; mean age 31.8 (range 23-41) years; mean height 1.74 (range 1.53-1.90) m; mean weight 83.7 (range 49.3-108.9) kg) were enrolled in the study. No participants had any disease or disorder that impacted their gait, as verified by self-reporting. All participants signed an informed consent approved by the Institutional Review Board of Purdue University. Two gait modes were examined: (1) a self-selected speed, and (2) a prescribed cadence, where the participant walked at a frequency set by a metronome. In the analysis, each pass across the bridge is considered as a trial. Six trials at a self-selected speed were completed, and five

trials at a prescribed cadence were completed, where the prescribed frequency was randomly selected between 1.7 and 2.3 Hz. A total of 615 trials were used in this study.

Several prior studies have sought to determine deterministic MSD biodynamic parameters for a single pedestrian during PSI. A summary of the reported values, as mean, standard deviation (SD), and/or the range of values, from those studies are summarized in Table 4.1. Despite this amount of effort dedicated to this activity, there is still a significant scarcity of results and a disparity in the damping and stiffness coefficient values obtained. Even for most of the studies conducted on a rigid surface, a wide range of results in the biomechanic characteristics are noticeable. Although some efforts have recently been conducted by [Zhang et al. \(2016\)](#), [Wang et al. \(2017\)](#), and [da Silva et al. \(2013\)](#) where the natural frequency and damping ratio are determined as functions of the pacing frequency, there is still no consensus among these studies regarding the biodynamic values and their impact on the inter-person variability. This lack of consistency plays a key role in any PSI analysis and must be considered in the analysis stage to meet serviceability-based design requirements.

Table 4.1.: Biodynamic parameters used/obtained in PSI studies.

Reference	Surface	m_p [kg]		c_p [kg · s ⁻¹]		k_p [N · m ⁻¹]	
		Mean	SD	Mean	SD	Mean	SD
Siegler et al., (1982) (Siegler et al., 1982)	Rigid					21850	
Pandy & Berme, (1988) (Pandy & Berme, 1988)	Rigid					12000	
Lee & Farley, (1998) (Lee & Farley, 1998)	Rigid					[12000-34500] ^a	
Fanning et al., (2005) (Fanning et al., 2005)	Moving			800		[5000-10000] ^a	
Geyer et al., (2006) (Geyer et al., 2006)	Rigid	81	3.5			14000	
Caprani et al., (2011) (C. Caprani et al., 2011)	Rigid	73.9	15.67	775.73		22500	2250
Kim & Park, (2011) (S. Kim & Park, 2011)	Rigid					[14000-28000] ^a	
da Silva et al., (2013) (da Silva et al., 2013)	Rigid	63.82	9.88	867.06		16684.66	1765.29
Shahabpoor et al., (2015) (Shahabpoor et al., 2015)	Moving	70		[665 - 792] ^a		[20900-24870] ^a	
Zhang et al., (2015) (Zhang et al., 2015)	Moving	73		521		10600	
Toso et al., (2016) (Toso et al., 2016)	Rigid	77.53 (45.97) ^b	13.88 (25.02) ^b	581.26 [294-1719] ^a		8126.39 [1000-22874] ^a	4431.09
Gomez et al., (2018) (Gomez et al., 2018)	Rigid/Moving	[56-97] ^a		[212.5-501.4] ^a		[14000-20000] ^a	

^a Range of values of biodynamic parameters used/obtained in the study.

^b Fraction of the body mass is considered to provide the inertia force generated by a walking pedestrian.

4.3 Results and discussion

In this section, the experimental data is used to quantify the uncertainties and to investigate their impact on the response of the coupled system. A comparison is made between the experimental and predicted responses to demonstrate the validity of the proposed approach. Various cases are considered in which the parameter ranges are determined for a single pedestrian in multiple trials (intra-person variability), or different pedestrians (inter-person variability) under specific conditions. For the sake of simplicity and to focus on the pedestrian variability, the beam's structural parameters are considered to be known. Thus, variations are not imposed on the structural subsystem parameters. In contrast, the pedestrian subsystem parameters such as, mass m_p , damping c_p , stiffness k_p , pace frequency F_p , and the vertical COM initial velocity $\dot{q}(t_o)$, are assumed to be uncertain-but-bounded parameters. Nominal parameters are chosen as the average value of the ranges obtained. To quantify the variability in each parameter, the relative magnitude of the uncertainty (RMU) (Skogestad & Postlethwaite, 2007; Elishakoff et al., 1994) is defined as a percentage using

$$\text{RMU} = \frac{\varepsilon_u - \varepsilon_l}{2\bar{\varepsilon}} \times 100\% \quad (4.17)$$

where ε_u , ε_l , and $\bar{\varepsilon}$, are the upper-bound, the lower-bound, and the mean values, respectively. The RMU for the m_p , c_p , k_p , F_p , and $\dot{q}(t_o)$ are denoted as pm , pc , pk , pf , and pq , respectively. In addition, the peak acceleration response (PAR) ratio is defined as the ratio between the largest $\ddot{y}_{L/2}^u$ and smallest $\ddot{y}_{L/2}^l$ values of the maximum absolute acceleration response at midspan. The PAR is used to quantify the impact of the variability by considering the range of experimental response produced by a single pedestrian in the time domain, and is computed as

$$\text{PAR} = \frac{\max |\ddot{y}_{L/2}^U|}{\max |\ddot{y}_{L/2}^L|}. \quad (4.18)$$

The parameter intervals are obtained based on several experimental tests conducted with a subject walking on a lively structural surface. By comparing the variations observed in the given measurement data with the robust envelope, developed based on the simulated responses, appropriate ranges for the parameters of the pedestrian model are estimated. This process is performed manually with only a few iterations, by changing the interval values to obtain the envelope that encompasses

the desired region. This procedure is simple yet systematic, and also takes advantage of the computational efficiency of the LFT approach.

The acceleration responses of the experimental data are plotted for comparison with the uPSI model predictions. Intra-subject variability is examined by comparing the responses of the same participant walking at (1) self-selected speed and (2) prescribed cadences. Inter-subject variability is examined by comparing different participants walking at (1) self-selected speed and (2) prescribed cadences. Figs. 4.9-4.13 each provide experimentally measured results for a visual comparison with the envelope of uncertain simulated results (*i.e.*, the uPSI model output). Each solid line represents the vertical acceleration recorded at the beam's midspan in a single test, while the gray region depicts the envelope of simulated responses. Also, an analysis based on the short-time Fourier transform is used to track the maximum of the power spectral density at each of the time points in the spectrogram. Then, the spectra of instantaneous frequencies versus time is obtained and plotted for each trial. Both the acceleration record (in (a) and (c)) and the instantaneous frequency (in (b) and (d)), are shown versus time. It can be observed from each figure, that the structural response remains at zero before the pedestrian enters the beam. The response clearly attenuates during a free vibration phase after the subject has exited the beam.

4.3.1 Response comparison for a walking subject using a metronome

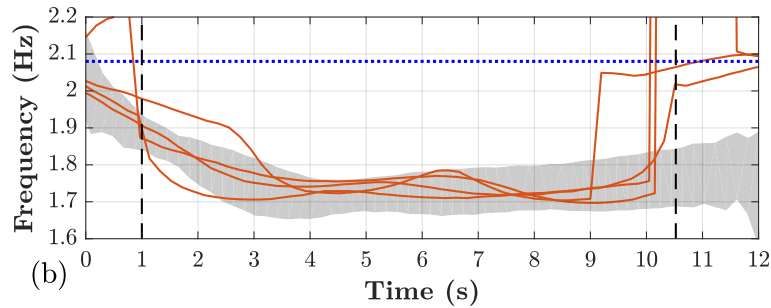
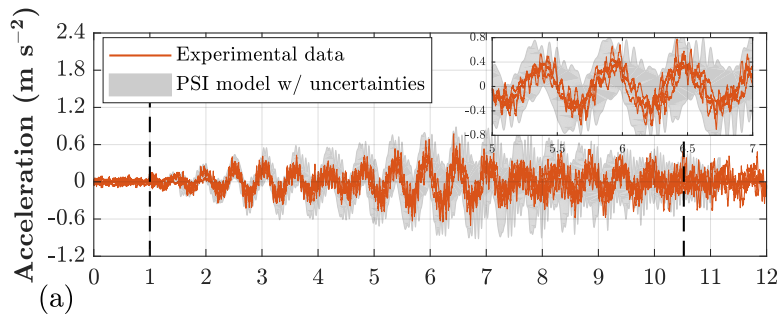
In this initial study, different trials are examined for a single pedestrian on the test structure. The measured responses are used to determine the uncertain parameter range, and the simulated responses are shown for a single subject to evaluate intra-person variability. Two subjects are considered with quite different physical characteristics. Each subject walks while following an audible beat with a specified frequency F_m produced by a metronome. Two representative plots showing the measured responses for each trial (solid line) and the simulated envelope of responses (gray region) are shown in Figs. 4.9 and 4.10 for the two different subjects. The data in these figures corresponds to the case in which the frequency of the metronome's beat F_m is set to 1.7 and 2.0 Hz. The body mass of each subject is measured directly in the lab, with a 1 kg variation assumed as modeling error. Other biodynamic parameter ranges for c_p , k_p , F_p , and $\dot{q}(t_o)$ are estimated by matching the bounded-responses of the model with the experimental measurements. Structural responses (Figs. 4.9 and

4.10) and biodynamic parameters with their variabilities (Table 4.2) are shown for two subjects with different masses walking at 1.7 and 2.0 Hz.

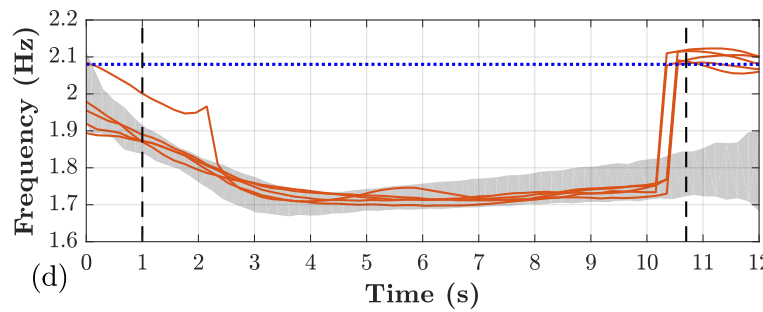
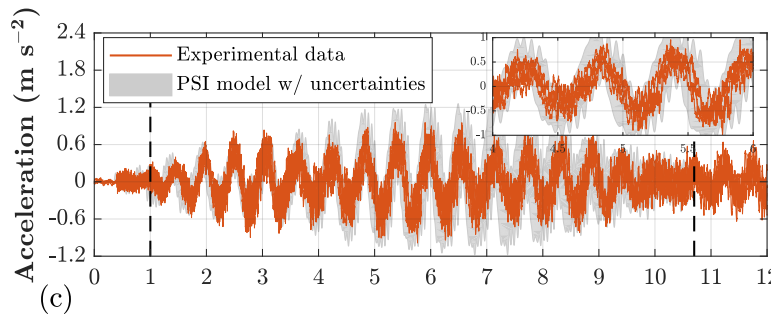
Note that when these two subjects walk at a frequency of $F_p = 1.7$ Hz, the maximum amplitude of the acceleration responses are relatively similar, even though the mass of the subject S-09 is almost double that of subject S-02. However, when they are instructed to walk with a gait frequency that is close to the natural frequency of the structure, the structural acceleration response produced by subject S-09 is approximately double that of the acceleration response with subject S-02. Also, note that the COM initial velocity parameter $\dot{q}(t_o)$ increases because the pedestrian must provide extra energy when the pace frequency is close to the vertical frequency of the structure. This implies that the subject expends more energy in the walking process to adapt and modulate gait at an unnatural pace frequency, consistent with published experimental observations (Holt et al., 1995). This also corresponds to an increase in the pedestrian stiffness during the gait cycle.

Table 4.2.: Perturbed biodynamic parameters obtained for a walking subject following an audible beat.

F_m [Hz]	Subject	m_p [kg]		k_p [$N \cdot m^{-1}$]		c_p [$kg \cdot s^{-1}$]		$\dot{q}(t_o)$ [$m \cdot s^{-1}$]		F_p [Hz]		PAR
		\bar{m}_p	pm [%]	\bar{k}_p	pk [%]	\bar{c}_p	pc [%]	$\bar{\dot{q}}(t_o)$	pq [%]	\bar{F}_p	pf [%]	
1.7	S-02	55	± 1.8	11000	± 9.1	200	± 50.0	0.45	± 11.1	1.71	± 2.9	1.57
2.0	S-02	55	± 1.8	15000	± 6.7	250	± 10.0	0.6	± 11.7	2.01	± 2.0	1.49
1.7	S-09	109	± 0.9	20000	± 15.0	500	± 10.0	0.4	± 12.5	1.71	± 1.8	1.16
2.0	S-09	109	± 0.9	24000	± 4.2	650	± 7.7	0.92	± 10.9	2.05	± 1.2	1.28

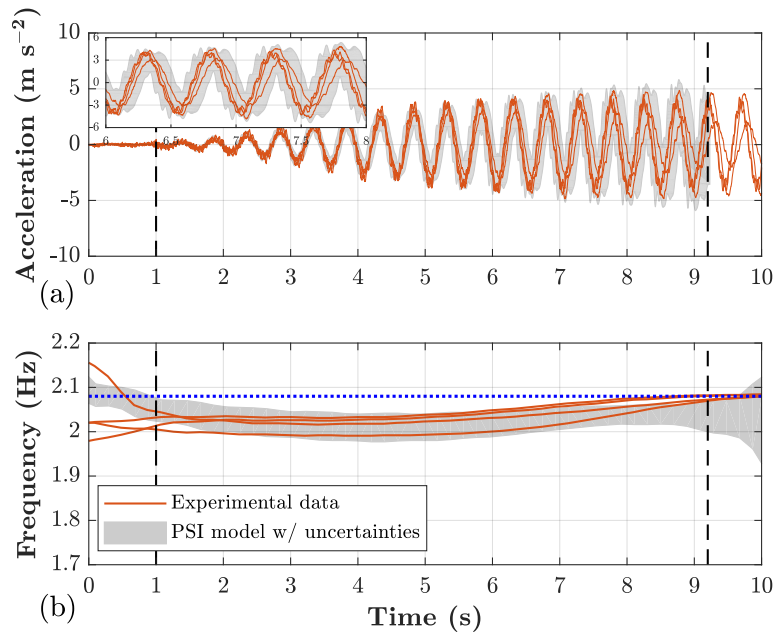


(a) Subject S-02.

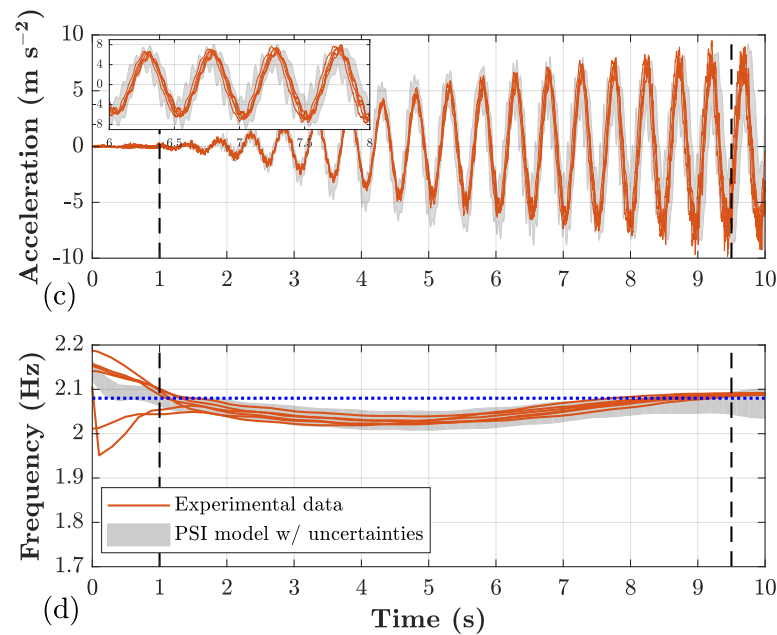


(b) Subject S-09.

Fig. 4.9.: Single experimental record for a subject walking on the structure (solid line) and uPSI model prediction (gray region) at $F_m = 1.7$ Hz. The two vertical dashed lines indicate when the pedestrian is walking on the beam. (a) and (c) Midspan acceleration amplitude; (b) and (d) Spectrum of instantaneous frequencies versus time. The horizontal dotted line in (b) and (d) represents the first vertical natural frequency of the bare structure.



(a) Subject S-02.



(b) Subject S-09.

Fig. 4.10.: Single experimental record for a subject walking on the structure (solid line) and uPSI model prediction (gray region) at $F_m = 2.0$ Hz. The two vertical dashed lines indicate when the pedestrian is walking on the beam. (a) and (c) Midspan acceleration amplitude; (b) and (d) Spectrum of instantaneous frequencies versus time. The horizontal dotted line in (b) and (d) represents the first vertical natural frequency of the bare structure.

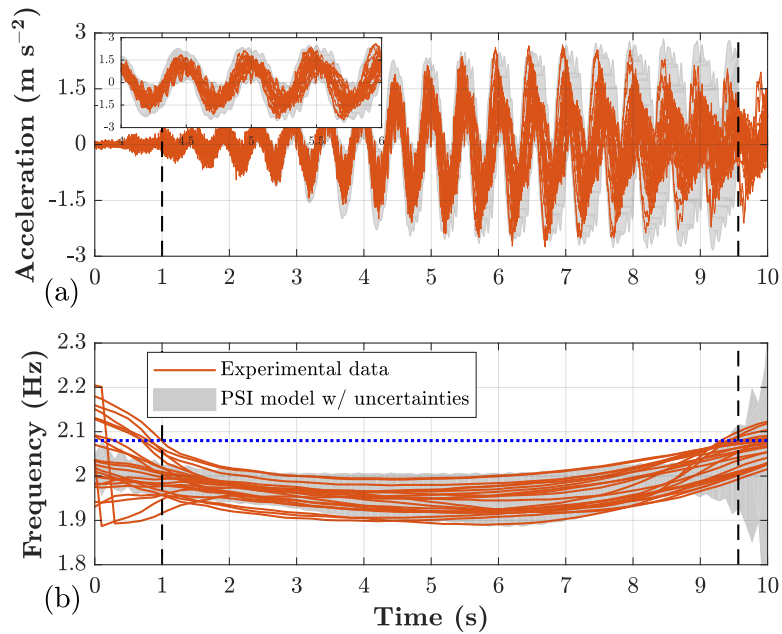
4.3.2 Response comparison for a single subject walking at a self-selected pace

In these tests, each subject walks at his/her self-selected and natural speed, producing structural responses and associated biodynamic parameters that are compared among the individual subjects to evaluate the intra-person variability. Structural responses (see Fig. 4.11) and biodynamic parameters with their variabilities (Table 4.3) are shown for two subjects with different masses walking freely on the structure. As shown in Fig. 4.11(a and b), several trials are performed with subject S-06. This subject demonstrates a self-selected pace frequency that has a small range from 1.89 to 1.97 Hz. This variability in the pace frequency might be produced by changes in the step length, changes in the subject horizontal walking speed, or simply from measurement error. However, the differences do affect the peak acceleration response values, which ranged from 1.22 to 2.69 $\text{m} \cdot \text{s}^{-2}$.

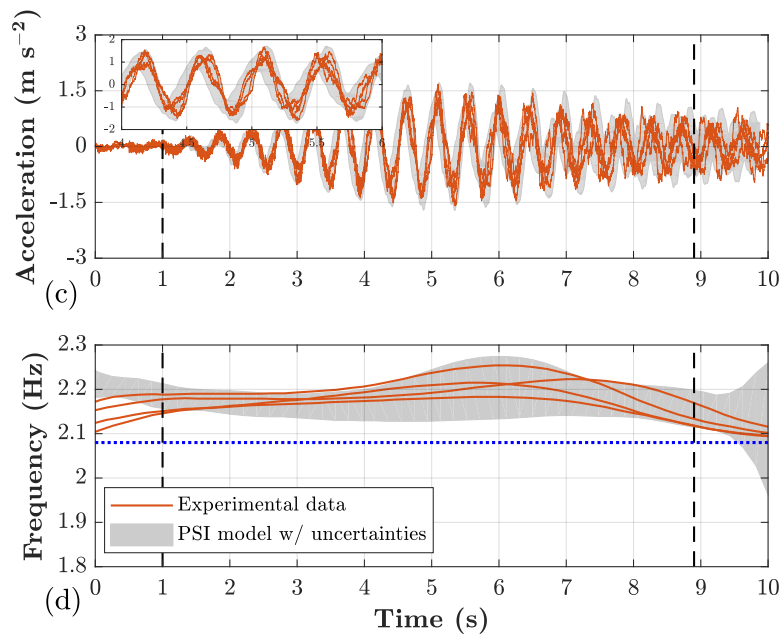
Subject S-15 exhibits very different results (see Fig. 4.11(c and d)). Here the self-selected pace frequency is higher than the first vertical frequency of the structure. The subject's pace frequency ranges from 2.18 to 2.24 Hz. However, the peak acceleration response varies much less here, with values ranging from 1.39 to 1.68 $\text{m} \cdot \text{s}^{-2}$, thus showing less sensitivity in the coupled dynamic response. Even for this subject, the parameter values and ranges obtained (see Table 4.3) produce a good correlation between the model response envelope and the observed data.

Table 4.3.: Perturbed biodynamic parameters obtained for a walking subject at self-selected pace frequency.

Subject	$\mathbf{m_p}$ [kg]		$\mathbf{k_p}$ [$\text{N} \cdot \text{m}^{-1}$]		$\mathbf{c_p}$ [$\text{kg} \cdot \text{s}^{-1}$]		$\mathbf{\dot{q}(t_o)}$ [$\text{m} \cdot \text{s}^{-1}$]		$\mathbf{F_p}$ [Hz]		PAR
	$\bar{\mathbf{m}}_p$	\mathbf{pm} [%]	$\bar{\mathbf{k}}_p$	\mathbf{pk} [%]	$\bar{\mathbf{c}}_p$	\mathbf{pc} [%]	$\bar{\mathbf{q}}(t_o)$	\mathbf{pq} [%]	$\bar{\mathbf{F}}_p$	\mathbf{pf} [%]	
S-06	77	± 1.3	8000	± 50.0	295	± 16.9	0.37	± 16.2	1.93	± 2.1	2.2
S-15	49	± 2.0	14000	± 14.3	400	± 12.5	0.5	± 10.0	2.21	± 1.4	1.2



(a) Subject S-06.



(b) Subject S-15.

Fig. 4.11.: Single experimental record for a subject walking on the structure (solid line) and uPSI model prediction (gray region) at self-selected speed. The two vertical dashed lines indicate when the pedestrian is walking on the beam. (a) and (c) Midspan acceleration amplitude; (b) and (d) Spectrum of instantaneous frequencies versus time. The horizontal dotted line in (b) and (d) represents the first vertical natural frequency of the bare structure.

From these results we conclude that individual test subjects, either when walking at self-selected speed or following a periodic beat, do not walk in a similar manner showing in every trial a spatial-temporal gait variation as shown in Chapter 3. This observation demonstrates an inability to consistently predict the walking patterns of any single subject. However, the PSI model with uncertainties is able to appropriately incorporate modeling errors to capture the broad range of responses obtained in the experimental data. This finding corroborates the concept of intra-subject variability discussed by Živanović (2006) who concludes that deterministic models have a limited ability to predict structural responses due to the use of a unique set of parameters.

4.3.3 Response comparison between subjects using the metronome

Next, to gain some insight into inter-subject parameter variability and its effects, the dynamic responses with different pedestrians are examined. For this analysis, the structural response is compared for fifteen subjects that walk following an audible beat. The experimental and simulated responses when the metronome is set to 1.8, 2.1, and 2.3 Hz are shown in Fig. 4.12(a-f). In these figures, each solid line represents a single experimental record for a different subject walking on the structure.

The parameter ranges needed to capture the variability of these subjects with different biodynamic characteristics are depicted in Table 4.4. Note that the mean value for the pedestrian mass is experimentally obtained in Section 4.2.1 and a variation of ± 30 kg is used in the analytic model. Also, the variability in the pedestrian model parameters, when multiple pedestrians are included, is considerably larger than those obtained when only the structural responses from a single pedestrian are analyzed (see Table 4.2). The increase in these parameters observed is attributed to the necessity of representing the inter-person variation in the parameters.

Table 4.4.: Perturbed biodynamic parameters obtained for walking subjects following an audible beat.

F_m [Hz]	m_p [kg]		k_p [$N \cdot m^{-1}$]		c_p [$kg \cdot s^{-1}$]		$\dot{q}(t_o)$ [$m \cdot s^{-1}$]		F_p [Hz]		PAR
	\bar{m}_p	pm [%]	\bar{k}_p	pk [%]	\bar{c}_p	pc [%]	$\bar{q}(t_o)$	pq [%]	\bar{F}_p	pf [%]	
1.8	85	± 35.3	8000	± 50.0	500	± 20	0.31	± 32.3	1.82	± 2.2	2.9
2.1	85	± 35.3	7000	± 28.6	350	± 28.6	0.82	± 30.5	2.12	± 0.9	1.7
2.3	85	± 35.3	12000	± 25	350	± 21.4	0.35	± 42.9	2.32	± 1.7	1.8

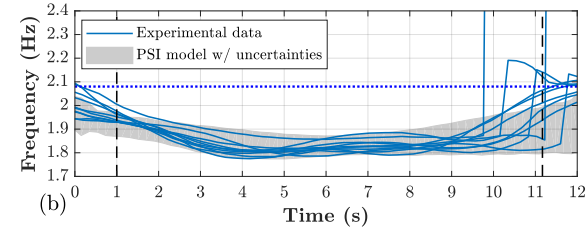
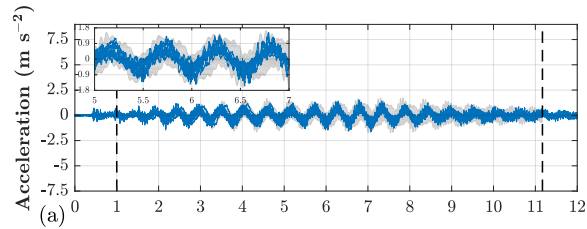
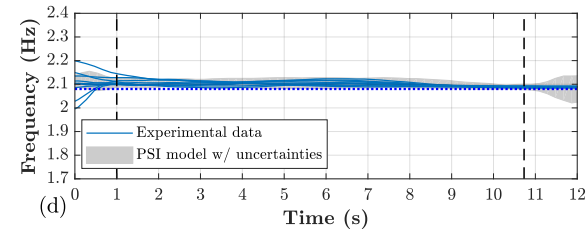
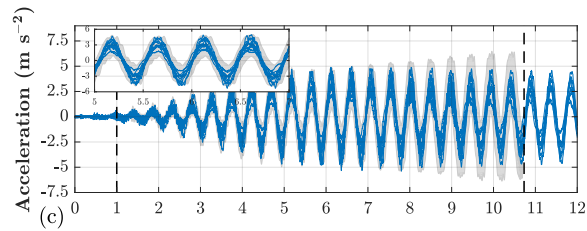
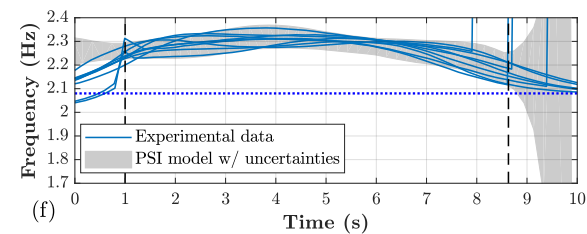
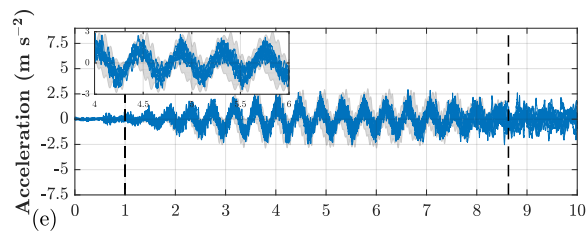
(a) $F_m = 1.8$ Hz.(b) $F_m = 2.1$ Hz.(c) $F_m = 2.3$ Hz.

Fig. 4.12.: Single experimental record for a different subject walking on the structure (solid line) and uPSI model prediction (gray region) following a metronome. (a), (c) and (e) Midspan acceleration amplitude; (b), (d) and (f) Spectrum of instantaneous frequencies versus time.

4.3.4 Response comparison between subjects walking freely

Finally, the structural response comparison produce by each subject walking at self-selected gait frequency is shown in Fig. 4.13. The simulated and experimental acceleration response in time domain is depicted in Fig. 4.13(a), while the instantaneous frequency of the response is shown in Fig. 4.13(b).

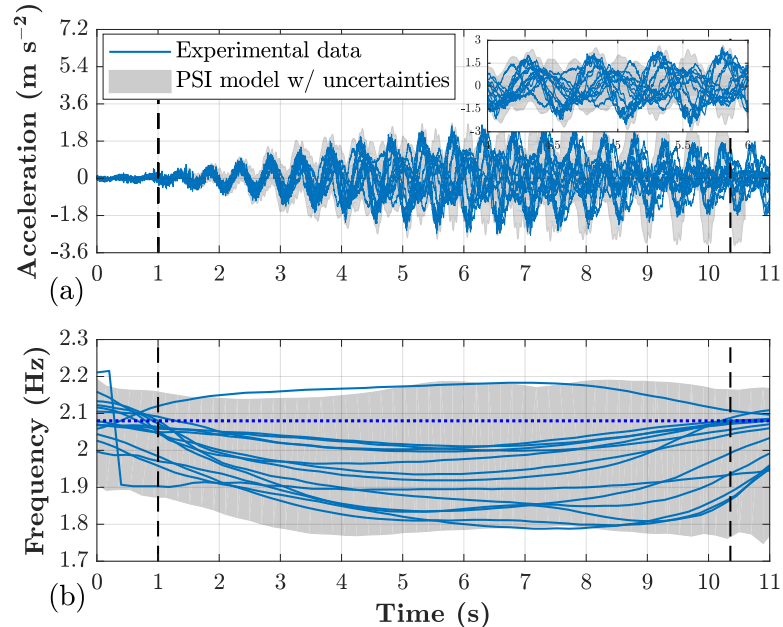


Fig. 4.13.: Single experimental record for a different subject walking on the structure (solid line) and uPSI model prediction (gray region) at self-selected speed. The two vertical dashed lines indicate when the pedestrian is walking on the beam. (a) Midspan acceleration amplitude; (b) Spectrum of instantaneous frequencies versus time. The horizontal dotted line in (b) represents the first vertical natural frequency of the bare structure.

The estimated ranges for the pedestrian parameters are given in Table 4.5. The PAR is 3.3, which indicates the substantial variation in the structural response produced by having different subjects. However, it should be noticed that the nominal value of $\dot{q}(t_o)$ remains lower indicating that when a subject walks at self-selected speed, he/she expends less energy to perform each gait cycle, consistent with published experimental observations (Holt et al., 1995).

The lack of consistency in the pedestrian's parameters verify the hypothesis, that it is important to consider the inter- and intra-subject variability. This need sug-

Table 4.5.: Perturbed biodynamic parameters obtained for walking subjects at self-selected pace frequency.

Subject	\mathbf{m}_p [kg]		\mathbf{k}_p [$\text{N} \cdot \text{m}^{-1}$]		\mathbf{c}_p [$\text{kg} \cdot \text{s}^{-1}$]		$\dot{\mathbf{q}}(t_o)$ [$\text{m} \cdot \text{s}^{-1}$]		\mathbf{F}_p [Hz]		PAR
	$\bar{\mathbf{m}}_p$	pm [%]	$\bar{\mathbf{k}}_p$	pk [%]	$\bar{\mathbf{c}}_p$	pc [%]	$\bar{\dot{\mathbf{q}}}(t_o)$	pq [%]	$\bar{\mathbf{F}}_p$	pf [%]	
All	85	± 35.3	18000	± 16.7	800	± 25	0.32	± 31.3	1.97	± 9.6	3.3

gests that parametric uncertainty should be incorporated when pursuing a robust and comprehensive analysis methodology that can inform the design process. By visually comparing the variation in the experimental data with the envelope of the simulated responses, good agreement is obtained and parameter uncertainties can be quantified using an LFT representations. The results imply, even for the same subject, that the biodynamic parameters c_p , k_p , and $\dot{q}(t_o)$ vary, and they also depend on the pace frequency F_p to compensate for changes in speed and levels of vibration.

Overall, the results demonstrate that the uPSI model predictions for the time-varying, coupled uncertain system can capture the recorded experimental accelerations. The estimated results with these models not only exhibit a bounded response that is similar to the experimental data, but also have good agreement with the time-dependent frequency variation of the response. Furthermore, it is observed that the nominal value and obtained ranges of the pedestrian biodynamic model, shown in Table 4.5, are within the variation ranges reported in earlier studies and documented here in Table 4.1. Thus, simulated bounded envelopes using the parameter ranges identified capture the interval of possible responses of this combined pedestrian-structure system in both the time and frequency domains. The uPSI model provides a comprehensive view of the possible variations in the response. It also demonstrates the importance of explicitly describing the uncertainty, and thus enabling robust design and analysis to meet realistic serviceability specifications.

4.4 Summary

In this chapter a pedestrian-structure interaction model that is intended to capture the variability of human biodynamic parameters is developed. The predicted responses are generated using a closed-loop configuration with a moving contact point to define the pedestrian location. The envelope for the experimental responses is obtained using the LFT with structured uncertainties, yielding closed-bound intervals

for the biodynamic parameters. Using several tests with a single subject, a parameter range is determined that captures the variability associated with a single subject. Then the response of the structure with several different subjects are examined, and the associated intervals are also determined to capture the variability in the biodynamic parameters for several different subjects.

5. EXPERIMENTAL AND NUMERICAL VIBRATION SERVICEABILITY ASSESSMENT OF A FOOTBRIDGE

5.1 Introduction

In this chapter an assessment of the vibration serviceability limit state of an in-service pedestrian bridge is performed. The approaches used in current guidelines are implemented to assess the serviceability criteria in a full scale footbridge based on normal operating conditions of the structure. The experimental program consists of both ambient response measurements and human-induced vibration to capture the dynamic characteristics of the operational footbridge. The identified fundamental vibration frequency in the vertical direction based on ambient measurements lies in a critical frequency range near the pace frequency, thus a vibration comfort assessment is required using the current design standards. To obtain the peak acceleration responses of the structure, experimental results for different human-induced load conditions are used. Then, numerical simulations using a pedestrian-structure interaction model are conducted to obtain the robust prediction response. These are used to demonstrate that the proposed methodology described in Chapter 4 can be easily adopted to assess the serviceability comfort limit in the design stage.

Although a crowd-loaded scenario is the ideal traffic case with different pedestrian densities, there are no common criteria regarding the number of individuals to assume in a crowd, the density of pedestrian traffic, or the degree of pace synchronization. Therefore, the complexity of the model becomes impractical and unrealistic. Besides, most of the guidelines use an estimated response for a single pedestrian modified by a factor to represent crowd-induced vibration on a structure (Van Nimmen et al., 2014). Hence, a simple but refined pedestrian-structure interaction model to account for the randomness in the dynamic properties of the walker is used here.

This chapter is organized as follows. Section 5.2 describes the experimental study conducted in a full scale pedestrian bridge. Ambient vibration measurements are used to estimate the operational modal characteristics of the bridge. An FE model is developed and updated based on the identified vibration frequencies and modal damping ratios. Section 5.3 presents the vibration serviceability assessment of the

footbridge and its comparison with current codes and standards. Several experimental human-induced load tests are conducted with one, two, and three pedestrians crossing the structure. The experimental bridge response data are then compared against the predicted structural response envelopes using the uncertain PSI model for different pace frequencies. Finally, the results from the experimental results and the acceptability comfort criteria are presented in the Summary.

5.2 Footbridge description and experimental setup

A pedestrian bridge is selected with the aim to assess the response of a modern structure under service conditions. The Hackberry Lane Pedestrian Bridge (see Fig 5.1), built in 2013 on the campus of the University of Alabama in the city of Tuscaloosa, is adopted to conduct a footbridge serviceability analysis in this study. The structure is an instrumented footbridge that exhibits dynamic interaction when crossed by pedestrians. The footbridge, based on a note in the original drawings, was designed in accordance with the [AISC \(2011\)](#). The crossbow bridge is made of steel and concrete with a span length of 44.35 m between abutments and a width of 3.65 m. Two trusses support a 6 in galvanized composite concrete floor deck with floor beams at regular intervals along the length of the bridge. In the design phase, the pedestrian bridge was analyzed for a uniform dead load of 90 psf and a live load of 85 psf, with allowed live load reduction up to 65 psf. An additional live load of 5 tons was included to consider light vehicle traffic on the bridge in the design.



Fig. 5.1.: Hackberry Lane pedestrian bridge in Tuscaloosa Alabama.

5.2.1 Full scale measurements

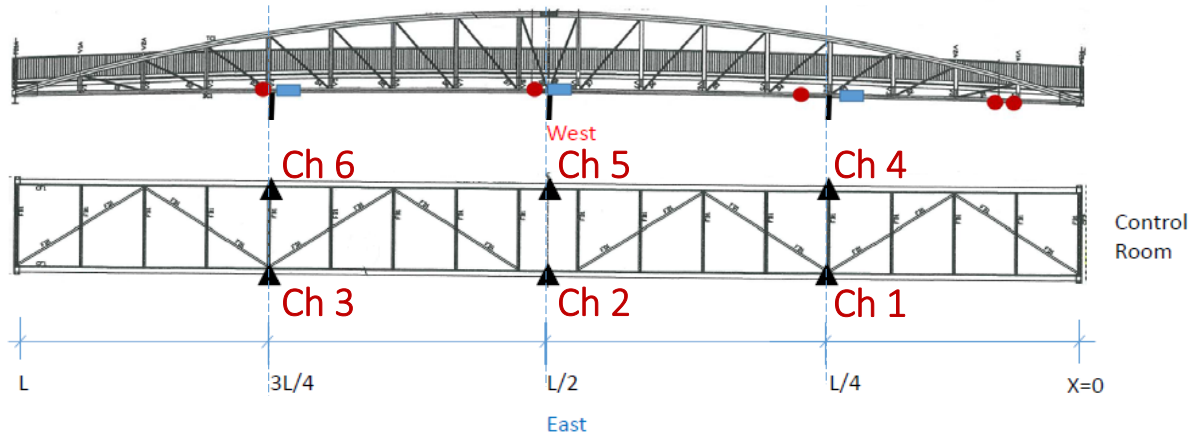
The pedestrian bridge is instrumented with six PCB 393B31 uniaxial accelerometers to capture vertical vibrations of the structure (see Fig. 5.2). The sensitivity of the sensors is ($\pm 5\%$) $10 \text{ V}\cdot\text{g}^{-1}$ with a frequency range of ($\pm 5\%$) 0.1 to 200 Hz. These sensors are connected to the data acquisition system with standard cables. The data acquisition software package used in the testing program was configured with a sampling frequency of 1024 Hz.

Ambient vibration tests are conducted to identify the natural frequencies, vibration modes, and modal damping ratios of the footbridge. The experimental data is analyzed to identify the modal characteristics of the bridge. Several different ambient acceleration response measurement sets are used in this analysis. The time history and time-frequency representation from a representative ambient experimental acceleration response recorded during the experiments (Channel No. 4 in Fig. 5.2) are shown in Fig. 5.3(a). Using the stochastic subspace identification (SSI) algorithm, an operational modal analysis using output-only measurements are conducted. The stabilization diagram together with the power spectral density (PSD) of the response are superimposed to identify the stable poles of the structure, as shown in Fig. 5.3(b). It is shown that stable frequencies associated with the predominant modes are found.

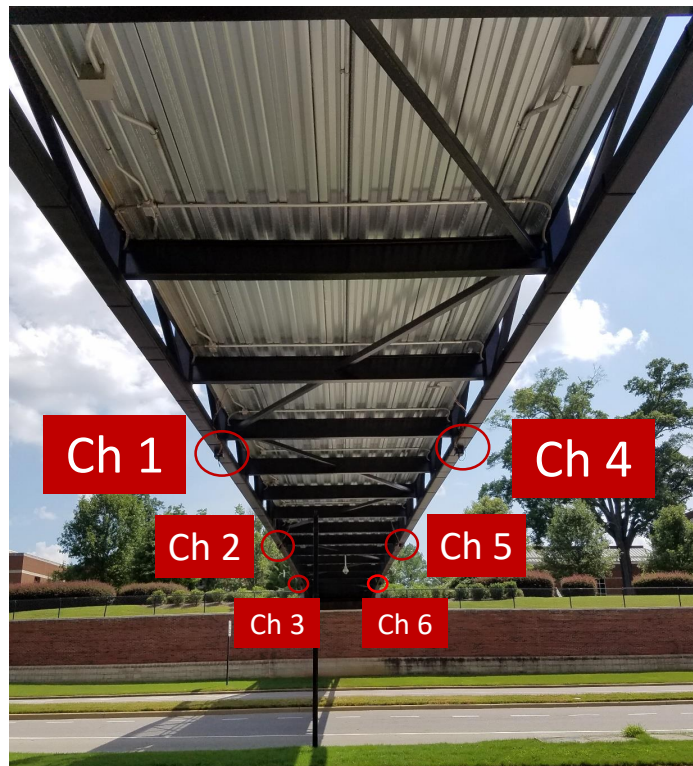
The first three vertical modes are at 2.26, 5.29 and 9.11 Hz, which correspond to the 1st, 4th and 6th mode shapes, respectively, as shown in Fig. 5.4. The damping ratios associated with the first three vertical modes are identified to be 1.1%, 0.97% and 0.88%. The first two torsional modes are at 2.64 Hz and 7.3 Hz with associated damping ratios of 0.97% and 1.91%, respectively. The torsional modes are the 2nd and 5th mode shapes. Although, there are no measurements taken in the lateral direction, a mode shape in this direction is obtained. The 3rd identified mode at 3.79 Hz is found to be associated with the 1st lateral mode based on the numerical model presented in Section 5.2.2.

5.2.2 Numerical modeling of the footbridge

Based on the structural drawings of the bridge (Lansdell et al., 2017; S. Zhou & Song, 2018), a 3-D finite element model (FEM) of the bridge is built assuming linear elastic behavior using SAP2000TM (Computer & structures, 2017). The structural members are modeled as beam elements with each node having 6-DOF. The



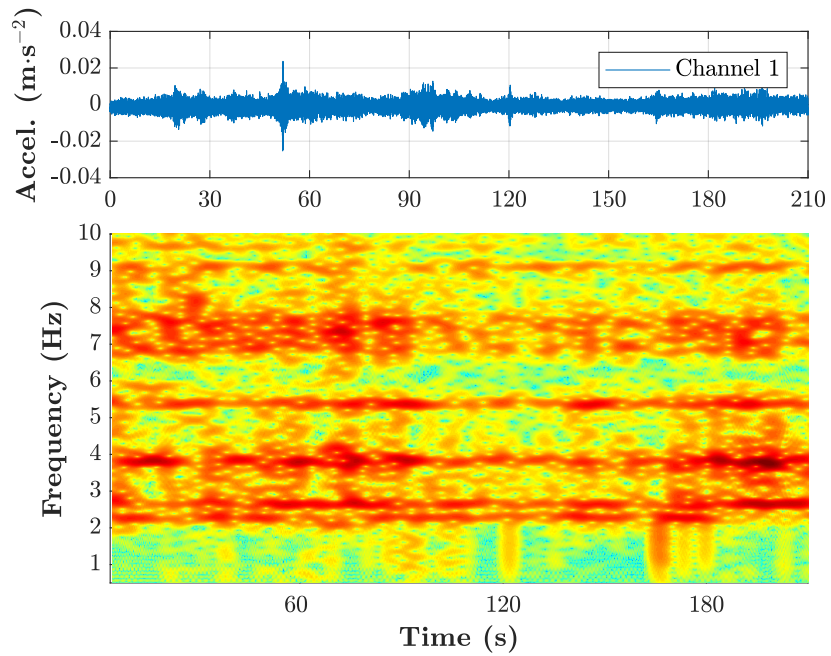
(a) Elevation and plan views of the footbridge structure.



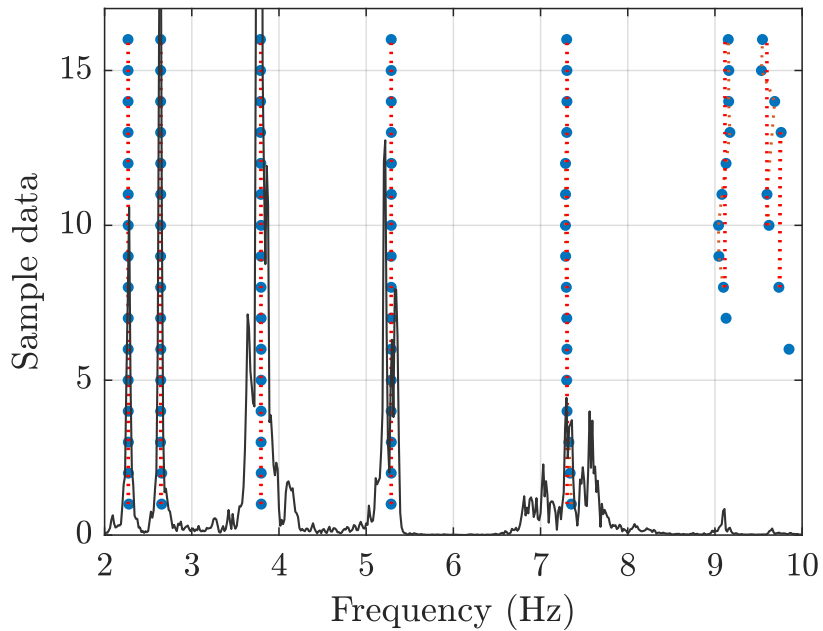
(b) Accelerometers in the vertical direction in the structure.

Fig. 5.2.: Details of the instrumented pedestrian bridge.

total number of DOF in the FE model is 1038, including the rotations as the boundary conditions at the supports. The geometry, element connectivity, superimposed loads, element sections, and material properties of the SAP2000 model are output to MATLABTM (MATLAB, 2017). The above-mentioned information is then used to



(a) Structural acceleration under ambient vibration and time-frequency representation of the measured responses of the bridge.



(b) Stabilization diagram obtained from SSI algorithm and power spectral density as reference.

Fig. 5.3.: Measured ambient response of the bridge (Channel No. 4).

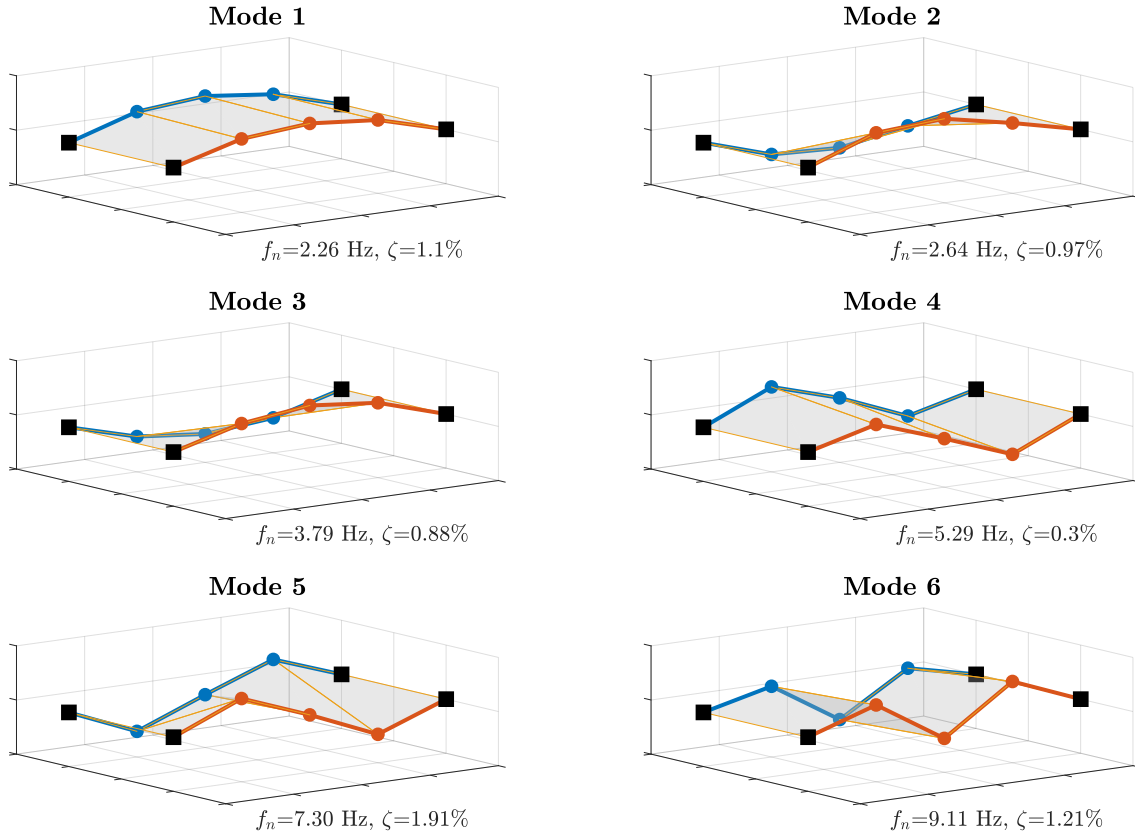


Fig. 5.4.: Identified mode shapes of the footbridge. Mode 1: 1st vertical. Mode 2: 1st torsional. Mode 3: 1st lateral . Mode 4: 2nd vertical. Mode 5: 2nd torsional. Mode 6: 3rd vertical.

develop a FEM able to be used to perform a dynamic analysis applying the framework described in Chapters 2 and 4.

To reduced the order of the FE model without loss of relevant and necessary information, a lumped mass matrix per element based upon their tributary areas with zero rotational mass is used in MATLAB. DOFs with small mass (less than 1% of the maximum value) are neglected and assumed as zero. Then, static condensation is applied by apportioning the mass and stiffness matrices into dynamic (non-zero mass) and zero mass DOF. Once this step is completed, the transformation matrix is determined, and the condensed mass and stiffness matrix are obtained. This series of operations reduces the model to 213-DOFs. These assumptions are confirmed by comparing the frequencies and mode shapes obtained with the SAP2000 model and the reduced model (see Fig. 5.5). The modal characteristics of the SAP2000 model,

which incorporates all vertical and rotational DOFs, is compared with the reduced model, which results in error values several orders of magnitude smaller than the initial model. Based on these results the DOF reduction applied to obtain a reduced order model seems to be realistic. The reduced model is compared based on the experimental modal analysis data to match, as close as possible, the first vertical mode shape and its corresponding frequency, as shown in Table 5.1.

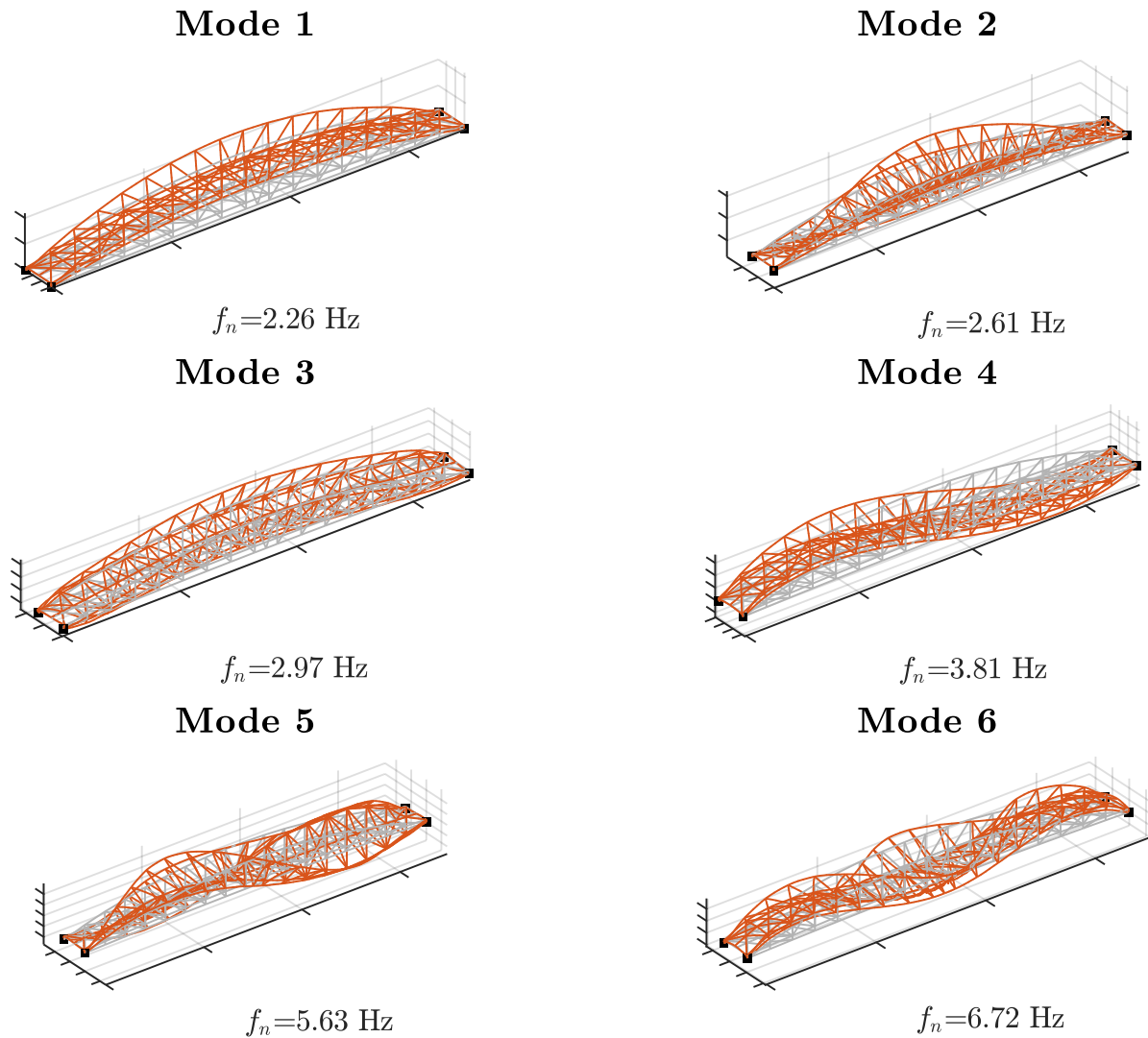


Fig. 5.5.: Analytical mode shapes of the footbridge. Mode 1: 1st vertical. Mode 2: 1st torsional. Mode 3: 1st lateral. Mode 4: 2nd vertical. Mode 5: 2nd torsional. Mode 6: 3rd vertical.

Table 5.1.: Experimental and FEM modal parameters of the footbridge.

Mode Shape	Experimental		SAP2000	MATLAB
	f_n [Hz]	ζ [%]	f_n [Hz]	f_n [Hz]
1 st vertical	2.26	1.10	2.26	2.26
1 st torsional	2.64	0.97	2.61	2.61
1 st lateral	3.79	0.88	2.97	2.97
2 nd vertical	5.29	0.30	3.81	3.81
2 nd torsional	7.30	1.91	5.63	5.63
3 rd vertical	9.11	1.21	6.72	6.72

Using the obtained experimental modal damping ratios (see Table 5.1), the damping matrix is formed by assuming proportional damping, as given by

$$\mathbf{C}_{\text{str}} = (\mathbf{\Phi}^\top)^{-1} \hat{\mathbf{C}}_{\text{str}} \mathbf{\Phi}^{-1} \quad (5.1)$$

where $\mathbf{\Phi}$ is the modal matrix and the $(\cdot)^\top$ symbol denotes the transpose operation. In this equation $\hat{\mathbf{C}}$ is

$$\mathbf{\Phi}^\top \mathbf{C}_{\text{str}} \mathbf{\Phi} = \hat{\mathbf{C}}_{\text{str}} = \begin{bmatrix} 2\zeta_1\omega_1m_1 & & & & \\ & 2\zeta_2\omega_2m_2 & & & \\ & & \ddots & & \\ & & & \ddots & \\ & & & & 2\zeta_n\omega_nm_n \end{bmatrix} \quad (5.2)$$

where ζ_i , ω_i and, m_i are the modal damping ratio, the natural frequency, and the generalized modal mass of the i -th mode shape, respectively.

5.3 Serviceability assessment for vertical vibration

The forced vibration response measurements of the footbridge are obtained when one, two, and three pedestrians walked along the structure. The pedestrians walk at a prescribed cadence where the pace frequency is synchronized by a metronome's beat. In the analysis, each pass across the bridge is considered as a trial. Several trials at a prescribed cadence are completed, where the metronome's frequency is set to 1.7, 1.9, 2.0, 2.1, 2.15, 2.2 and 2.3 Hz. Here, comparisons are made between the measured vertical acceleration responses of this footbridge, the uncertain PSI model

prediction using the obtained ranges of the biodynamic parameters in Chapter 4, and the serviceability standards in current guidelines.

5.3.1 Experimental assessment of pedestrian-induced vibration

The serviceability is examined by comparing the responses of the same participant walking at different prescribed cadences. Distinct trials are investigated for different pedestrian load conditions to evaluate the vibration levels on a footbridge. The pedestrian walked while following an audible beat with a specified frequency F_m produced by a metronome. Two representative plots showing the measured acceleration responses for each trial (solid line) and their corresponding time-frequency representations, are depicted in Fig. 5.6 for one pedestrian and in Appendix B for two and three synchronized pedestrian, respectively. The experimental results in these figures correspond to the cases in which the frequency of the metronome's beat was set to 1.7, 1.9, 2.2, and 2.3 Hz. Note that when the pedestrian walk following the beat at 2.2 Hz, the maximum amplitude of the acceleration response is obtained. Thus, resonance effects are produced in the pedestrian bridge. Even for only one pedestrian (see Fig. 5.6), the amplitude of the vertical acceleration response reached $0.6 \text{ m}\cdot\text{s}^{-2}$ when the pace frequency is near the first vertical natural frequency of the structure.

Horizontal stripes in time-frequency plots show the qualitative energy content due to the dominant harmonics of the pedestrian load that excite a particular mode shape. For instance, the pedestrian, in Fig. 5.6(a), follows the metronome's beat walking at 1.7 Hz. Then, induced harmonics appear at 1.7, 3.4, 5.1, 6.8 Hz and so on. Hence, the 2nd vertical mode of the structure at 5.3 Hz is excited by the 3rd harmonic of the load showing a dark red stripe at that frequency. Similar effect happens when the metronome is set to 1.9 Hz (see Fig. 5.6(b)). The harmonics of the pedestrian load produce responses in the vertical mode shapes at 2.26, 5.3, 9.1 Hz, as well as in the torsional modes at 2.64 and 7.3 Hz. It means that the input energy provided by the pedestrian is spread and dissipated in different modes without increasing the structural response. However, when the pedestrian walks at 2.2 Hz (see Fig. 5.6(c)), the energy that is input by the walking force is concentrated mostly in the first mode, producing a resonant condition that increases the response of the bridge. Finally, when the metronome's beat is set to 2.3 Hz, the 1st and 3rd modes of the structure are excited by the 1st and 4th harmonics of the walking load, respectively (see Fig. 5.6(d)).

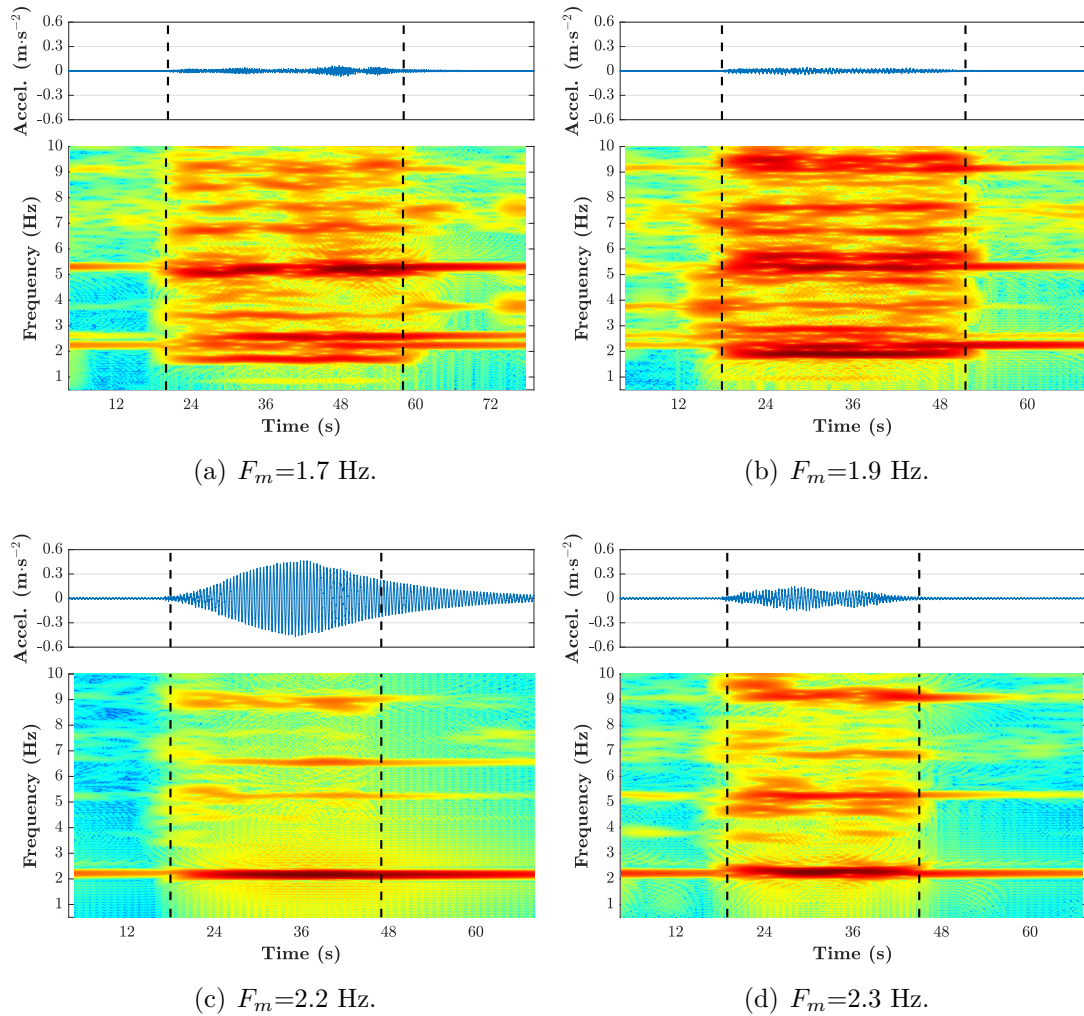


Fig. 5.6.: Vertical accelerations due to a pedestrian walking at different frequencies (Channel No. 04).

Similar behavior can be distinguished when two and three synchronized pedestrians walk along the footbridge as shown in Appendix B.

5.3.2 Comparison with current standards

The vibration serviceability requirement in current guidelines is a two-step procedure (Gheitsi et al., 2016). First, a limit value for the vibration frequency is compared with the natural frequencies of the footbridge. If the structure does not meet this requirement because one or more frequencies lie in the critical frequency

range specified for the code, the second step needs to be conducted. The second step includes a more comprehensive dynamic analysis, where the structural acceleration response is obtained since the fundamental frequencies are close enough to the pace frequency and its harmonics. Then, vibration comfort is assessed comparing the acceleration results with the maximum allowable acceleration values recommended in current guidelines (see Table 1.2). The design codes evaluated in this study are: AASHTO (2009), ISO-10137 (2007), Eurocode-5 (EN 1995-2, 2004), and Sétra (2006). Even when these standards are based on frequency and acceleration criteria, all of them have different comfort limit approaches to account for the acceptability of vibration.

The experimental results show that the natural frequency at 3.79 Hz associated with the lateral mode shape of the footbridge is in accordance with the frequency criterion in the guidelines. This confirms there is no risk of resonance under medial lateral pedestrian load. Therefore, this case is not analyzed in this study. However, the frequency of the first mode in vertical direction (2.26 Hz) lies in the critical frequency range established by the mentioned codes (see Fig. 5.7(a)). As a result, the acceleration response of the bridge at the midspan needs to be verified. The maximum vertical acceleration for one (Fig. 5.7(b)), two, and three (Fig. 5.7(c)) pedestrians are assessed in terms of vibration comfort levels. The comparison between the experimental peak accelerations and the maximum allowable values in the codes, as well as the comfort regions established by Sétra (2006), are reported in Fig. 5.7(b and c) for one and three pedestrians, respectively.

For one pedestrian crossing the bridge (see Fig. 5.7(b)) the predicted maximum acceleration calculated with Sétra (2006) (dashed-dotted line) and Eurocode-5 (EN 1995-2, 2004) (dash line) are $0.18 \text{ m}\cdot\text{s}^{-2}$ and $0.26 \text{ m}\cdot\text{s}^{-2}$, respectively. Notice that these peak accelerations limits are lower than those obtained during the experimental test when the metronome was set to 2.2 Hz. At this pace frequency the footbridge peak acceleration reached $0.6 \text{ m}\cdot\text{s}^{-2}$ exceeding the maximum comfort region established by Sétra (2006). The vertical acceleration limit defined by ISO-10137 (2007) is not a function of the number of pedestrians because it is established as an upper limit to keep the vibration in a comfortable level. Thus, the limit value for this code remains the same, no matter the number of pedestrians walking on the bridge.

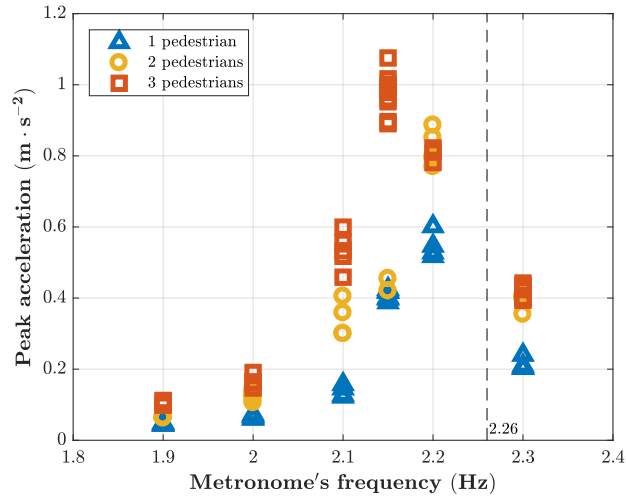
For three synchronized pedestrian (see Fig. 5.7(c)), the experimental peak accelerations recorded at $F_m=2.15 \text{ Hz}$, exceed the maximum allowable acceleration limits established by Eurocode-5 (EN 1995-2, 2004), Sétra (2006) and ISO-10137 (2007),

whose maximum predicted values are 0.26, 0.31 and $0.7 \text{ m}\cdot\text{s}^{-2}$, respectively. It should be mentioned that the density of the pedestrian crowd is defined as the number of pedestrians over the deck (Sétra, 2006; Heinemeyer et al., 2007). For this test, the density due to three pedestrians on the bridge is $0.02 \text{ pedestrians}\cdot\text{m}^{-2}$. Because this value is found to be extremely low considering the location of the footbridge on the University campus, it is very likely that a dense traffic condition might occur. For a dense traffic load Sétra (2006) and Hivoss (Heinemeyer et al., 2007) suggest $0.8 \text{ pedestrians}\cdot\text{m}^{-2}$ as the density considered in the design, representing a group of 140 synchronized pedestrians over the bridge at the same time. Using this pedestrian density value, the estimated peak acceleration on the bridge is $1.9 \text{ m}\cdot\text{s}^{-2}$, which is in the minimum comfort region.

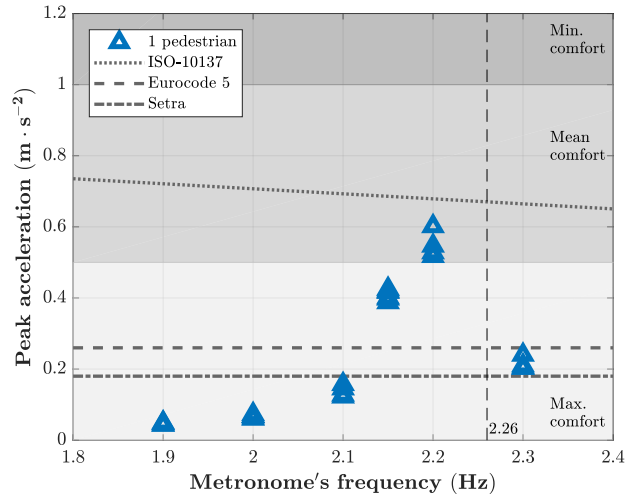
It can be seen in Fig. 5.7(b and c) that under walking-induced loads, the levels of accelerations exceed the recommended limits proposed by the considered guidelines. These results are in agreement with the pedestrian perception of vibrations during the experiments. Thus, the acceptance criteria for human serviceability conditions of the footbridge are not suitable, even for only one pedestrian, hence, vibration comfort is not assured.

5.3.3 Numerical prediction of the structural response

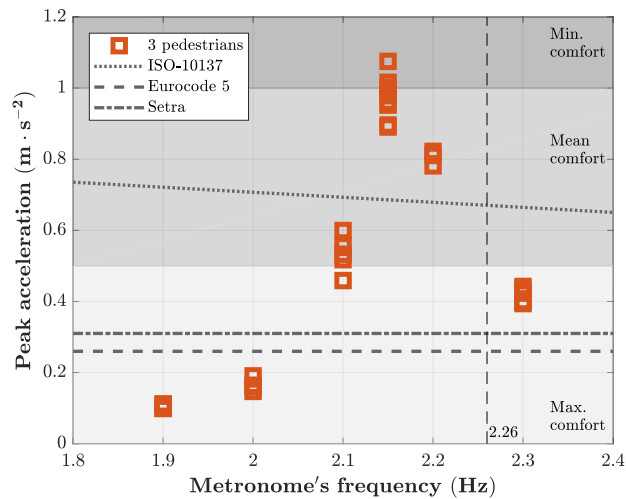
Finally, a simulation using the framework developed in this dissertation is used to demonstrate that the pedestrian-structure behavior can be successfully anticipated in the design stage. A comparison is made between the experimental and predicted responses to demonstrate the validity of the approach proposed in Chapters 2 and 4. The robust response prediction of the footbridge is conducted using the modular framework developed in Chapter 2. Because the human influence on the structure has revealed considerable randomness that is not considered in any code, the pedestrian is modeled as an uncertain dynamic subsystem represented by a single SDOF oscillator. To represent the variability of the pedestrian's dynamic characteristics, uncertainties are included in the pedestrian subsystem following the procedure established in Chapter 4. The pedestrian subsystem parameters such as, mass m_p , damping c_p , stiffness k_p , pace frequency F_p , and the vertical body COM initial velocity $\dot{q}(t_o)$, are assumed to be uncertain-but-bounded parameters. The biomechanic parameter ranges in Table 4.5 are used to model a single pedestrian under a specific pace frequency condition. The structural parameters of the footbridge are considered



(a) Midspan peak acceleration as a function of the metronome's frequency.



(b) One pedestrian.



(c) Three pedestrians.

Fig. 5.7.: Vibration serviceability assessment of a footbridge under pedestrian-induced loads.

to be known. Thus, variations on the structural subsystem parameters are not taken into account.

The experimental and simulated responses when the metronome is set to 1.7, 2.2, and 2.3 Hz are shown in Fig. 5.8(a-c). The prescribed frequencies at 1.7 and 2.3 Hz are chosen to represent the minimum and maximum credible pace frequency of a pedestrian. Due to the dynamic characteristics of the bridge, the level of interactions between the pedestrian and structure at these frequencies is low. However, a high level of interaction is noticeable when F_m is set 2.2 Hz. Each solid line represents the vertical acceleration recorded at the midspan of the footbridge in a single test, while the gray region depicts the envelope of simulated response. By visually comparing the variation in each trial in the experimental test with the envelope of the simulated responses, good agreement is obtained. The PSI model with uncertainties is able to appropriately incorporate modeling errors to capture the broad range of responses exhibiting a bounded response that is similar to the experimental data. Therefore, it is observed that the simulated bounded envelopes using the parameter ranges identified in Chapter 4 capture the interval of possible responses of this combined pedestrian-structure system.

To perform a robust estimate of the structural response, parametric uncertainties should be incorporated into the analysis prior to the design stage. Prediction of the bridge's dynamic response obtained according to current codes might differ from the real value of an operational bridge revealing, in some cases, unexpected behavior. Therefore, this framework can easily be applied for a serviceability assessment to address the vibration effects under pedestrian-induced loads considering the inter- and intra-subject variability. This type of analysis, performed at design stage, can help to determine if there is a need for an adjustment in the structural design or implementation of an energy dissipation device.

5.4 Summary

This chapter presents the vibration serviceability assessment of an in-service footbridge under controlled walking-induced load. An experimental program including ambient measurements as well as pedestrian-induced vibration is conducted to obtain the dynamic characteristics of the footbridge in both empty and in-service conditions. A reduced order numerical model is built and used with the framework developed in this dissertation to consider pedestrian uncertainties and interactions. Experi-

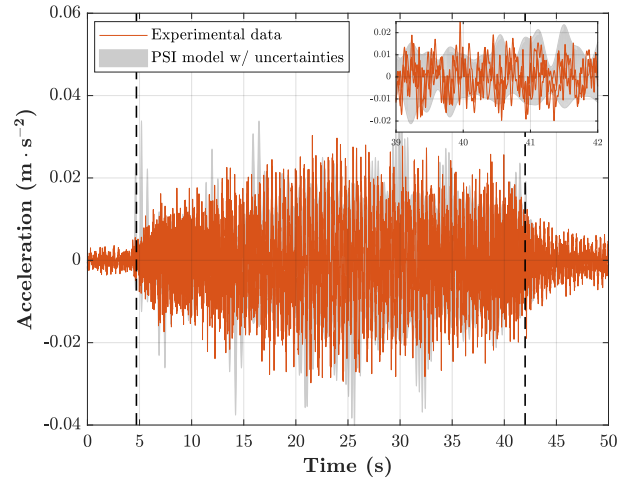
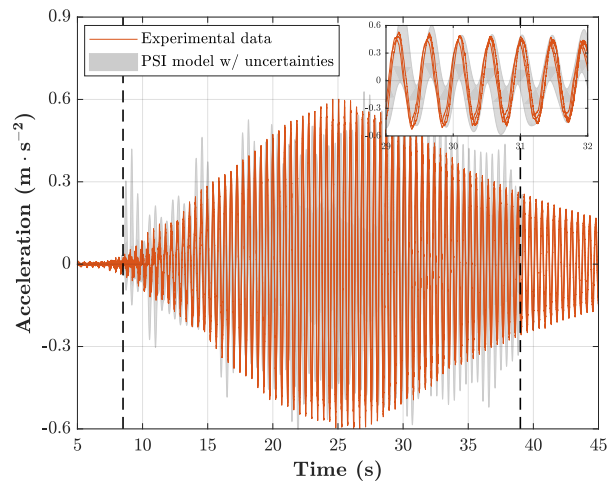
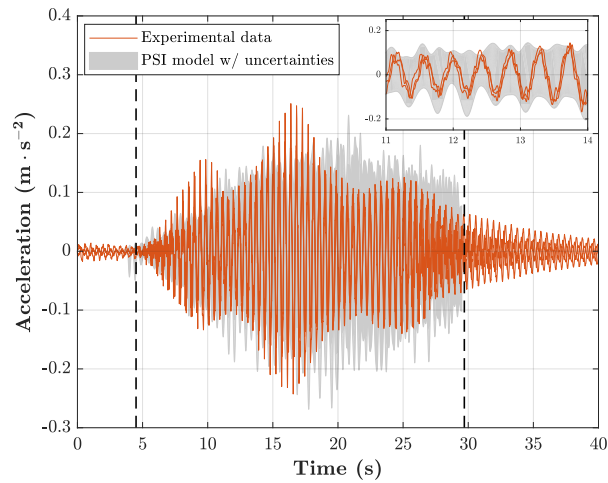
(a) $F_m = 1.7$ Hz.(b) $F_m = 2.2$ Hz.(c) $F_m = 2.3$ Hz.

Fig. 5.8.: Midspan acceleration amplitude of three experimental trials for a pedestrian walking on the footbridge (solid line) and uncertain PSI model prediction (gray region). The two vertical dashed lines indicate when the pedestrian enters and leaves the bridge.

tal responses for different pedestrian load conditions are used to obtain observations of the dynamic behavior of the bridge. Serviceability verification of the footbridge is performed using current standards and guidelines. Two general alternatives are typically considered to enhance the serviceability performance of a footbridges. The first option is to increase the stiffness of the structure to shift its natural frequencies out of the range excited by pedestrians. This criterion is the first to be considered in any design code. However, the stiffening solution will also increase the mass and sometimes could be very intrusive. The second option is to increase the damping of the bridge to reduce the resonant response. However, this alternative is not explicitly defined in any code or standard. Thus, further investigation should be conducted to design and implement dissipative devices in the analysis and design stages of the structure.

The assessment results show that the predicted maximum acceleration responses by Eurocode-5 ([EN 1995-2, 2004](#)), [Sétra \(2006\)](#), and [ISO-10137 \(2007\)](#) differ from the experimental results obtained for controlled single pedestrian and synchronized crowd conditions. The recorded experimental acceleration data of the bridge exceed the acceptable comfort limits established by these guidelines. The peak acceleration of the structure is underestimated when the pace frequency is close to the fundamental frequency. Consequently, a more comprehensive dynamic analysis is required to estimate reliable vibration levels, particularly when the fundamental frequency in vertical direction of the bridge lies in the pace frequency range (between 1.6 to 2.4 Hz) where vibration problems are expected.

Finally, the framework developed in this dissertation is used to predict pedestrian-structure behavior during the design stage. The simulated bounded envelope responses using the parameter ranges identified in [Chapter 4](#) show good agreement with the experimental data. It demonstrates that the proposed uncertain PSI model is able to capture the interval of possible responses of this combined pedestrian-structure system when the uncertainties are described explicitly, thus enabling robust design and analysis to meet realistic serviceability specifications.

6. CONCLUSIONS AND RECOMMENDATIONS

In this dissertation, rational analyses of pedestrian-structure interaction have been performed to properly incorporate these dynamic effects toward more realistic structural designs. A comprehensive analysis and experimental program was conducted to quantify both the spatial-temporal variations in gait characteristics when a pedestrian is influenced by vertical vibrating conditions and the sensitivity of the structural response to walking-induced loads including biodynamic parameter variations. The common point of interest between human motor behavior, feedback systems and serviceability design of structures results in significant contributions in diverse fields. By blurring these research boundaries, the understanding of pedestrian-structure interaction is pushed further, enabling structural designers to perform an appropriate analysis and design that achieve desirable performance with realistic response variations. Thus, key knowledge yielding better understanding and modeling of the effects of pedestrian-induced dynamic actions on a structure was developed in this dissertation.

To take into consideration pedestrian-structure interaction effects, a sequential strategy is proposed to be incorporated into the structural analysis and design. In the future, this approach might be followed to become a simple but effective design procedure. First, a refined PSI model to account for the interaction and randomness in the dynamic properties of a walker must be used. Although a crowd-loaded scenario is the ideal traffic case with different pedestrian densities, there are no common criteria regarding the number of individuals to assume in a crowd, the density of pedestrian traffic, nor the degree of pace synchronization. Therefore, the complexity of the model becomes impractical and unrealistic. Thus, a novel substructuring model that is able to simulate the interaction between a pedestrian and structure adequately was developed in this dissertation for improved structural response prediction.

Furthermore, by studying the influence of a lively structure on the pedestrian gait characteristics, the kinematic variation in terms of step length, step width, pace frequency, and gait speed were found to have significant differences on a stationary surface as compared to a moving surface under walking condition. The results showed a pedestrian's tendency to modify and adapt one's gait based on the amplitude and

the frequency of the vibration, which is likely either for stability balance or metabolic energy minimization. Based on these results, the assessment of these gait changes in the design process could be meaningful for the serviceability of pedestrian structures they must be included at the design stage using the values indicated in Table 3.2.

Then, an explicit description of the pedestrian variability must be used to obtain a robust design model fully capable of meeting realistic serviceability specifications. A systematic approach to combine the developed feedback model with gait variability and intra- and inter-subject biodynamic uncertainties was implemented to provide a robust model suited to highlight the sensitivity of the structural response to pedestrian parameter randomness. Based on these variations, appropriate ranges for the uncertain biodynamic parameters of the pedestrian were determined in Table 4.5 and can be used by generating an arbitrary number of simulations to assess the structural responses. Thus, these findings highlight the effect of human-structure interaction and emphasize the importance of including this variability in high-fidelity models.

A serviceability verification of a footbridge was performed using the acceptable comfort limits established by current standards and guidelines. The assessment showed that the recorded experimental acceleration data of the bridge differed from the estimated peak acceleration response obtained using the equations provided by guidelines. It can be concluded that there is no unified agreement in the serviceability assessment procedures to account for vibration comfort levels. Even the most advanced standards and guidelines need to be carefully considered in the design stage due to unforeseen results. Therefore, for any pedestrian structure, whose fundamental frequency in vertical direction lies in the range of the pace frequency (between 1.6 to 2.4 Hz), a comprehensive procedure must be conducted as an alternative to reduce the structural vibration.

First, structural design processes currently assume the pedestrian load as static, which might be not appropriate when the vertical frequency of the structure is between 1.6 and 2.4 Hz. A simple pedestrian-structure model must be used to include the bidirectional forces between the coupled system. Second, design guidelines must reconsider the frequency criterion where the fundamental frequency needs to be high enough to avoid dynamic amplification under pedestrian activities to offer other options when, for aesthetic or economic reasons, the frequency of the system cannot be increased to guideline limits. Increasing the stiffness to shift the natural frequencies of a footbridge out of the range excited by pedestrians might be unrealistic and even unreasonable. Decreasing the mass it is also not easy in pedestrian structures where

non-structural elements are not pervasive. Therefore, for any pedestrian structure, whose fundamental frequency in vertical direction lies in the range of the pace frequency (between 1.6 to 2.4 Hz), the use of supplemental devices such as a tuned mass damper (TMD) and/or damper devices is recommended to decrease annoying excessive vibration that is present even under low traffic conditions. The results and methodologies here establish a clear understanding of walking-induced load effects in structures, yielding rational knowledge for improving analysis procedures and design guidelines for pedestrian structures where vibration leads to a reduction in serviceability.

6.1 Future research perspectives

Some recommendations for future studies to improve the concepts and methodologies developed in this dissertation include:

- The proposed substructured model is presented and shown to be effective in modeling the coupled dynamics associated with pedestrian-structure interaction. The results demonstrated that the PSI model provides an effective and reliable approach to simulate the interaction. Furthermore, the flexibility of this framework could easily incorporate different pedestrian activities and more complex models, of either pedestrians or bridges, and could also be used as a framework to consider advanced damping devices or structural control systems.
- In the proposed models, PSI and uncertain PSI, the single and double phase portions of the pedestrian stance is not distinguished. Future improvements should consider the possibility to model each leg as a spring and damper to consider a more natural stride in the simulation. Furthermore, the possibility of separation of the pedestrian from the bridge should be considered. This model could readily be extended in the future to consider a running or jumping human, or to consider variable walking speeds, as needed.
- This study provides a more complete spatial and temporal analysis of the human gait parameters when the pedestrian is influenced under vertical vibrating conditions. The results provide a better understanding of the pedestrian intra-subject gait changes on a lively surface. These findings will enable structural engineers to incorporate gait changes in realistic pedestrian models in the analysis and design of structures. However, an extensive statistical analysis with

more test subjects, at both moving and rigid surfaces, will refine parameters regarding the gait variability ranges. Then, their implementation with the PSI model will yield high-fidelity pedestrian-induced load models providing a better serviceability prediction of the structural response.

- The frequency criterion in guidelines where the fundamental frequency needs to be high enough to avoid dynamic amplification under pedestrian activities should be reconsidered. Fundamental frequencies higher than 5 Hz are unrealistic for structures with longer spans. Even 3 Hz is a very strict criterion that might not control the vibration requirements for serviceability and safety conditions. The guidelines should allow an alternative design approach to add external damping to reduce the response, if the fundamental frequency of the structure is between 1.6 and 2.4.
- The response of the pedestrian-structure system is dominated by the pedestrian-induced load that behaves as a quasi-periodic load with very well defined harmonic components. Thus, the effectiveness of a tuned mass damper (TMD) is considerably less than that expected due to the fact that conventional TMDs are highly sensitive for the variability of the excitation and the modal changes of the system. An optimal design of a TMD capable to take the transient loading and the dynamic effects of the pedestrian-structure interaction into account, should be further studied to decrease the footbridge response and improve the serviceability requirements.
- Currently modal analysis is extensively used in PSI due to their ability to represent a MDOF system into a set of SDOF. However, the assumption of proportional damping is often used and undamped modes which uncouple the mass and stiffness matrices do simultaneously uncouple the damping matrix. However, the influence of a crowd-structure system, where is well know that the human body is a highly damped system, might not allow to decouple the equation of motions due to non-proportionally damped modes in the coupled system. Further analysis in grandstands and theatres where people are sitting would be an ideal scenario to evaluate if the assumption of proportional modes is still valid.

References

- AASHTO. (2009). *LRFD guide specifications for the design of pedestrian bridges* (No. T-5 (WAI 31)).
- AISC. (2011). *Steel construction manual* (14th ed.). American Institute of Steel Construction.
- Alexander, R. (1995). Simple models of human movement. *Applied Mechanics Reviews*, 48(8), 461. doi: 10.1115/1.3005107
- Archbold, P., Keogh, J., Caprani, C., & Fanning, P. (2011). A parametric study of pedestrian vertical force models for dynamic analysis of footbridges. In *Evaces – experimental vibration analysis for civil engineering structures* (pp. 35–44). Varenna, Italy.
- ASCE-7/10. (2010). *Minimum design loads for buildings and other structures* (Vol. 7). American Society of Civil Engineers.
- Bachmann, H., Ammann, W. J., Deischl, F., Eisenmann, J., Floegl, I., Hirsch, G. H., ... others (1995). *Vibration problems in structures: practical guidelines*. Birkhäuser.
- Bailey, J., Mata, T., & Mercer, J. A. (2017). Is the Relationship Between Stride Length, Frequency, and Velocity Influenced by Running on a Treadmill or Overground? *International journal of exercise science*, 10(7), 1067–1075.
- Begue, J., Caderby, T., Peyrot, N., & Dalleau, G. (2018). Influence of gait speed on free vertical moment during walking. *Journal of Biomechanics*, 75, 186–190. doi: 10.1016/j.jbiomech.2018.05.011
- Blekherman, A. N. (2005). Swaying of pedestrian bridges. *Journal of Bridge Engineering*, 10(2), 142–150. doi: 10.1061/(ASCE)1084-0702(2005)10:2(142)
- Bocian, M., Macdonald, J. H. G., & Burn, J. F. (2013). Biomechanically inspired modeling of pedestrian-induced vertical self-excited forces. *Journal of Bridge Engineering*, 18(12), 1336–1346. doi: 10.1061/(ASCE)BE.1943-5592.0000490

- Brand, M., Sanjayan, J., & Sudbury, A. (2017). Dynamic response of pedestrian bridges for random crowd-loading. *Australian Journal of Civil Engineering*, 3(1), 27–38. doi: 10.1080/14488353.2007.11463918
- Bro2004. (2004). *Vägverkets allmänna tekniska beskrivning för nybyggande och förbättring av broar*. Svensk Byggtjänst, Stockholm, Sverige.
- Brownjohn, J., Pavic, A., & Omenzetter, P. (2004). A spectral density approach for modelling continuous vertical forces on pedestrian structures due to walking. *Canadian Journal of Civil Engineering*, 31(1), 65–77. doi: 10.1139/103-072
- Brownjohn, J., Racic, V., & Chen, J. (2015). Universal response spectrum procedure for predicting walking-induced floor vibration. *Mechanical Systems and Signal Processing*, 70-71, 1–15. doi: 10.1016/j.ymsp.2015.09.010
- Bruno, L., & Corbetta, A. (2017). Uncertainties in crowd dynamic loading of footbridges : A novel multi-scale model of pedestrian traffic. *Engineering Structures*, 147, 545–566. doi: 10.1016/j.engstruct.2017.05.066
- BS5400, B. S. A. (1978). *Steel, concrete and composite bridges—part 2: Specification for loads; appendix c: Vibration serviceability requirements for foot and cycle track bridges*. Great Britain.
- Cahill-Rowley, K., & Rose, J. (2017). Temporal-spatial reach parameters derived from inertial sensors: Comparison to 3D marker-based motion capture. *Journal of Biomechanics*, 52, 11–16. doi: 10.1016/j.jbiomech.2016.10.031
- Caprani, C., & Ahmadi, E. (2016). Formulation of human-structure system models for vertical vibration. *Journal of Sound and Vibration*, 377, 346–367. doi: 10.1016/j.jsv.2016.05.015
- Caprani, C., Keogh, J., Archbold, P., & Fanning, P. (2011). Characteristic vertical response of a footbridge due to crowd loading. In *Proceedings of the 8th international conference on structural dynamics (eurodyn 2011), leuven, belgium* (pp. 90–106).
- Caprani, C. C., Keogh, J., Archbold, P., & Fanning, P. (2012). Enhancement factors for the vertical response of footbridges subjected to stochastic crowd loading. *Computers and Structures*, 102-103, 87–96. doi: 10.1016/j.compstruc.2012.03.006

- Chaussé, E. (1906). *Code of building laws and regulations of the city of montreal*. Guertin printing Company.
- Choi, J. S., Kang, D. W., Seo, J. W., & Tack, G. R. (2017). Fractal fluctuations in spatiotemporal variables when walking on a self-paced treadmill. *Journal of Biomechanics*, *65*, 154–160. doi: 10.1016/j.jbiomech.2017.10.015
- Collins, S. H., & Kuo, A. D. (2013). Two independent contributions to step variability during over-ground human walking. *PLoS ONE*, *8*(8), 1–11. doi: 10.1371/journal.pone.0073597
- Computer, & structures, S., Inc. (2017). *Static and dynamic finite element analysis of structures*. Berkeley, California, USA.
- Cunha, A., & Moutinho, C. (1999). Active control of vibrations in pedestrian bridges. In *Conference of the european association for structural dynamics (eurodyn'99)* (Vol. 2, pp. 783–788).
- Dallard, P., Fitzpatrick, T., Flint, A., Low, A., Smith, R., Willford, M., & Roche, M. (n.d.). London Millenium bridge: pedestrian-induced lateral vibration. *Journal of Bridge Engineering*(6), 412–417.
- Dang, H. V., & Živanović, S. (2013). Modelling pedestrian interaction with perceptibly vibrating footbridges. *FME Transactions*, *41*(4), 271–278.
- Dang, H. V., & Živanović, S. (2015). Experimental characterisation of walking locomotion on rigid level surfaces using motion capture system. *Engineering Structures*, *91*, 141–154. doi: 10.1016/j.engstruct.2015.03.003
- Dang, H. V., & Živanović, S. (2016). Influence of low-frequency vertical vibration on walking locomotion. *Journal of Structural Engineering*, *142*(04016120), 1–12. doi: 10.1061/(ASCE)ST.1943-541X.0001599.
- Danion, F., Varraine, E., Bonnard, M., & Pailhous, J. (2003). Stride variability in human gait: The effect of stride frequency and stride length. *Gait and Posture*, *18*(1), 69–77. doi: 10.1016/S0966-6362(03)00030-4
- da Silva, F. T., Brito, H. M. B. F., & Pimentel, R. L. (2013). Modeling of crowd load in vertical direction using biodynamic model for pedestrians crossing footbridges. *Canadian Journal of Civil Engineering*, *40*(July), 1196–1204.

- DIN-Fachbericht. (2003). *Din-fachbericht 102*. Deutsches Instiut für Normung, Betonbrücken.
- Dingwell, J. B., Cusumano, J. P., Cavanagh, P. R., & Sternad, D. (2001). Local dynamic stability versus kinematic variability of continuous overground and treadmill walking. *Journal of Biomechanical Engineering*, *123*(1), 27. doi: 10.1115/1.1336798
- Dyke, S. J., Spencer, B. F., Quast, P., Sain, M. K., C, K. D., & Soong, T. T. (1996). Acceleration feedback control of mdof structures. *Journal of Engineering Mechanics*, *122*(9), 907–918.
- Eckhardt, B., Ott, E., Strogatz, S. H., Abrams, D. M., & McRobie, A. (2007). Modeling walker synchronization on the Millennium bridge. *Physical Review E - Statistical, Nonlinear, and Soft Matter Physics*, *75*(2), 1–10. doi: 10.1103/PhysRevE.75.021110
- Elishakoff, I., Li, Y. W., & Starnes, J. H. (1994). A deterministic method to predict the effect of unknown-but-bounded elastic moduli on the buckling of composite structures. *Computer Methods in Applied Mechanics and Engineering*, *111*(1-2), 155–167. doi: 10.1016/0045-7825(94)90043-4
- Ellingwood, B., & Tallin, A. (1984). Structural serviceability: floor vibrations. *J. Struct. Eng.*, *110*(2), 401–418. doi: 10.1061/(ASCE)0733-9445(1984)110:2(401)
- EN 1991-2, E. C. f. S. (2002). *Eurocode 1 - actions on structures – part 2: General actions -traffic loads on bridges*. European Committee for Standardization CEN,Brussels, Belgium.
- EN 1995-2, E. C. f. S. (2004). *Eurocode 5 - design of timber structures – part 2: bridges*. Authority: The European Union Per Regulation 305/2011, Directive 98/34/EC, Directive 2004/18/EC,Brussels, Belgium.
- Fanning, P., Archbold, P., & Pavic, A. (2005). A novel interactive pedestrian load model for flexible footbridges. In *Proceeding of the 2005 society for experimental mechanics annual conference on experimental and applied mechanics* (pp. 7–9). Portland, OR.

- Ferrarotti, A., & Tubino, F. (2016). Generalized equivalent spectral model for serviceability analysis of footbridges. *Journal of Bridge Engineering*, *21*(12), 942–954. doi: doi.org/10.1061/(ASCE)BE.1943-5592.0000963
- Fujino, Y., Pacheco, B., Nakamura, S. I., & Warnitchai, P. (1993). Synchronization of human walking observed. *Earthquake Engineering & Structural Dynamics*, *22*(December 1993), 741–758.
- Fujino, Y., Sun, L., Pacheco, B. M., Member, A., & Chaiseri, P. (1992). Tuned liquid damper (TLD) for suppressing horizontal motion of structures. *Journal of Engineering Mechanics*, *118*(10), 2017–2030.
- García-Diéguez, M., & Zapico-Valle, J. L. (2017). Statistical modeling of the relationships between spatiotemporal parameters of human walking and their variability. *Journal of Structural Engineering*, *143*(12), 04017164. doi: 10.1061/(ASCE)ST.1943-541X.0001899
- García-diéguez, M., & Zapico-Valle, J. L. (2018). Sensitivity of the vertical response of footbridges to the frequency variability of crossing pedestrians. *Vibration*, 290–311. doi: 10.3390/vibration1010020
- Geyer, H., Seyfarth, A., & Blickhan, R. (2006). Compliant leg behaviour explains basic dynamics of walking and running. *Proceeding of the royal society of London: Biological science*, *1603*(273), 2861–2867. doi: 10.1098/rspb.2006.3637
- Gheitasi, A., Ozbulut, O. E., Usmani, S., Alipour, M., & Harris, D. K. (2016). Experimental and analytical vibration serviceability assessment of an in-service footbridge. *Case Studies in Nondestructive Testing and Evaluation*, *6*, 79–88. doi: 10.1016/j.csndt.2016.11.001
- Gomez, D., Dyke, S., & Rietdyk, S. (2018). Experimental verification of a substructure-based model to describe pedestrian-bridge interaction. *Journal of Bridge Engineering*, *23*(4), 1–14. doi: 10.1061/(ASCE)BE.1943-5592.0001204
- Gomez, D., Dyke, S. J., & Maghareh, A. (2015). Enabling role of hybrid simulation across NEES in advancing earthquake engineering. *Smart Structures and Systems*, *15*(3), 913–929.
- Gomez, D., Dyke, S. J., & Rietdyk, S. (2019a). Spatial-temporal assessment of stride variability in walking-induced vibration. , (under review)..

- Gomez, D., Dyke, S. J., & Rietdyk, S. (2019b). Structured uncertainty for a pedestrian-structure interaction model. *Journal of Sound and Vibration*, (under review)..
- Gomez, D., Silva, C., Dyke, S., & Thomson, P. (2015). Interactive platform to include human-structure interaction effects in the analysis of footbridges. In *Proceedings of the XXXIII conference and exposition on structural dynamics (IMAC 2015)* (pp. 1110–1117). Orlando, FL.
- Grieve, D. W., & Gear, R. J. (1966). The relationships between length of stride, step frequency, time of swing and speed of walking for children and adults. *Ergonomics*, *9*(5), 379–399. doi: 10.1080/00140136608964399
- Gu, D.-W., Petkov, P., & Konstantinov, M. M. (2005). *Robust control design with matlab®*. Springer Science & Business Media.
- Hausdorff, J. M., Rios, D. A., & Edelberg, H. K. (2001). Gait variability and fall risk in community-living older adults: A 1-year prospective study. *Archives of Physical Medicine and Rehabilitation*, *82*(8), 1050–1056. doi: 10.1053/apmr.2001.24893
- Heinemeyer, C., Keil, A., Schlaich, M., Goldack, A., Trometer, S., Lukic, M., . . . Caetano, E. (2007). *Human induced vibrations of steel structures design of footbridges (HIVOSS)*.
- Henriques, A. A. (2008). Efficient analysis of structural uncertainty using perturbation techniques. *Engineering Structures*, *30*(4), 990–1001. doi: 10.1016/j.engstruct.2007.06.007
- Holt, K. G., Jeng, S. F., Ratcliffe, R., & Hamill, J. (1995). Energetic cost and stability during human walking at the preferred stride frequency. *Journal of Motor Behavior*, *27*(2), 164–178. doi: 10.1080/00222895.1995.9941708
- Huo, L., Qu, C., & Li, H. (2016). Robust control of civil structures with parametric uncertainties through D-K iteration Linsheng. *The Structural Design of Tall and Special Buildings*, *25*(August 2015), 158–176. doi: 10.1002/tal
- Ingólfsson, E., & Georgakis, C. (2011). A stochastic load model for pedestrian-induced lateral forces on footbridges. *Engineering Structures*, *33*(12), 3454–3470. doi: 10.1016/j.engstruct.2011.07.009

- ISO-10137. (2007). *Bases for design of structures - serviceability of buildings and walkways against vibrations*. International standard, Switzerland.
- Jimenez-Alonso, J. F., Saez, A., Caetano, E., & Magalhaes, F. (2016). Vertical crowd – structure interaction model to analyze the change of the modal properties of a footbridge. *Journal of Bridge Engineering*, 1–19. doi: 10.1061/(ASCE)BE.1943-5592.0000828.
- Johnson, L. J. (1905). *New data on the weight of a crowd of people*. Association of Engineering Societies.
- Jordan, K., Challis, J. H., & Newell, K. M. (2007). Walking speed influences on gait cycle variability. *Gait and Posture*, 26(1), 128–134. doi: 10.1016/j.gaitpost.2006.08.010
- Joshi, V., & Srinivasan, M. (2015). Walking on a moving surface: energy-optimal walking motions on a shaky bridge and a shaking treadmill can reduce energy costs below normal. *Mathematical, physical and engineering science*, 471(2174), 1–19. doi: 10.1038/161375b0
- Joshi, V., & Srinivasan, M. (2018). Walking crowds on a shaky surface: Stable walkers discover Millennium Bridge oscillations with and without pedestrian synchrony. *Biology Letters*, 14(10). doi: 10.1098/rsbl.2018.0564
- Kim, A., Kim, J., Rietdyk, S., & Ziaie, B. (2015). A wearable smartphone-enabled camera-based system for gait assessment. *Gait & posture*, 42(2), 138–44. doi: 10.1016/j.gaitpost.2015.05.001
- Kim, S., & Park, S. (2011). Leg stiffness increases with speed to modulate gait frequency and propulsion energy. *Journal of Biomechanics*, 44(7), 1253–1258. doi: 10.1016/j.jbiomech.2011.02.072
- Krenk, S. (2012). Dynamic response to pedestrian loads with statistical frequency distribution. *Journal of Engineering Mechanics*, 138(10), 1275–1281. doi: 10.1061/(ASCE)EM.1943-7889.0000425
- Lansdell, A., Song, W., & Dixon, B. (2017). Development and testing of a bridge weigh-in-motion method considering nonconstant vehicle speed. *Engineering Structures*, 152, 709–726. doi: 10.1016/j.engstruct.2017.09.044

- Lee, C. R., & Farley, C. T. (1998). Determinants of the center of mass trajectory in human walking and running. *The Journal of Experimental Biology*, *201*, 2935–2944.
- LondonTown. (2015). *Millennium bridge*. (Retrieved from <http://www.londontown.com/>. Online; accessed 19 February 2015)
- Macdonald, J. (2009). Lateral excitation of bridges by balancing pedestrians. *Proceedings of the Royal Society A: Mathematical, Physical and Engineering Sciences*, *465*(2104), 1055–1073. doi: 10.1098/rspa.2008.0367
- Maki, B. (1997). Gait changes in older adults: predictors of falls or indicators of fear? *American geriatrics society*, *45*, 313–320.
- Marinova, D., & Stavroulakis, G. (2007). Robust control design of a smart building structure. *Journal of Theoretical and Applied Mechanics*, *45*(1), 73–90.
- MATLAB. (2017). *version 9.2 (r2017a)*. The MathWorks Inc., Natick, Massachusetts.
- McAndrew Young, P. M., & Dingwell, J. B. (2012). Voluntarily changing step length or step width affects dynamic stability of human walking. *Gait and Posture*, *35*(3), 472–477. doi: 10.1016/j.gaitpost.2011.11.010
- Mochon, S., & McMahon, T. (1980). Ballistic walking: an improved model. *Mathematical Biosciences*, *52*, 241–260. doi: 10.1017/CBO9781107415324.004
- Moens, D., & Vandepitte, D. (2007). Interval sensitivity theory and its application to frequency response envelope analysis of uncertain structures. *Computer Methods in Applied Mechanics and Engineering*, *196*(21-24), 2486–2496. doi: 10.1016/j.cma.2007.01.006
- Moore, R. E., Kearfott, R. B., & Cloud, M. J. (2009). *Introduction to interval analysis* (Vol. 110). Siam.
- Moreno, C. P., & Thomson, P. (2010). Design of an optimal tuned mass damper for a system with parametric uncertainty. *Annals of Operations Research*, *181*(100), 783–793. doi: 10.1007/s10479-010-0726-x

- Nakamura, S. I., & Fujino, Y. (2002). Lateral vibration on a pedestrian cable-stayed bridge. *Structural Engineering International: Journal of the International Association for Bridge and Structural Engineering (IABSE)*, *12*(4), 295–300. doi: 10.2749/101686602777965162
- Nowak, A. S., & Collins, K. R. (2012). *Reliability of structures*. CRC Press.
- ONT95. (1995). *Ontario highway bridge design code ont95*. Ontario Government, Ontario, Canada.
- Onyshko, S., & Winter, D. (1980). A mathematical model for the dynamics of human locomotion. *Journal of Biomechanics*, *13*(4), 361–368. doi: 10.1016/0021-9290(80)90016-0
- Ortiz, A. R., & Caicedo, J. M. (2019). Modeling the effects of a human standing on a structure using a closed loop-control system. *Journal of Engineering Mechanics*, *145*(5), 04019025. doi: 10.1061/(ASCE)EM.1943-7889.0001583
- Packard, A. K. (1998). *What's new with μ : Structured uncertainty in multivariable control* (Unpublished doctoral dissertation). University of California.
- Pandy, M. G., & Berme, N. (1988). Synthesis of human walking: A planar model for single support. *Journal of Biomechanics*, *21*(12), 1053–1060.
- Paw, Y. C., & Balas, G. J. (2008). Parametric uncertainty modeling for LFT model realization. *Proceedings of the IEEE International Symposium on Computer-Aided Control System Design*, 834–839. doi: 10.1109/CACSD.2008.4627338
- Pedersen, L., & Frier, C. (2010). Sensitivity of footbridge vibrations to stochastic walking parameters. *Journal of Sound and Vibration*, *329*(13), 2683–2701. doi: 10.1016/j.jsv.2009.12.022
- Pfeil, M., Amador, N., Pimentel, R., & Vasconcelos, R. (2014). Analytic – numerical model for walking person – footbridge structure interaction. In *Proceedings of the 9th international conference on structural dynamics, eurodyn 2014* (pp. 1079–1086). Porto, Portugal.
- Piccardo, G., & Tubino, F. (2009). Simplified procedures for vibration serviceability analysis of footbridges subjected to realistic walking loads. *Computers and Structures*, *87*(13-14), 890–903. doi: 10.1016/j.compstruc.2009.04.006

- Poovarodom, N., Kanchanosot, S., & Warnitchai, P. (2003). Application of non-linear multiple tuned mass dampers to suppress man-induced vibrations of a pedestrian bridge. *Earthquake Engineering and Structural Dynamics*, *32*(7), 1117–1131. doi: 10.1002/eqe.265
- Qin, J. W., Law, S. S., Yang, Q. S., & Yang, N. (2013a). Finite element analysis of pedestrian-bridge dynamic interaction. *Journal of Applied Mechanics*, *81*(4), 041001.
- Qin, J. W., Law, S. S., Yang, Q. S., & Yang, N. (2013b). Pedestrian-bridge dynamic interaction, including human participation. *Journal of Sound and Vibration*, *332*(4), 1107–1124.
- Racic, V., & Brownjohn, J. (2011). Stochastic model of near-periodic vertical loads due to humans walking. *Advanced Engineering Informatics*, *25*(2), 259–275. doi: 10.1016/j.aei.2010.07.004
- Racic, V., Pavić, A., & Brownjohn, J. (2009). Experimental identification and analytical modelling of human walking forces: Literature review. *Journal of Sound and Vibration*, *326*(1-2), 1–49. doi: 10.1016/j.jsv.2009.04.020
- Ricciardelli, F., & Pizzimenti, A. D. (2007). Lateral walking-induced forces on footbridges. *Journal of Bridge Engineering*, *12*(6), 677–688. doi: 10.1061/(ASCE)1084-0702(2007)12:6(677)
- Roberts, T. M. (2003). Synchronised pedestrian excitation of footbridges. *Proceedings of ICE, Bridge Engineering*, *156*(4), 155–160.
- Roos, I. (2009). *Human induced vibration on footbridges: Application and comparison of pedestrian load models* (Unpublished master's thesis). Delft University of Technology, Netherlands.
- Sachse, R., Pavic, A., & Reynolds, P. (2003). Human-structure dynamic interaction in civil engineering dynamics: A literature review. *Shock and Vibration Digest*, *35*(1), 3–18.
- Sekiya, N., Nagasaki, H., Ito, H., & Furuna, T. (1997). Optimal walking in terms of variability in step length. *Journal of Orthopedic and Sports Physical Therapy*, *26*(5), 266–272.

- Sétra. (2006). Footbridges, assessment of vibrational behaviour of footbridges under pedestrian loading. In *Technical guide, service d'études techniques des routes et autoroutes*. Paris, France.
- Shahabpoor, E., Pavic, A., & Racic, V. (2013). Using MSD model to simulate human-structure interaction during walking. In *Topics in dynamics of civil structures, volume 4: Proceedings of the 31st imac, a conference on structural dynamics, 2013* (Vol. 4, pp. 357–364). doi: 10.1007/978-1-4614-6555-3
- Shahabpoor, E., Pavic, A., & Racic, V. (2015). Identification of Mass-Spring-Damper model of walking humans. *ASCE J.Construction*, 912–923. doi: 10.1061/9780784479117.078
- Siegler, S., Seliktar, R., & Hyman, W. (1982). Simulation of human gait with the aid of a simple mechanical model. *Journal of Biomechanics*, 15(6), 415–425.
- Skogestad, S., & Postlethwaite, I. (2007). *Multivariable feedback control: analysis and design* (Vol. 2). Wiley New York.
- Skyscrapercity. (2015). *Solferino bridge*. (Retrieved from <http://www.skyscrapercity.com/>). Online; accessed 22 September 2015)
- Stevenson, R. (1821). Description of bridges of suspension. *The Edinburgh Philosophical Journal*, 5(10), 237–256.
- Strogatz, S. H., Abrams, D. M., McRobie, A., Eckhardt, B., & Ott, E. (2005). Theoretical mechanics: crowd synchrony on the Millennium Bridge. *Nature*, 438(7064), 43–44. doi: 10.1038/43843a
- Svoboda, Z., Bizovska, L., Janura, M., Kubonova, E., Janurova, K., & Vuillerme, N. (2017). Variability of spatial temporal gait parameters and center of pressure displacements during gait in elderly fallers and nonfallers: A 6-month prospective study. *PLoS ONE*, 12(2), 1–11. doi: 10.1371/journal.pone.0171997
- Tilden, C. J. (1913). Kinetic effects of crowds. *Transactions of the American Society of Civil Engineers*, 76(1), 2107–2126.
- Toso, M. A., Gomes, H. M., Da Silva, F. T., & Pimentel, R. L. (2016). Experimentally fitted biodynamic models for pedestrian-structure interaction in walking situations. *Mechanical Systems and Signal Processing*, 72-73, 590–606.

- Toso, M. A., Gomes, H. M., Silva, F. T., & Pimentel, R. L. (2013). A biodynamic model fit for vibration serviceability in footbridges using experimental measurements in a designed force platform for vertical load gait analysis. In *Icem15: 15th international conference on experimental mechanics* (Vol. 22, pp. 23–33). Porto, Portugal.
- Tubino, F. (2017). Human-structure interaction in pedestrian bridges: A probabilistic approach. *Procedia Engineering*, *199*, 2883–2888. doi: 10.1016/j.proeng.2017.09.584
- Van Nimmen, K., Lombaert, G., De Roeck, G., & Van den Broeck, P. (2014). Vibration serviceability of footbridges: Evaluation of the current codes of practice. *Engineering Structures*, *59*(0), 448–461. doi: 10.1016/j.engstruct.2013.11.006
- Van Nimmen, K., Lombaert, G., De Roeck, G., & Van den Broeck, P. (2014). Vibration serviceability of footbridges: Evaluation of the current codes of practice. *Engineering Structures*, *59*, 448–461.
- Venini, P. (1998). Robust control of uncertain structures. *Science*, *67*, 165–174. doi: 10.1016/S0045-7949(97)00168-5
- Venuti, F., Bruno, L., & Bellomo, N. (2007). Crowd dynamics on a moving platform: Mathematical modelling and application to lively footbridges. *Mathematical and Computer Modelling*, *45*(3-4), 252–269. doi: 10.1016/j.mcm.2006.04.007
- Wang, H., Chen, J., & Brownjohn, J. M. (2017). Parameter identification of pedestrian’s spring-mass-damper model by ground reaction force records through a particle filter approach. *Journal of Sound and Vibration*, *411*, 409–421. doi: 10.1016/j.jsv.2017.09.020
- Whittington, B. R., & Thelen, D. G. (2009). A Simple mass-spring model with roller feet can induce the ground reactions observed in human walking. *Journal of Biomechanical Engineering*, *131*(1), 011013. doi: 10.1115/1.3005147
- Whittle, M. W. (2014). *Gait analysis: an introduction*. Butterworth-Heinemann.
- Winter, D. A. (2009). *Biomechanics and motor control of human movement*. John Wiley & Sons.

- Wolmuth, B., & Surtees, J. (2003). Crowd-related failure of bridges. *Proceedings of the ICE: Civil Engineering*, 156(3), 116–123. doi: 10.1680/cien.2003.156.3.116
- Yamasaki, M., Sasaki, T., & Torii, M. (1991). Sex difference in the pattern of lower limb movement during treadmill walking. *Applied physiology*(62), 99–103.
- Ylli, K., Hoffmann, D., Willmann, A., Becker, P., Folkmer, B., & Manoli, Y. (2015). Energy harvesting from human motion : Exploiting swing and shock excitations. *Smart Materials and Structures*, 24(2), 25029. doi: 10.1088/0964-1726/24/2/025029
- Zhang, M., Georgakis, Qu, W., & Chen, J. (2015). SMD model parameters of pedestrians for vertical human-structure interaction. *IMAC XXXIII A Conference and Exposition on Structural Dynamics*. doi: 10.1007/978-3-319-15248-6_33
- Zhang, M., Georgakis, C. T., & Chen, J. (2016). Biomechanically excited SMD model of a walking pedestrian. *Journal of Bridge Engineering*, 21(8), C4016003. doi: 10.1061/(ASCE)BE.1943-5592.0000910
- Zhou, K., & Doyle, J. C. (1998). *Essentials of robust control* (Vol. 104). Prentice hall Upper Saddle River, NJ.
- Zhou, S., & Song, W. (2018). Environmental-effects-embedded model updating method considering environmental impacts. *Structural Control and Health Monitoring*, 25(3), 1–22. doi: 10.1002/stc.2116
- Zijlstra, W. (2004). Assessment of spatio-temporal parameters during unconstrained walking. *European Journal of Applied Physiology*, 92(1-2), 39–44. doi: 10.1007/s00421-004-1041-5
- Živanović, S. (2006). *Probability-based estimation of vibration for pedestrian structures due to walking* (Unpublished doctoral dissertation). University of Sheffield.
- Živanović, S., Diaz, I. M., & Pavić, A. (2009). Influence of walking and standing crowds on structural dynamic properties. In *Proceedings of the the 27th imac conference*. Orlando, Florida USA.
- Živanović, S., Pavić, A., & Ingólfsson, E. (2010). Modelling spatially unrestricted pedestrian traffic on footbridges. *ASCE Journal of Structural Engineering*, 136(10), 1296–1308.

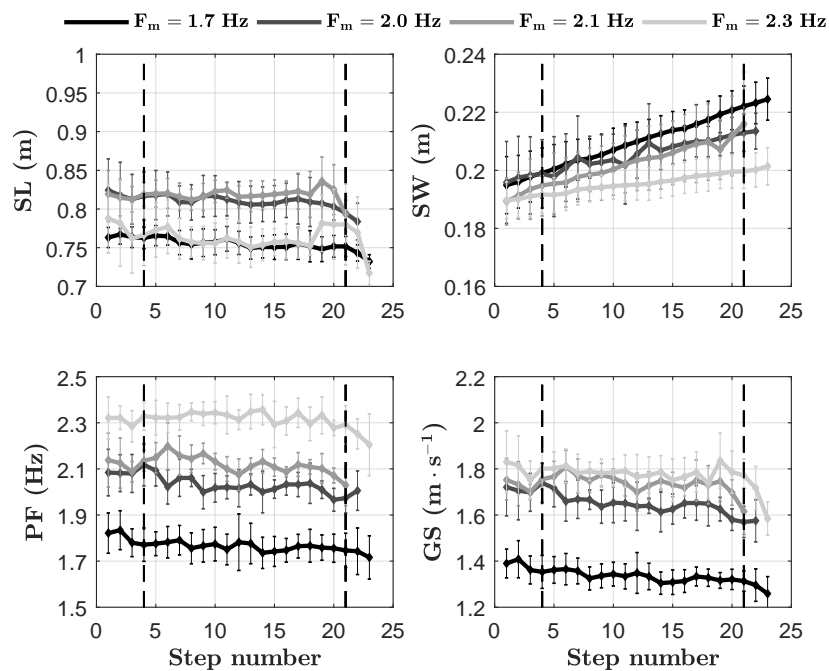
- Živanović, S., Pavić, A., & Reynolds, P. (2005). Vibration serviceability of footbridges under human-induced excitation: A literature review. *Journal of Sound and Vibration*, 279(1-2), 1–74. doi: 10.1016/j.jsv.2004.01.019
- Živanović, S., Pavić, A., & Reynolds, P. (2007). Probability-based prediction of multi-mode vibration response to walking excitation. *Engineering Structures*, 29(6), 942–954. doi: 10.1016/j.engstruct.2006.07.004
- Zuo, D., Hua, J., & Van Landuyt, D. (2012). A model of pedestrian-induced bridge vibration based on full-scale measurement. *Engineering Structures*, 117–126. doi: 10.1016/j.engstruct.2012.06.015

APPENDICES

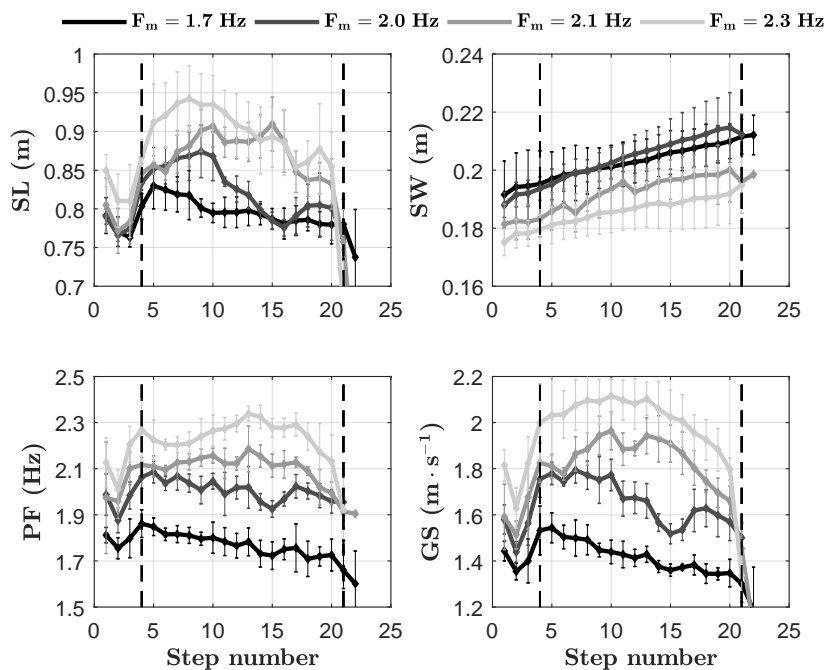
A. GAIT VARIABILITY

Gait kinematic characteristic comparison when the pedestrian walked on overground and on the moving surface. Two gait modes are examined: (1) prescribed cadence, where the participant walked at a frequency (F_m) set by a metronome, and (2) self-selected speed. Each pass on the moving surface or on the floor is considered a trial. The median values were obtained for each pedestrian's kinematic parameter vs. step number. Because less than ten trials per test were performed, the median is used here. To provide a measure of the variability, the median absolute deviation (MAD) is used for its insensitivity to outliers. The MAD of a dataset is the median of the absolute values between the i -th data point, x_i , and the median of the dataset as

$$\text{MAD} = \text{median} (|x_i - \text{median}(x_i)|). \quad (\text{A.1})$$

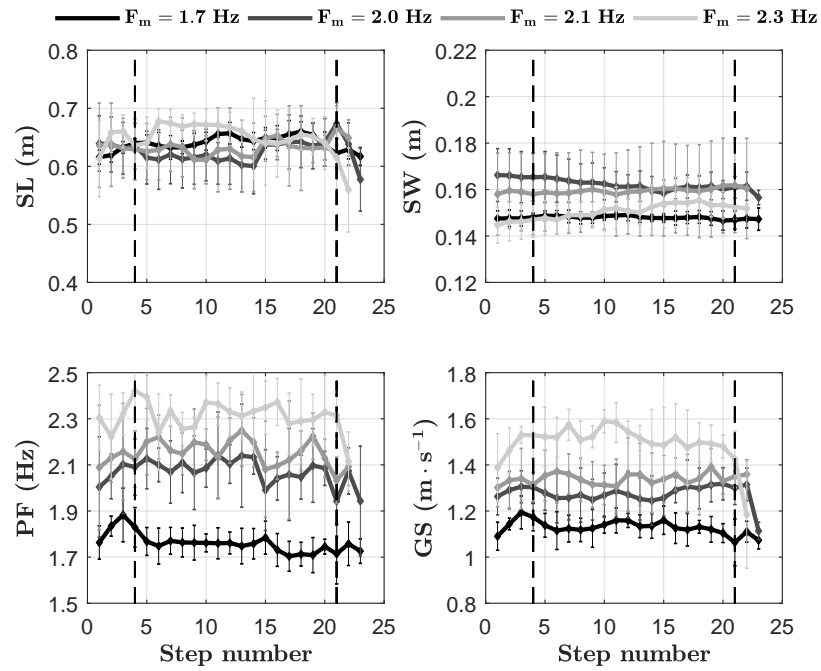


(a) Stationary surface.

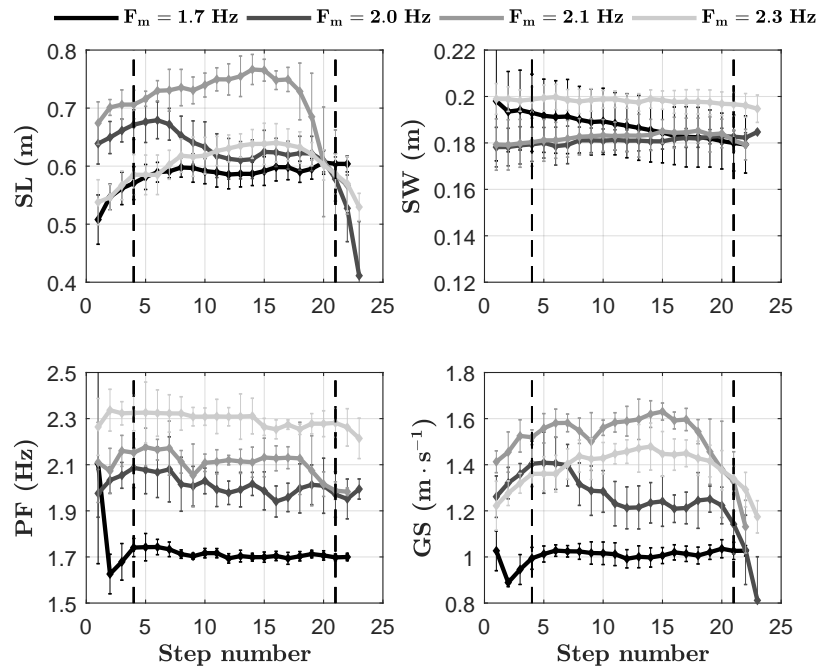


(b) Moving surface.

Fig. A.1.: Prescribed cadence: Subject S-1.

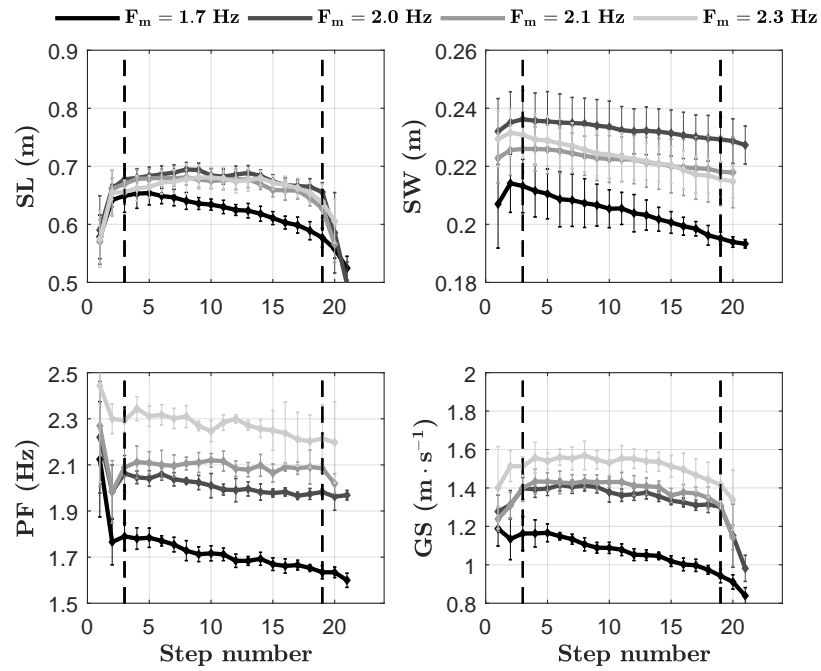


(a) Stationary surface.

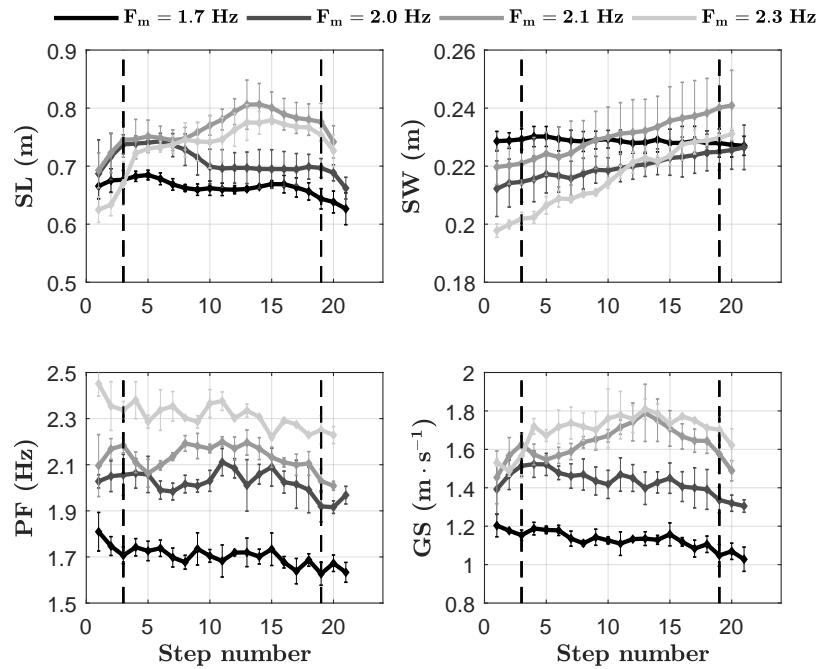


(b) Moving surface.

Fig. A.2.: Prescribed cadence: Subject S-2.

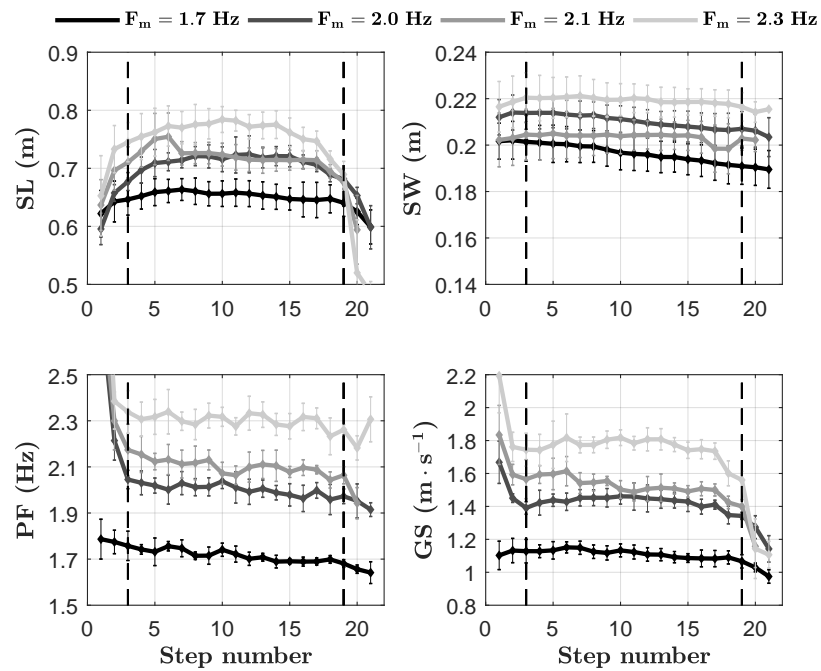


(a) Stationary surface.

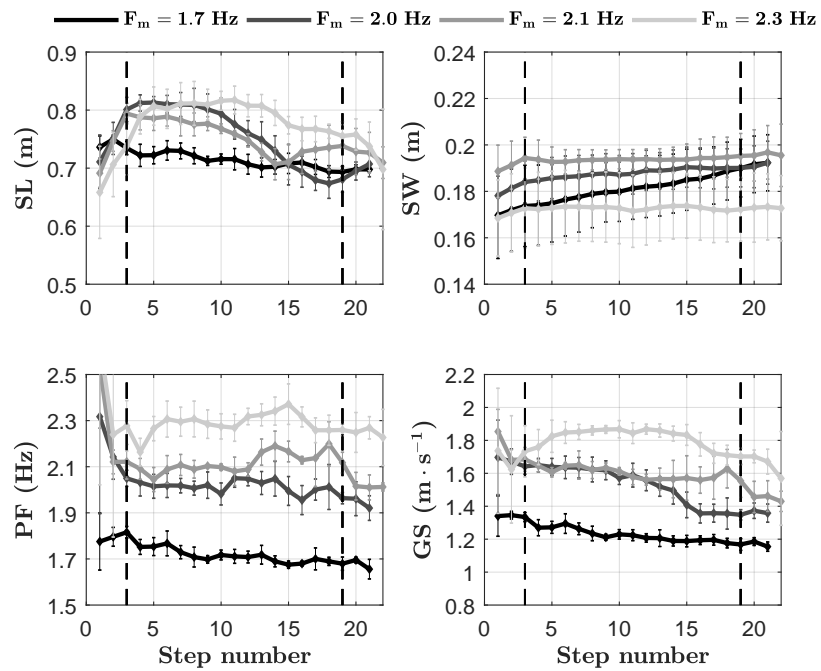


(b) Moving surface.

Fig. A.3.: Prescribed cadence: Subject S-3.

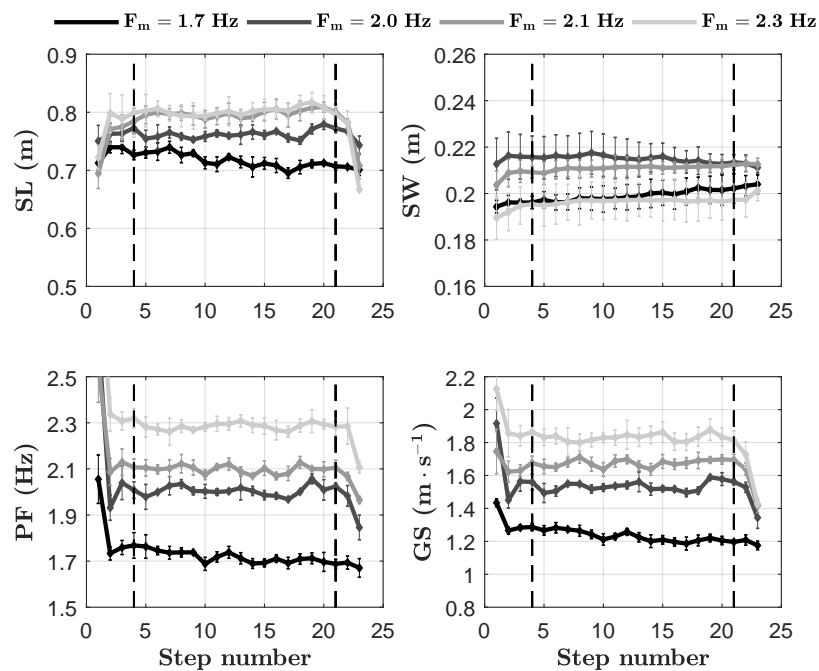


(a) Stationary surface.

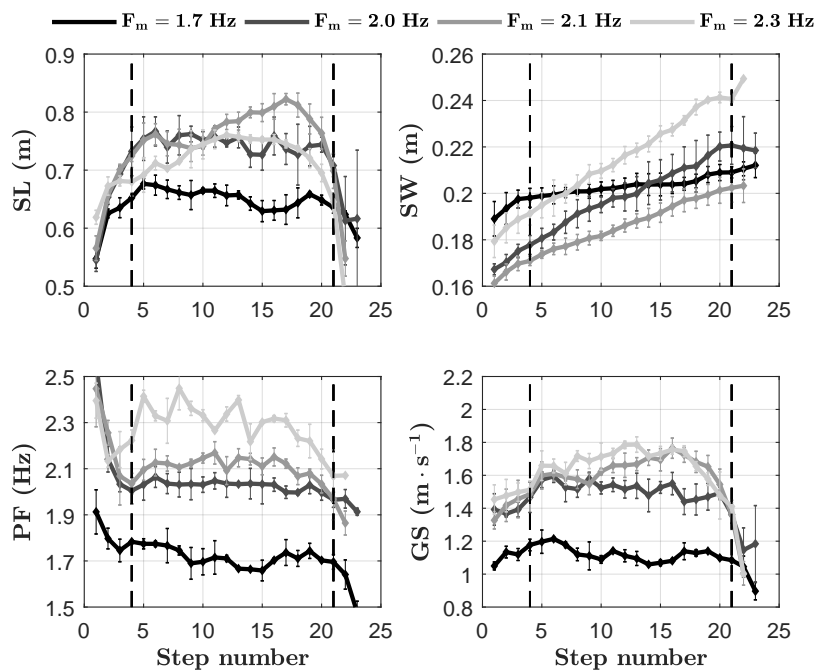


(b) Moving surface.

Fig. A.4.: Prescribed cadence: Subject S-4.

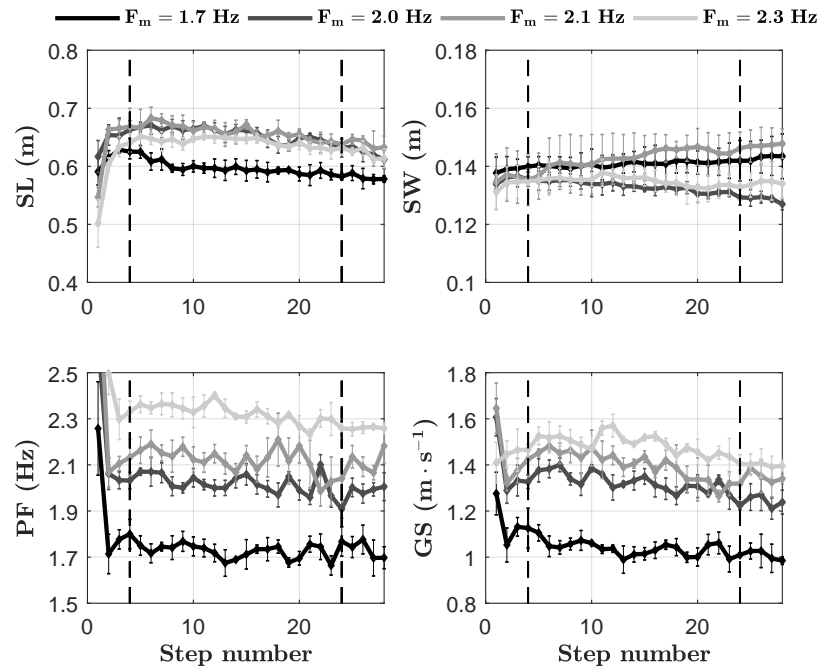


(a) Stationary surface.

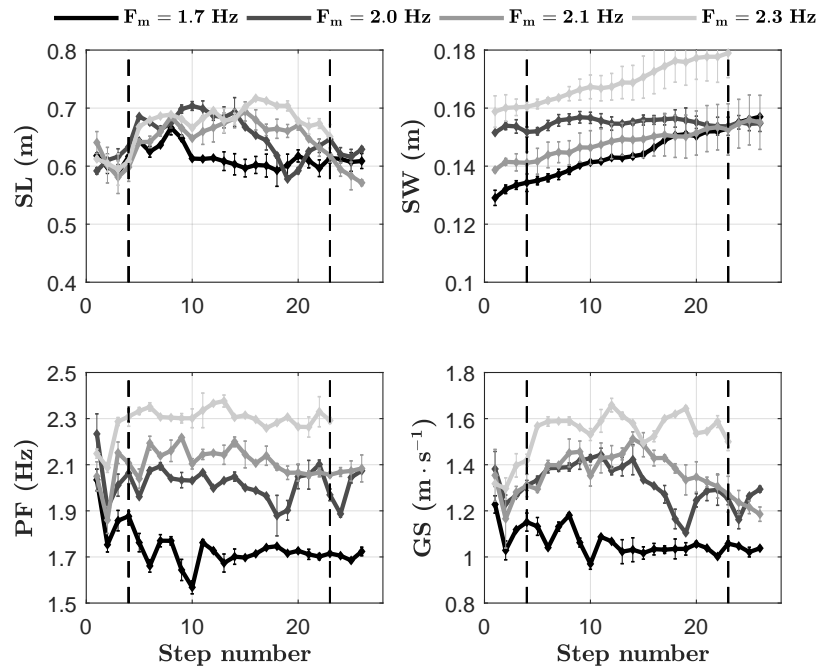


(b) Moving surface.

Fig. A.5.: Prescribed cadence: Subject S-5.



(a) Stationary surface.



(b) Moving surface.

Fig. A.6.: Prescribed cadence: Subject S-6.

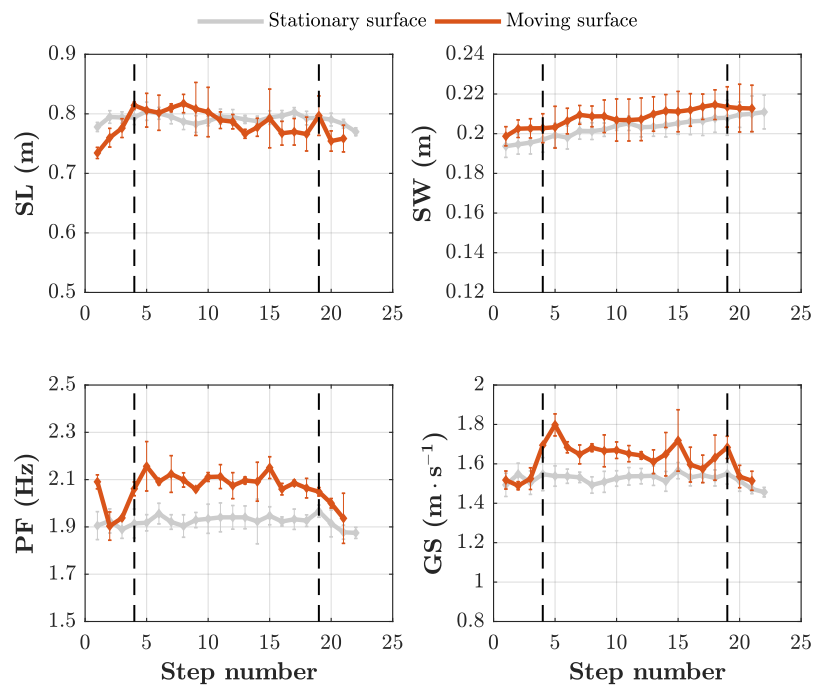


Fig. A.7.: Self-selected pace: Subject S-1.

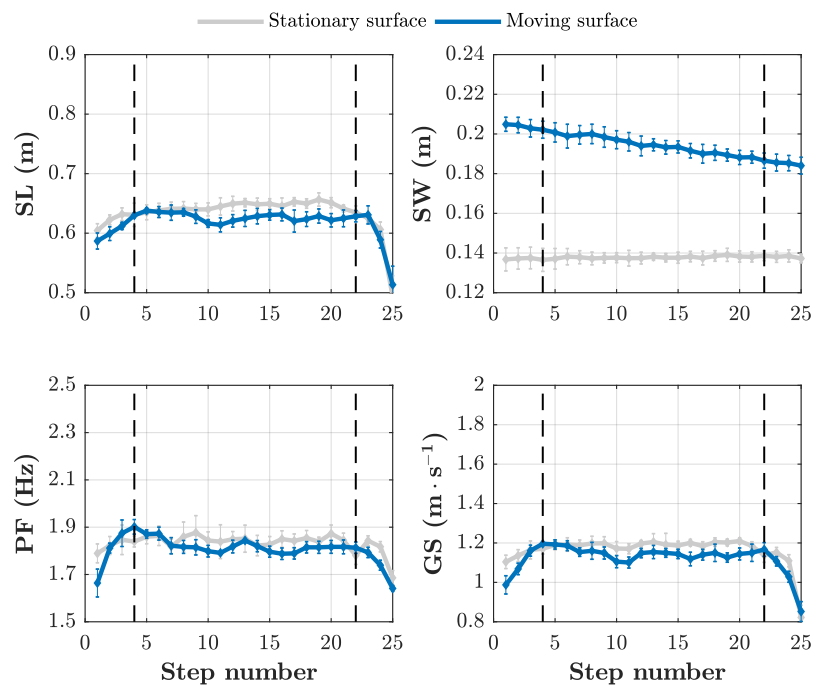


Fig. A.8.: Self-selected pace: Subject S-2.

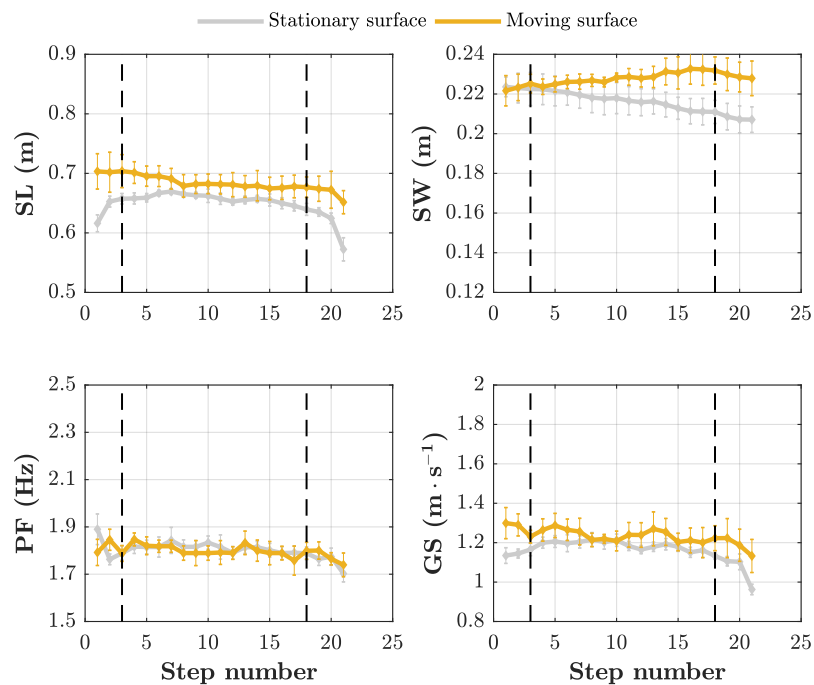


Fig. A.9.: Self-selected pace: Subject S-3.

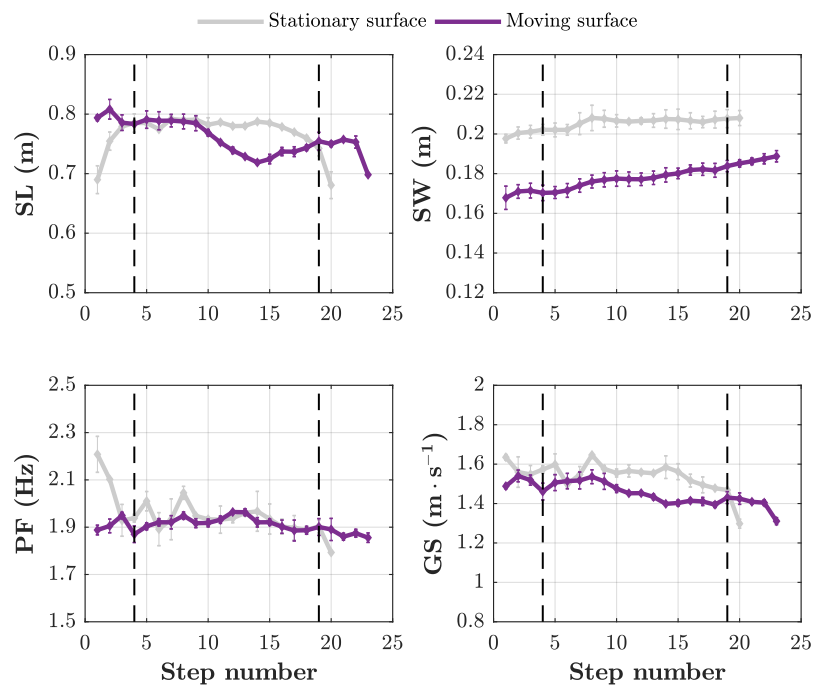


Fig. A.10.: Self-selected pace: Subject S-4.

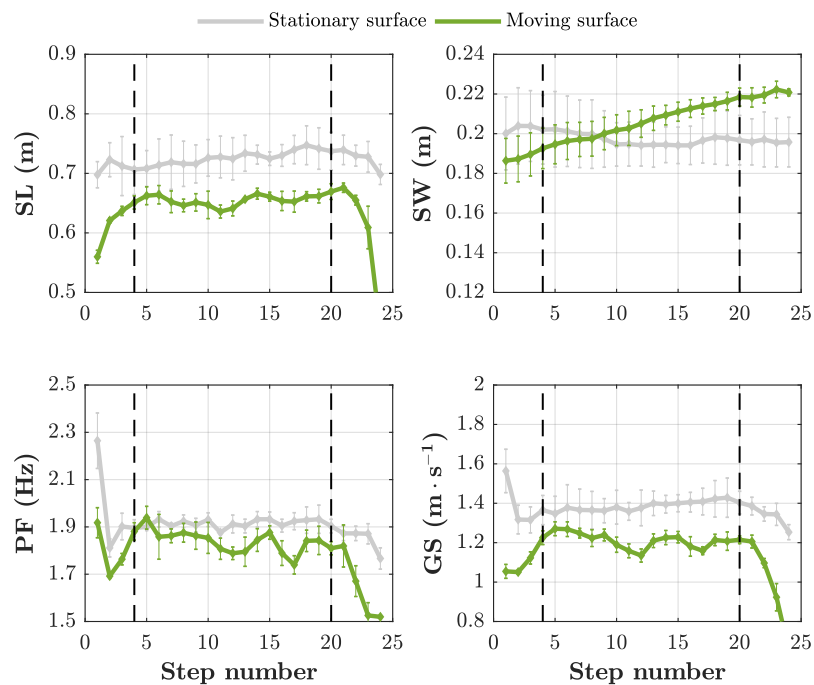


Fig. A.11.: Self-selected pace: Subject S-5.

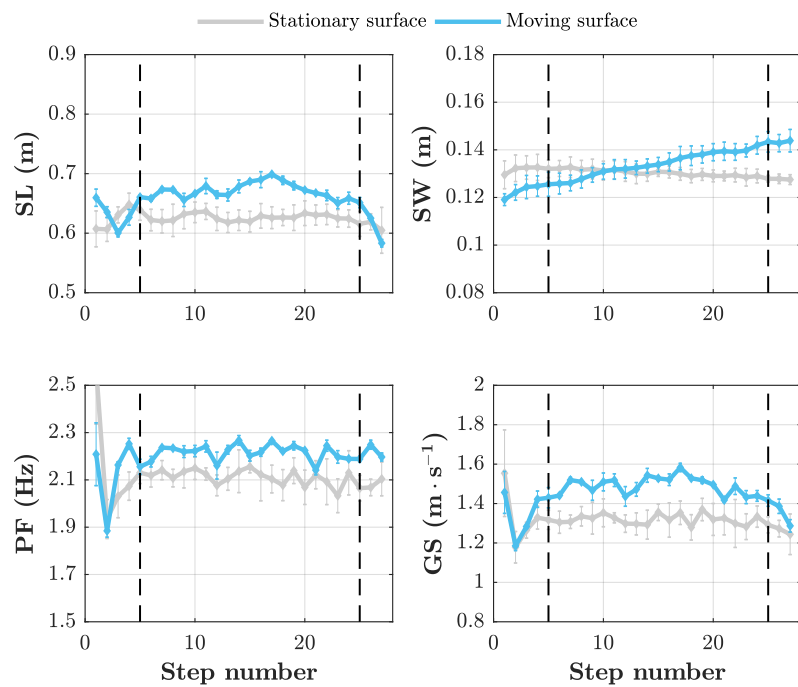


Fig. A.12.: Self-selected pace: Subject S-6.

B. STRUCTURAL RESPONSE FOR DIFFERENT PEDESTRIAN LOAD CONDITIONS

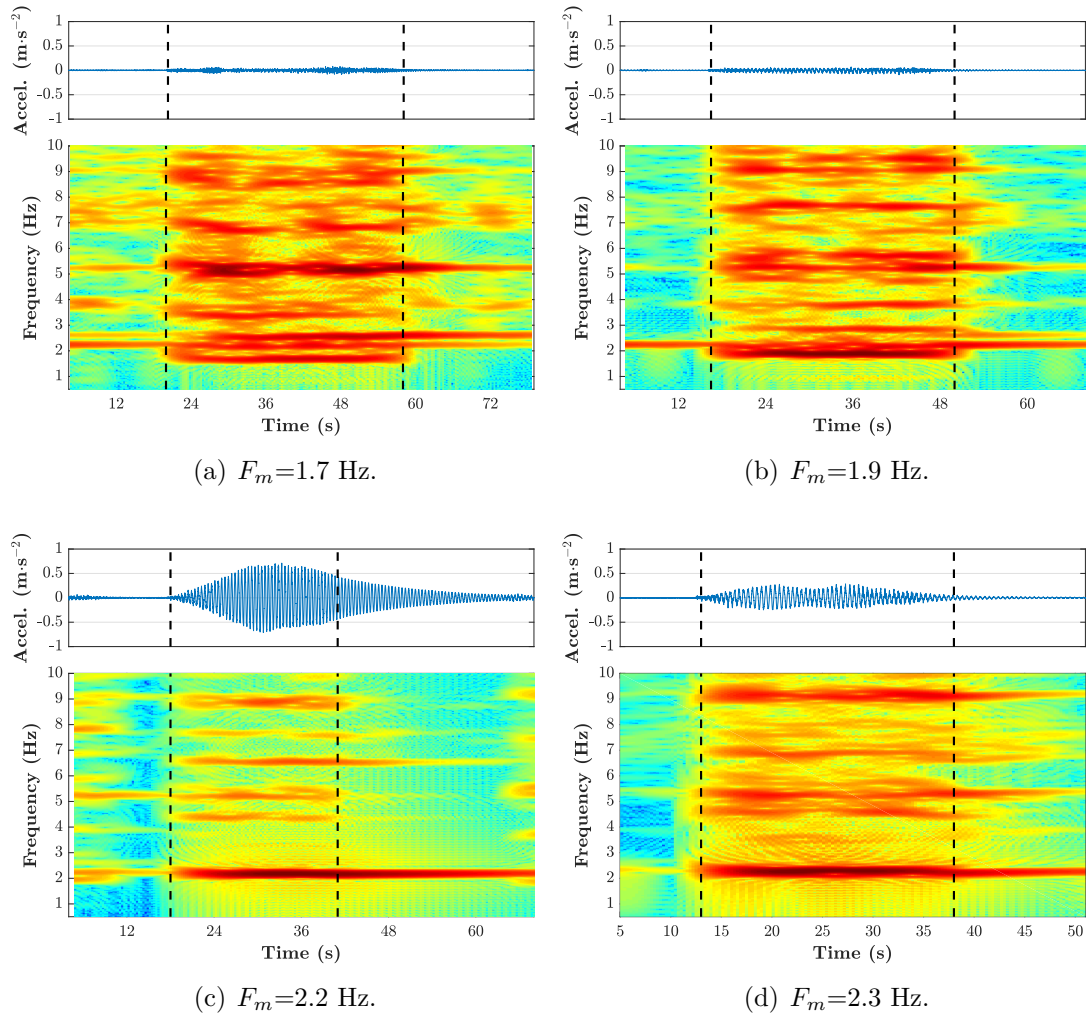


Fig. B.1.: Vertical accelerations due to two pedestrians walking at different frequencies (Channel No. 4).

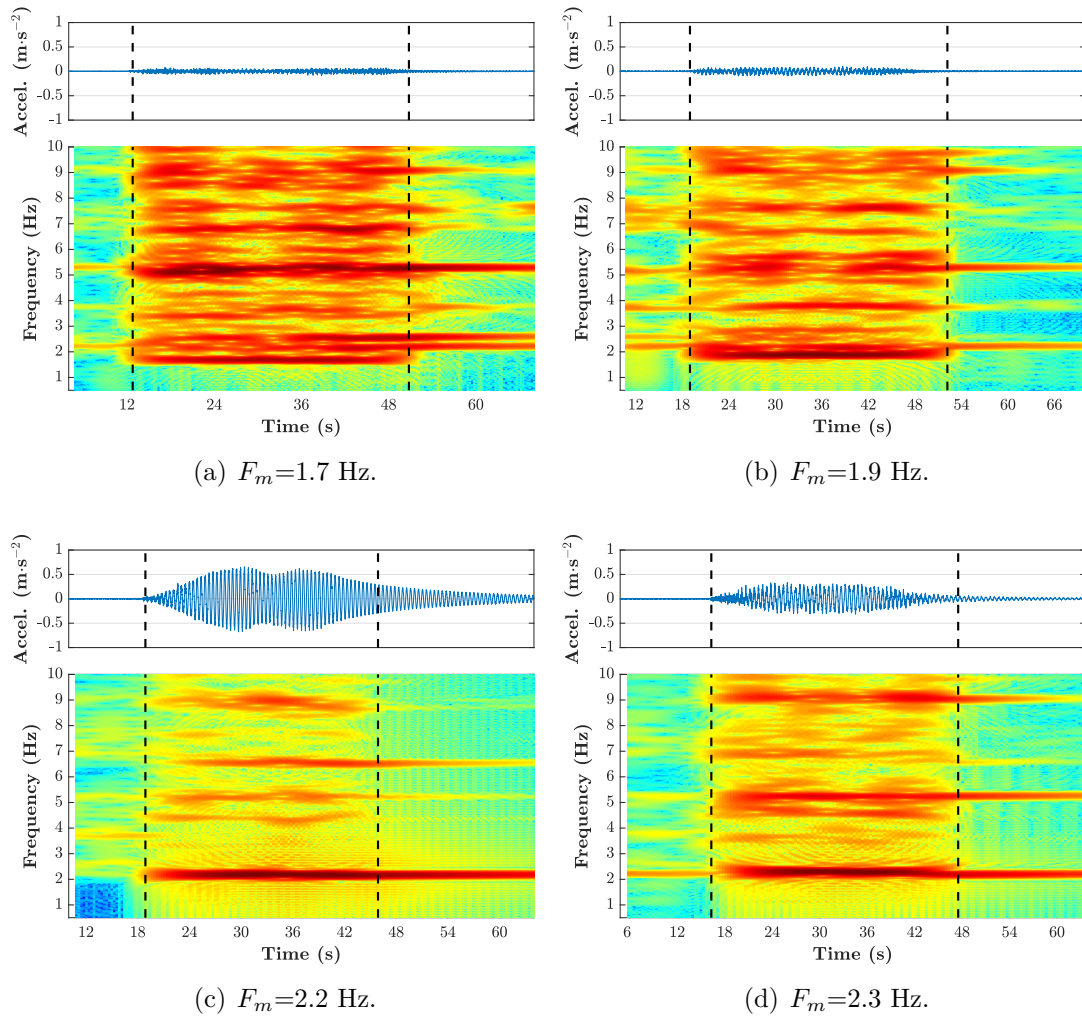


Fig. B.2.: Vertical accelerations due to three pedestrians walking at different frequencies (Channel No. 4).